University of Cape Town

MSc Thesis

Quantum States on Spheres in the Presence of Magnetic Fields

Author:
Ruach Pillay Slayen

Supervisor:
J Murugan
J Shock

University of Cape Town

A thesis submitted in fulfillment of the requirements for the degree of MSc

in the

Laboratory for Quantum Gravity and Strings
Mathematics and Applied Mathematics
Faculty of Science

July 6, 2019

The copyright of this thesis vests in the author. No quotation from it or information derived from it is to be published without full acknowledgement of the source. The thesis is to be used for private study or non-commercial research purposes only.

Published by the University of Cape Town (UCT) in terms of the non-exclusive license granted to UCT by the author.

University of Cape Town

Abstract

The study of quantum states on the surface of various two-dimensional geometries in the presence of strong magnetic fields has proven vital to the theoretical understanding of the quantum Hall effect. In particular, Haldane's seminal study of quantum states on the surface of a compact geometry, the sphere, in the presence of a monopole magnetic field, was key to developing an early understanding of the fractional quantum Hall effect. Most of the numerous studies undertaken of similar systems since then have been limited to cases in which the magnetic fields are everywhere constant and perpendicular to the surface on which the charged particles are confined.

In this thesis, we study two novel variations of Haldane's spherical monopole system: the 'squashed sphere' in the presence of a monopole-like magnetic field, and the sphere in the presence of a *dipole* magnetic field. In both cases the magnetic field is neither perpendicular nor constant with respect to the surface on which the charged particles are confined. Furthermore, the spherical dipole system has vanishing net magnetic flux. For the 'squashed sphere' system we find the lowest Landau level single-particle Hilbert space, and it is shown that the effect of the squashing is to localise the particles around the equator. For the spherical dipole system we find the entire single-particle Hilbert space and energy spectrum. We show that in the strong-field limit the spectrum exhibits a Landau level structure, as in the spherical monopole case. Unlike in the spherical monopole case, each Landau level is shown to be infinitely degenerate. The emergence of this Landau level structure is explained by the tendency of a strong dipole field to localise particles at the poles of the sphere.

Acknowledgements

Firstly, I would like to thank the Nation Institute for Theoretical Physics (NITheP) for the funding that made the completion of this MSc degree possible.

To my supervisors Dr. Jonathan Shock and Prof. Jeff Murugan, thank you for the support, academic and otherwise, that you have given me for the duration of my student years. To the service and administrative staff of the UCT Mathematics and Applied Mathematics department, thank you for the work you do, without which very little could be accomplished by anybody else.

To my parents Mike and Thikam, thank you for instilling in me the value of taking pride in whatever I do, and for unconditionally (and too often thanklessly) supporting me at every step.

To Asher, Leila, Nombuso, La'eeqa, Brian and Nishal, thank you for the strict regime of reading and exercise that got me through. To all of you and to Luthando and Ntokozo; the last few years would not have been bearable without you.

Finally, to my grandfather Dr. C.N. Pillay, thank you for your support and your belief in the importance of all of my studies, interests and commitments; and for, in your 90^{th} year, beginning to read about quantum mechanics so that we could talk about this work.

Contents

Chapter 1

Introduction

1.1 Background and Motivation

The Quantum Hall Effect

The simple set up of a two-dimensional electron gas in the presence of a strong magnetic field, provides the backdrop to some of the most remarkable phenomena in condensed matter, and indeed in all of physics [23]. These phenomena are collectively referred to as the *quantum Hall effect* (QHE). The QHE has fundamental significance as an example of macroscopic scale quantum mechanical effects [1], has links to deep ideas in the mathematical study of topology, and is central to the cutting edge of technological research into topological insulators/superconductors and quantum computing. These factors, among many others, are testament to how fruitful the study of this simple system has proven to be to modern science.

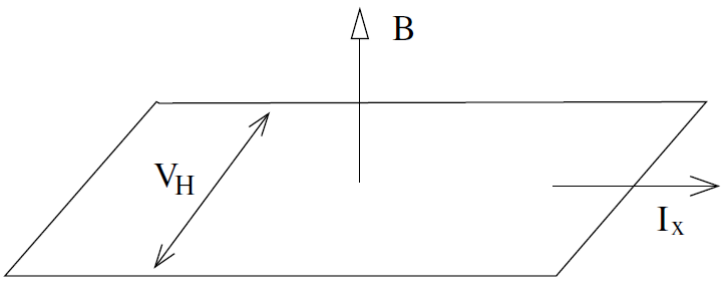

Figure 1.1: Set up for the classical Hall effect [23].

Prior to the discovery of the QHE, its classical counterpart was discovered by Edwin Hall in 1879. The *classical* Hall effect can be observed in the system of an electrical conductor with a current I_x flowing perpendicular to an applied magnetic field B (see Figure 1.1). The current carrying electrons experience a Lorentz force due to the applied field and accumulate on one side of the conductor. This produces a potential difference transverse to the direction of the current, called the *Hall voltage* V_H, given by

$$V_H = \rho_{xy} I_x \,. \tag{1.1}$$

The proportionality constant ρ_{xy} is known as the *Hall resistivity*[1]. The *longitudinal resistivity* is given by $\rho_{xx} = V_x/I_x$, where V_x is the potential difference across the conductor in the direction of current flow.

[1]That the Hall resistivity is equal to the transverse resistance is a fact unique to two-dimensional systems.

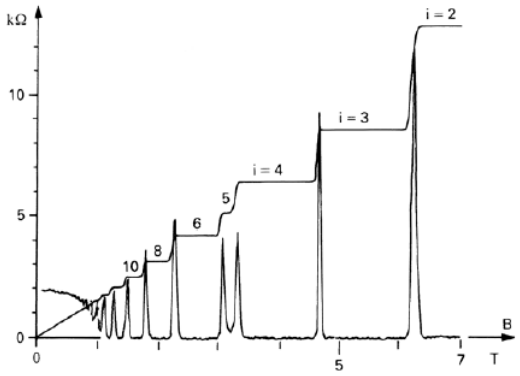

Figure 1.2: Resistivities in the integer quantum Hall effect [23].

A century later in 1980, von Klitzing performed the first experiments exploring the quantum regime of the Hall effect [2]. The resistivities were again measured, this time using very strong applied magnetic fields at very low temperatures. The result obtained is known as the *integer* quantum Hall effect (IQHE), for which von Klitzing received the 1985 Nobel prize. The Hall resistivity were found to take *precisely quantised* values,

$$\rho_{xy} = \frac{2\pi\hbar}{e^2}\frac{1}{\nu}, \quad \nu \in \mathbb{Z}, \tag{1.2}$$

where the value of ν is measured to be an integer with incredible accuracy[2]. Plotted as a function of magnetic field strength, the Hall resistivity ρ_{xy} has a series of plateaux at the quantised values in increasing order, separated by sharp jumps (see Figure 1.2). The longitudinal resistivity, on the other hand, vanishes when ρ_{xy} sits on a plateau and spikes precisely when ρ_{xy} jumps from one plateau to the next.

This quantisation of the resistivity in the IQHE has been found to be robust and independent of all microscopic details of the system, such as the type of semiconductor material and the purity of the sample [1]. This characteristic is known as *universality*.

Two years after the discovery of the IQHE, Tsui and Störmer again measured the resistivities, this time using samples with less *disorder*[3]. They found the emergence of new resistivity plateaux with values given by (1.2) but for *fractional* values $\nu \in \mathbb{Q}$ [3]. This result is known as the fractional quantum Hall effect (FQHE). Subsequently, samples with less disorder were measured, resulting in a proliferation of observed plateaux at various rational values of ν, commonly but not exclusively with odd denominators.

Theoretical Results

Theoretically, the plateaux observed in the IQHE are straight-forwardly explained. Electron-electron interactions can be ignored, greatly simplifying the problem. Using standard quantum mechanics, the electrons in the conductor can then be shown to occupy highly degenerate energy eigenstates known as *Landau levels*, which form the conceptual bedrock of the various phenomena of the QHE. Fascinatingly, the existence of precise integer quantisation was shown to be intimately linked to the 'messy' physics of disorder[4] [23]. One year after its experimental discovery, Laughlin [7], and later Halperin [43] were able to clarify the roles of extended and localised states in the QHE using the idea of gauge invariance.

To explain the FQHE, interactions between electrons could no longer be neglected, making the problem both more difficult and much richer. Laughlin laid down the building blocks of the theory by explaining the $\nu = 1/m$

[2]Consequently the QHE is used to maintain the standard of electrical resistivity and to measure the ratio of fundamental constants $2\pi\hbar/e^2$ [23].

[3]Disorder here refers to the prevalence of symmetry-breaking impurities, contained to some degree in all experimental samples.

[4]A random potential introduced to model disorder in the sample has the effect of 'trapping' electron orbits. The fact that these localised orbits are unable to carry current across the length of the conductor gives rise to the quantisation of the Hall resistivity.

FQHE ground states for m an odd integer [6], for which he shared the Nobel prize with Tsui and Störmer in 1998. Further research into the FQHE has been profoundly productive, yielding amongst other things the discovery of some of the most exotic states of quantum matter in contemporary physics: localised collective excitations of the FQHE fluid called *anyons*. Anyons are in general neither fermions or bosons, possess fractional charge and fractional statistics [13] and can themselves form collective excitations. This latter fact gives rise to the idea of the *hierarchy of states*, first suggested by Haldane [11] and built upon by Halperin [44], and expanded into the *composite fermion* framework by Jain [45]. These theoretical innovations allowed for the iterative explanation of many more filling fractions beyond those covered in Laughlin's original work. Moore and Read [47] and later Read and Rezayi [48] proposed further FQHE states to explain yet more of the observed filling fractions.

Moving from the wavefunction oriented microscopic approach of Laughlin, a more coarse-grained approach to understanding the FQHE was found in the effective field theories known as *Chern-Simons theories* [50, 51, 52]. These theories were able to reproduce many results obtained using the microscopic perspective, provide new insights on the QHE, and provide many cases of fruitful study for the rapidly expanding research area of *field theory dualities* [49].

Topological States of Matter

The physics of anyons, fundamental to our understanding of the FQHE, is intimately connected to the topology of loops in two-dimensional space. But the link between the QHE and topology is far more fundamental than this. The *TKNN invariant* [46] (named for Thouless, Kohomot, Nightingale and den Nijs) relates the precise quantization of the Hall resistivity to Chern numbers, topological invariants associated to the curvature of the system's Hamiltonian parameter space via the Berry phase [42]. The QHE thus serves as the prototypical example of an entirely new type of order for phases of matter: *topological order*. The concept of topological order was a break from Landau's symmetry breaking paradigm, which was until then believed to account for all states of matter.

While phases of matter within the symmetry breaking paradigm are characterised by a symmetry group and associated local order parameter, certain theoretical spin liquids were found to have different chiral spin states which are indistinguishable from the perspective of symmetry groups [14]. Topological order[5] was the concept introduced to fill this gap. New quantum numbers such as the non-Abelian Berry phase, edge excitations, ground state degeneracy [61] and topological entanglement entropy [16] were introduced to characterise and define the different topological orders. Having been developed to describe the as-yet purely theoretical spin liquids, this notion of topological order found practical application in the FQHE fluid. Further important application of these ideas include the hugely active research area of topological insulators [53] and topological superconductors [54].

Compact Geometries

The theoretical and experimental manifestations of the QHE highlighted thus far have all been in the context of planar geometry: the two-dimensional surface to which the electron gas is confined has been flat. We now address the QHE on the surface of curved and, in particular, compact surfaces via a discussion of Haldane's contribution to Laughlin's seminal theoretical work on the FQHE [6].

Laughlin's proposed FQHE states, by virtue of being formulated for a planar system, had to be confined by an external potential in order to localise the states within a finite area. This external confining potential then breaks the system's translational invariance and introduces the additional physics associated with the existence of a boundary, such as edge modes.

In 1983, Haldane considered a geometrical variation of this planar system first considered in the 1930s by Dirac and others [20, 21]: charged particles moving on the surface of a sphere which encloses a magnetic monopole at its center [11]. While 'unphysical' due to the magnetic monopole, this spherical monopole system replicates many of the key features of its planar counterpart. As with the perpendicular magnetic field in the planar system, the monopole field gives rise to a constant, perpendicular magnetic field through the surface of the sphere. By considering

[5]The name is motivated by the fact that the low energy effective description of the chiral spin states is a *topological quantum field theory* [60].

a compact geometry, a finite surface area is achieved without the existence of a boundary, avoiding the physics of edge states. This makes the spherical system an ideal context in which to explore the bulk physics of the Landau problem. It is also better suited to numerical simulation and to a simpler treatment of the thermodynamic limit than its planar counterpart [32].

Since Haldane's innovation, QHE states on a huge variety of compact and non-compact, curved and flat two-dimensional manifolds have been studied extensively. Dunne's synthesis [17] of the spherical monopole system and the planar system into a common framework (which he then applies to hyperbolic space) laid the groundwork for prescriptions for IQHE [56] and FQHE [4] states on surfaces of arbitrary curvature. Particular studies have included those of tori [55], cylinders [63] and higher genus Riemann surfaces [61]. Although largely theoretical at present, such studies have greatly enriched our understanding of experimentally observable states: studies of ground states on curved surfaces were found to provide a complete description of the QHE on a flat background, to imply geometric reasons for quantization and to uncover universal features of the QHE inaccessible to calculations in flat space [4]. All dissipation-free transport coefficients at low energies of the QHE were found to be understood as the response of the ground state to changes in scalar curvature on a closed manifold [4]. These results have both highlighted the importance of geometry, as opposed to topology, in our understanding of the QHE [57, 58, 59] and have centered the importance of compact geometries in particular.

Astrophysical Quantum Matter and Inhomogeneous Magnetic Fields

Phenomenology, specifically of the tabletop variety, is an important reason why the various and varied phenomena of the QHE have generated so much excitement since their discovery. However, such tabletop experiments are constrained by the intensity of the magnetic fields that can be produced on Earth[6]. If we want to learn more about quantum matter interacting with stable magnetic fields stronger than the $\sim \mathcal{O}(100)$T fields achievable in terrestrial laboratories [62], we can look elsewhere in the cosmos. Neutron stars, specifically their most powerfully magnetic manifestations, magnetars, exhibit magnetic fields that range in strength from $10^4 - 10^{11}$T, making them some of the most intense in the known Universe. In this age of precision multi-messenger observations, we have access to volumes of astrophysical data that offer an unprecedented glimpse into the physics of these gigantic generators. While much effort is directed toward probing the interior of neutron stars, there is also a considerable amount to be learnt from their surface (see, for example, [64] for some recent developments in neutron star atmospheric physics). A key motivation for some of the work done in this thesis was piqued by the question: *Are there astrophysical signatures of topological quantum matter*?

One crucial difference between the physics of a two-dimensional gas of electrons on the surface of a neutron star and the Haldane sphere is that, in the former, the magnetic field is primarily *dipole* in nature[7]. Consequently, the net magnetic flux is zero. While the study of charged classical particles in dipole fields in three-dimensional space has a long history in the geophysical context of cosmic rays and auroral phenomena [65], our engagement with the existing literature on the topic of two-dimensional quantum states in the presence of strong magnetic fields yielded no results about dipole fields. We observed that, in general, little attention has been given to two-dimensional quantum states in inhomogeneous magnetic fields. In the context of planar systems, the work done has been focussed either on relatively small variations from homogeneity, such as fields which approach a uniform value at large distances [5], or on highly constrained variations, such as fields which are monotonic functions of radial distance [8]. In the context of compact surfaces, the work done assumes small variations over a large constant background [4]. None of this allows for the case of particular interest to us: a compact surface through which the net magnetic flux vanishes.

We were thus lead to consider a novel variation of Haldane's spherical monopole system: the spherical dipole system, obtained by simply replacing the magnetic monopole at the centre of the sphere with a magnetic dipole. The primary question we sought to answer was: *would such a system exhibit a Landau level structure?*

With the physically realisable dipole field replacing that of the monopole, and as experimentalists' abilities to grow

[6]While $\sim 10^{14}$T magnetic fields are achievable in heavy-ion collisions such as at the LHC, these are out of equilibrium and exist on time scales too short to be relevant for our purposes.

[7]Although it must be pointed out that it is likely not *pure* dipole. Like the sun, there are multipole moments that decay rapidly with radius. We thank Bryan Gaensler for reminding us of this.

two-dimensional graphene surfaces are continually expanding, the spherical dipole system could indeed be physically realisable in the future. It may present an opportunity to empirically test some of the theoretical predictions for quantum Hall states on compact geometries. While this would require the extension of our results to the relativistic case relevant for graphene, we hope our work can serve as a first step and useful reference point to this end.

1.2 Overview of this Thesis

In this thesis we will be describing the quantum mechanics of charged particles confined to various two-dimensional spherical (and spheroidal) surfaces in the presence of magnetic fields.

We begin by considering two simple geometries in the case of a constant, perpendicular magnetic field: the plane and the sphere, in **Chapter 2** and **Chapter 3** respectively. These systems are well understood and none of our work here is original. We begin by presenting and solving the classical systems. We then closely follow [17] in solving the quantum formulation of the problem. In both cases we find the full single particle Hilbert space, first using an *analytic approach* based on solving a second-order linear differential equation, then using an *algebraic approach* in which we reduce the problem to a first-order linear differential condition via the use of raising and lowering operators. The special relationship between these two systems, with all features of the planar system emerging in the infinite radius limit of the corresponding features of the spherical monopole system, is emphasized in both approaches.

In **Chapter 4** we present the framework, also developed in [17], for treating the general system of charged particles constrained to the surface of any two-dimensional Kähler manifold in a constant, perpendicular magnetic field. Our results for the planar and spherical monopole system then emerge as special cases of this general framework. Following [4], we then extend this framework to allow us to solve for the lowest Landau level states for a two dimensional compact surface in the case of a *non-constant, non-perpendicular* magnetic field.

In **Chapter 5** we apply the framework developed in Chapter 4 to the system of charged particles confined to the surface of the oblate spheroid, or the 'squashed sphere'. We present a perturbative result for the lowest Landau level single particle states in the case of both perpendicular and non-perpendicular monopole-like magnetic field configurations. The work in this chapter is original.

In **Chapter 6**, we tackle the spherical dipole system. We first consider the classical problem and the trajectories of various classical solutions. Next we present the *Mathieu function* solutions to the quantum problem, which are then argued to be unphysical. We then present the *angular oblate spheroidal* solutions to the quantum problem, which account for the entire single-particle Hilbert space. We analyse these wavefunctions and their energy spectrum in various limits: the weak-field limit, the free particle, near the north pole, and the strong-field limit. We dedicate substantially more attention to the last case, where it is shown that the energy spectrum acquires a Landau level structure. The work in this chapter is original and has been submitted for publication [40].

In **Chapter 7**, we conclude the thesis by presenting a summary of its content and key results, as well as a number of possible directions for future research. **Appendix A** then contains a number of Laguerre and Jacobi polynomial relations relevant to the calculations in Chapters 2 and 3, while in **Appendix B** we derive the conformal map used to construct the squashed sphere in Chapter 5.

Chapter 2

The Planar System

We begin by considering the simplest system in which the physics of Landau levels and the associated phenomena of the QHE emerge: charged particles confined to a plane in the presence of a constant, perpendicular magnetic field. Following [17], we find the full single-particle Hilbert space and spectrum using both an analytic and algebraic approach, and analyse the wavefunctions found. We begin with a brief consideration of the classical problem.

2.1 Classical Dynamics

The Lagrangian for a non-relativistic particle of charge e and mass m moving in a background magnetic field $\mathbf{B} = \nabla \times \mathbf{A}$ is given by

$$L = \frac{1}{2} m \dot{\mathbf{x}}^2 + e \dot{\mathbf{x}} \cdot \mathbf{A} \,, \tag{2.1}$$

in units of $c = 1$. Note that under a gauge transformation $\mathbf{A} \to \mathbf{A} + \nabla\alpha$, the relevant term in the Lagrangian changes as

$$\begin{aligned} \dot{\mathbf{x}} \cdot \mathbf{A} \quad &\longrightarrow \quad \dot{\mathbf{x}} \cdot \mathbf{A} + \dot{\mathbf{x}} \cdot \nabla\alpha & (2.2) \\ &= \quad \dot{\mathbf{x}} \cdot \mathbf{A} + \dot{\alpha} \,, & (2.3) \end{aligned}$$

resulting in the Lagrangian changing by a total derivative: $L \to L + e\dot{\alpha}$. This leaves any equations of motion derived from (2.1) invariant.

The canonical momentum associated with our Lagrangian is

$$\mathbf{p} \equiv \frac{\partial L}{\partial \dot{\mathbf{x}}} = m\dot{\mathbf{x}} + e\mathbf{A} \,, \tag{2.4}$$

which differs from the *mechanical momentum* $\boldsymbol{\pi} \equiv m\dot{\mathbf{x}}$.

The Hamiltonian is then given by the usual Legendre transformation of the Lagrangian

$$\begin{aligned} H &= \dot{\mathbf{x}} \cdot \mathbf{p} - L & (2.5) \\ &= \frac{1}{2m} (\mathbf{p} - e\mathbf{A})^2 \,. & (2.6) \end{aligned}$$

Notice that this is just the Hamiltonian of a point particle in the absence of any magnetic field $H = \frac{1}{2} m \dot{\mathbf{x}}^2$. The fact that the vector potential does not feature is the statement that the magnetic field does no work and therefore does not affect the energy of the system. However the vector potential remains important to our description of the system, as we see when we consider our canonical variables, $\mathbf{x}$ and $\mathbf{p}$. The fact that they are canonical means that they satisfy the following Poisson bracket relations

$$\{x_i, p_j\} = \delta_{ij} \,, \qquad \{x_i, x_j\} = \{p_i, p_j\} = 0 \,, \tag{2.7}$$

where the Poisson bracket is given by

$$\{f,g\} = \frac{\partial f}{\partial x_i}\frac{\partial g}{\partial p_i} - \frac{\partial f}{\partial p_i}\frac{\partial g}{\partial x_i}\,. \tag{2.8}$$

However, $\mathbf{p}$ is clearly not gauge invariant as it depends linearly on the gauge potential. As a quantity which depends on our choice of gauge we know that it cannot have physical meaning. On the other hand, the mechanical momentum $\boldsymbol{\pi} = m\dot{\mathbf{x}}$ is manifestly gauge invariant. However, it is not a canonical variable, as can be seen by checking that the Poisson bracket of the mechanical momentum with itself is non-vanishing

$$\{\pi_i,\pi_j\} = \{p_i - eA_i, p_j - eA_j\} = e\Big(\frac{\partial A_j}{\partial x_i} - \frac{\partial A_i}{\partial x_j}\Big) = e\epsilon_{ijk}B_k\,. \tag{2.9}$$

The classical equation of motion following from the Lagrangian (2.1) is

$$m\ddot{\mathbf{x}} = e\dot{\boldsymbol{x}}\times\mathbf{B}\,, \tag{2.10}$$

which is simply the Lorentz force law. The general solution for electrons confined to move in the x_1x_2-plane in a perpendicular magnetic field $\mathbf{B} = (0,0,B)$ is then given by

$$x_1(t) = X_1 - R\sin(\omega_B+\phi)\,, \qquad x_2(t) = X_2 + R\cos(\omega_B+\phi)\,. \tag{2.11}$$

These solutions describe electrons moving in fixed circular closed orbits. The radius R, center (X_1,X_2) and phase ϕ of the circular orbit are constants of integration, while the frequency with which the particle orbits is given by the *cyclotron frequency*

$$\omega_B = \frac{eB}{m}\,. \tag{2.12}$$

2.2 Quantum Mechanics

2.2.1 Analytic Approach

Single-Particle States

We now progress to the quantum formulation of the problem, following the treatment given in [17]. The canonical commutation relations following from the Poisson brack relations (2.7) are

$$[x_i,p_j] = i\hbar\delta_{ij}\,, \qquad [x_i,x_j] = [p_i,p_j] = 0\,, \tag{2.13}$$

whilst from (2.9) the mechanical momentum satisfies

$$[\pi_x,\pi_y] = ie\hbar B\,. \tag{2.14}$$

Setting $\hbar = m = e = 1$ in (2.5), the Hamiltonian for a system of non-interacting charged particles moving in the plane in a perpendicular uniform magnetic field of strength $B>0$ is given by

$$H = \frac{1}{2}(-i\boldsymbol{\nabla} - \mathbf{A})^2\,. \tag{2.15}$$

We choose to work in the symmetric gauge

$$A^i = -\frac{B}{2}\varepsilon^{ij}x^j\,. \tag{2.16}$$

Note that this choice of gauge preserves azimuthal rotational symmetry (rotational symmetry about the origin); we therefore expect angular momentum to be a good quantum number with which to label energy eigenstates. Changing to complex coordinates

$$z = \sqrt{B/2}(x^1 + ix^2)\,, \tag{2.17}$$

$$\bar{z} = \sqrt{B/2}(x^1 - ix^2)\,. \tag{2.18}$$

which we have rescaled by $\sqrt{B/2}$ for convenience, our Hamiltonian (2.15) can now be written as

$$H = B\Big(- \partial\bar{\partial} - \frac{1}{2}(z\partial - \bar{z}\bar{\partial}) + \frac{1}{4}z\bar{z}\Big)\,, \tag{2.19}$$

where

$$\partial \equiv \frac{\partial}{\partial z} = \sqrt{2/B}(\partial_1 - i\partial_2)\,, \tag{2.20}$$

$$\bar{\partial} \equiv \frac{\partial}{\partial \bar{z}} = \sqrt{2/B}(\partial_1 + i\partial_2)\,, \tag{2.21}$$

are the holomorphic and anti-holomorphic derivatives respectively.

Before proceeding to solve for the eigenstates, we perform a prudent redefinition of our single-particle Hilbert space which will greatly simplify our efforts. We first define *reduced eigenstates* [35, 36] $\hat{\Psi}$ in terms of the full eigenstates Ψ as follows

$$\Psi(z,\bar{z}) = e^{-|z|^2/2}\hat{\Psi}(z,\bar{z}) \tag{2.22}$$

where we have extracted the *measure factor* $e^{-|z|^2/2}$. The reduced eigenstates will be identified with elements of the Hilbert space, while the measure factor will appear in the measure of the Hilbert space inner product,

$$\begin{aligned}\langle f|g\rangle &\equiv \int d\mu(z)\overline{f(z,\bar{z})}g(z,\bar{z})\,,\\ d\mu(z) &= \frac{1}{2\pi i}e^{-|z|^2}dzd\bar{z}\,.\end{aligned} \tag{2.23}$$

For each full operator A which acts on full eigenstates as $A\Psi = a\Psi$, we would like to define the *Hilbert space operator* $\hat{A}$ which acts on the reduced states to return the same eigenavalue: $\hat{A}\hat{\Psi} = a\hat{\Psi}$. The necessary relation between such operators is given by conjugation

$$\hat{A} = e^{|z|^2/2}Ae^{-|z|^2/2}\,, \tag{2.24}$$

as can be simply verified:

$$\hat{A}\hat{\Psi} = e^{|z|^2/2}Ae^{-|z|^2/2}\hat{\Psi} = e^{|z|^2/2}A\Psi = e^{|z|^2/2}a\Psi = a\hat{\Psi}\,. \tag{2.25}$$

Using the prescription (2.24) we find the Hilbert space Hamiltonian operator corresponding to (2.19) to be given by

$$\hat{H} = B\Big(- \partial\bar{\partial} + \bar{z}\bar{\partial} + \frac{1}{2}\Big)\,. \tag{2.26}$$

The anti-holomorphic derivatives in the first two terms imply that the ground states of the Hamiltonian are holomorphic wavefunctions

$$\hat{\Psi}_{\rm LLL} = f(z)\,, \tag{2.27}$$

satisfying $\bar{\partial}f(z) = 0$. They all have ground state energy $B/2$. The corresponding full states are eigenstates of the full Hamiltonian (2.19) given by

$$\Psi_{\rm LLL} = e^{-|z|^2/2}f(z)\,. \tag{2.28}$$

Note that we have found infinitely many ground state eigenfunctions which are all degenerate in energy. These states constitute what is known as the *lowest Landau level*, henceforth referred to as the LLL.

The standard planar angular momentum operator, given in polar coordinates by $J = -i\partial_\phi$, is given in our coordinates by

$$J = z\partial - \bar{z}\bar{\partial} = \hat{J}\,. \tag{2.29}$$

Note that the reduced and full form of the operator are identical. It is easily verified that J commutes with H, as we would expect given the azimuthal rotational symmetry of the problem. To find the excited states of our Hamiltonian,

we will therefore look for simultaneous eigenstates of energy and angular momentum. We choose as our ansatz the most general form of an angular momentum eigenstate,

$$\hat{\Psi} = z^m P(|z|^2)\,, \tag{2.30}$$

where P is some function to be determined and single valuedness requires that $m \in \mathbb{Z}$. That this is an angular momentum eigenstate with eigenvalue m is most easily verified by changing to complex polar coordinates $z = re^{i\phi}$:

$$\hat{J}\hat{\Psi} = -i\partial_\phi\big(r^m e^{im\phi} P(r^2)\big) = m\hat{\Psi}\,. \tag{2.31}$$

Requiring that $\hat{\Psi}$ also be an energy eigenstate then allows us to impose

$$\hat{H}\hat{\Psi} = E\hat{\Psi} \quad \Rightarrow \quad B\Big(-\partial\bar{\partial} + \bar{z}\bar{\partial} + \frac{1}{2}\Big)z^m P = Ez^m P\,. \tag{2.32}$$

Changing variables to $x \equiv |z|^2$, we recover the following differential equation for P

$$x\frac{d^2P}{dx^2} + (m+1-x)\frac{dP}{dx} + \Big(\frac{E}{B} - \frac{1}{2}\Big)P = 0\,. \tag{2.33}$$

We recognise this as having the form of a *Laguerre differential equation*

$$xf'' + (m+1-x)f' + nf = 0\,, \tag{2.34}$$

which has as solutions the *generalised Laguerre polynomials*

$$L_n^m(x) \equiv \frac{1}{n!}e^x x^{-m}\frac{d^n}{dx^n}(e^{-x}x^{n+m}) \tag{2.35}$$

$$= \sum_{j=0}^{n}\frac{(-1)^j}{j!}\binom{n+m}{n-j}x^j\,, \tag{2.36}$$

which are defined for $n \in \mathbb{Z}$, $n \geq 0$ and $j \geq -n$. Comparing (2.34) with (2.33) we make the identification

$$E = B\Big(n + \frac{1}{2}\Big) \tag{2.37}$$

Our reduced single-particle eigenstates are thus given by

$$\begin{aligned}\hat{\Psi}_n^m(z,\bar{z}) &= \mathcal{N}z^m L_n^m(|z|^2)\\ E_{B,n} &= B\Big(n+\frac{1}{2}\Big)\\ n &= 0,1,2,...\\ m &= -n, -n+1, ...\end{aligned} \tag{2.38}$$

where $\mathcal{N}$ is a normalisation constant.

The $n = 0$ case corresponds to our LLL states (2.30) found earlier by inspection. We see that the rest of our spectrum is composed of infinitely many evenly spaced energy levels labelled by the positive integer n. Since the spectrum is independent of m, each level is infinitely degenerate. These highly degenerate energy levels are known as *Landau levels* and are a feature of the physics of charged particles on two-dimensional surfaces in constant perpendicular magnetic fields. Within a Landau level, degenerate states are distinguished by their angular momentum quantum number m. The LLL states all have non-negative angular momentum while the higher Landau levels contain states with negative angular momentum.

Normalisation

Returning to the normalisation constant $\mathcal{N}$, we would like to choose it such that our reduced wavefunctions satisfy orthonormality with respect to the inner product (2.23),

$$\left\langle \hat{\Psi}_n^m \middle| \hat{\Psi}_{n'}^{m'} \right\rangle = \frac{\mathcal{N}^2}{2\pi i} \int dz d\bar{z} e^{-|z|^2} z^m \bar{z}^{m'} L_n^m(|z|^2) L_{n'}^{m'}(|z|^2) \,. \tag{2.39}$$

To solve for $\mathcal{N}$, we change to complex polar coordinates,

$$\left\langle \hat{\Psi}_n^m \middle| \hat{\Psi}_{n'}^{m'} \right\rangle = \frac{\mathcal{N}^2}{\pi} \int dr d\phi e^{-r^2} e^{i(m-m')\phi} r^{m+m'+1} L_n^m(r^2) L_{n'}^{m'}(r^2) \tag{2.40}$$

$$= 2\mathcal{N}^2 \delta_{m,m'} \int dr e^{-r^2} r^{2m+1} L_n^m(r^2) L_{n'}^m(r^2) \,, \tag{2.41}$$

where in the second equality we have done the ϕ integral to obtain $2\pi\delta_{m,m'}$. Changing coordinates to $x = r^2$, we find

$$\left\langle \hat{\Psi}_n^m \middle| \hat{\Psi}_{n'}^{m'} \right\rangle = \mathcal{N}^2 \delta_{m,m'} \int dx e^{-x} x^m L_n^m(x) L_{n'}^m(x) \,. \tag{2.42}$$

The integral here is of a known form [18] which expresses the orthogonality of the Laguerre polynomials on the interval $[0, \infty)$ with respect to the weight $e^{-x}x^m$:

$$\int_0^\infty dx e^{-x} x^m L_n^m(x) L_{n'}^m(x) = \delta_{n,n'} \frac{(n+m)!}{n!} \,. \tag{2.43}$$

We therefore identify our normalisation constant

$$\mathcal{N} = \sqrt{\frac{n!}{(n+m)!}} \,. \tag{2.44}$$

With this choice, our wavefunctions (2.38) are orthonormal with respect to both quantum numbers:

$$\left\langle \hat{\Psi}_n^m \middle| \hat{\Psi}_{n'}^{m'} \right\rangle = \delta_{n,n'} \delta_{m,m'} \,. \tag{2.45}$$

Additionally, they form a complete set of functions [19], spanning the entire single-particle Hilbert space.

2.2.2 Algebraic Approach

Single-Particle States

We now introduce a simple algebraic formulation of the Hilbert space structure described above. We begin by introducing two sets of harmonic oscillator step operators [28, 29, 30, 31]

$$\begin{aligned} a^\dagger &\equiv \partial - \bar{z}/2 \,, \\ a &\equiv -\bar{\partial} - z/2 \,, \\ b^\dagger &\equiv -\bar{\partial} + z/2 \,, \\ b &\equiv \partial + \bar{z}/2 \,. \end{aligned} \tag{2.46}$$

These satisfy the commutation relations

$$[a, a^\dagger] = [b, b^\dagger] = 1 \,. \tag{2.47}$$

with all other commutators vanishing. We recognise (2.47) as the Heisenberg algebra commutation relations. We then write our energy and angular momentum operators in terms of these step operators

$$H = B\Big(a^\dagger a + \frac{1}{2}\Big) \,, \tag{2.48}$$

$$J = b^\dagger b - a^\dagger a \,. \tag{2.49}$$

Looking at H and the commutation relations for a and $a^\dagger$, we immediately note that $a^\dagger$ and a can be interpreted as energy raising and lowering operators respectively, in analogy with the standard harmonic oscillator system. Clearly $b^\dagger$ and b commute with the Hamiltonian and therefore leave energy invariant when acting on states. Let us now establish an interpretation for $b^\dagger$ and b and establish the effects of all operators on angular momentum. We first note that

$$[J,a] = [b^\dagger b - a^\dagger a, a] = -[a^\dagger, a]a = a \tag{2.50}$$

$$,[J,b] = [b^\dagger b - a^\dagger a, b] = [b^\dagger, b]b = -b\,. \tag{2.51}$$

Similarly, we find

$$[J,a^\dagger] = -a^\dagger\,, \tag{2.52}$$

$$[J,b^\dagger] = b^\dagger\,. \tag{2.53}$$

These results establish $b^\dagger$ and b respectively as angular momentum raising and lowering operators which leave energy invariant. They allow us to move between the degenerate states of different angular momentum within any particular Landau level. On the other hand, $a^\dagger$ and a are angular momentum lowering and raising operators respectively, which simultaneously raise and lower energy. They allow us to move between states in different Landau levels. It then follows that the composite operators $a^\dagger b^\dagger$ and ab act as energy raising and lowering operators respectively which leave angular momentum invariant.

As before, we now examine the corresponding operators which act directly on our Hilbert space as defined above. Using the prescription (2.24) we find

$$\hat{a}^\dagger = \partial - \bar{z}\,, \tag{2.54}$$

$$\hat{a} = -\bar{\partial}\,, \tag{2.55}$$

$$\hat{b}^\dagger = -\bar{\partial} + z\,, \tag{2.56}$$

$$\hat{b} = \partial\,, \tag{2.57}$$

and

$$\hat{H} = B(\hat{a}^\dagger\hat{a} + 1/2)\,, \tag{2.58}$$

$$\hat{J} = \hat{b}^\dagger\hat{b} - \hat{a}^\dagger\hat{a}\,. \tag{2.59}$$

These reduced operators satisfy the same commutation relations as the corresponding full operators in (2.47). Now note that

$$\begin{aligned}\langle f|\hat{a}g\rangle &= \int dzd\bar{z}e^{-|z|^2}\bar{f}\big(-\bar{\partial}g\big) = \int dzd\bar{z}\bar{\partial}\big(e^{-|z|^2}\bar{f}\big)g \\ &= \int dzd\bar{z}e^{-|z|^2}(-z+\bar{\partial})\bar{f} = \int dzd\bar{z}e^{-|z|^2}\overline{(\partial-\bar{z})f}g \\ &= \big\langle \hat{a}^\dagger f\big|g\big\rangle\,.\end{aligned} \tag{2.60}$$

Likewise it can be verified that

$$\Big\langle f\Big|\hat{b}g\Big\rangle = \Big\langle \hat{b}^\dagger f\Big|g\Big\rangle\,. \tag{2.61}$$

Thus $\hat{a}$ and $\hat{a}^\dagger$ (and $\hat{b}$ and $\hat{b}^\dagger$) are truly adjoints, unlike their corresponding full operators.

The action of these operators on the Hilbert space reduced wavefunctions is given by

$$\hat{a}^\dagger\hat{\Psi}^j_n = \sqrt{n+1}\hat{\Psi}^{j-1}_{n+1}\,, \tag{2.62}$$

$$\hat{a}\hat{\Psi}^j_n = \sqrt{n}\hat{\Psi}^{j+1}_{n-1}\,, \tag{2.63}$$

$$\hat{b}^\dagger\hat{\Psi}^j_n = \sqrt{n+j+1}\hat{\Psi}^{j+1}_n\,, \tag{2.64}$$

$$\hat{b}\hat{\Psi}^j_n = \sqrt{n+j}\hat{\Psi}^{j-1}_n\,, \tag{2.65}$$

which can be verified in terms of our explicit solutions (2.38) using the differential-difference and difference relations for the Laguerre polynomials in Appendix A. Note that $\hat{b}\hat{\Psi}_n^{-n} = 0$, which tells us that the minimum angular momentum allowed for a state in the n^{th} Landau level is $j = -n$. On the other hand since $\hat{b}^\dagger \hat{\Psi}_n^j = 0$ has no solution, we see that there is no maximal allowed angular momentum state.

To recover explicit expressions for our wavefunctions, we know that $\hat{\Psi}_0^0$ is our 'vacuum' state in the sense that it is annihilated both by the energy lowering operator, yielding

$$0 = \hat{a}\hat{\Psi}_0^0 = -\bar{\partial}\hat{\Psi}_0^0 \quad \Rightarrow \quad \hat{\Psi}_0^0 = f(z)\,, \tag{2.66}$$

and by the angular momentum lowering operator, yielding

$$0 = \hat{b}\hat{\Psi}_0^0 = \partial f(z) \quad \Rightarrow \quad f(z) = 1\,. \tag{2.67}$$

Having found our vacuum state $\hat{\Psi}_0^0 = 1$, we obtain states of higher angular momentum by acting on this vacuum state with the angular momentum raising operator,

$$\hat{\Psi_0^m} = (\hat{b}^\dagger)^m \hat{\Psi}_0^0 = (-\bar{\partial} + z)^m \hat{\Psi}_0^0 = z^m\,. \tag{2.68}$$

Note that we have recovered, up to normalisation, the explicit form of our LLL states as in (2.38). Finally, we include the exponential measure factor to get our full LLL eigenstates,

$$\Psi_0^m = z^m e^{-|z|^2/2}\,. \tag{2.69}$$

The full set of explicit expressions for higher Landau level (2.38) states can also be recovered in the algebraic approach by applying the energy raising operator to our LLL states. We will not do this here.

Degeneracy Counting

While we have established that on the infinite plane the LLL is infinitely degenerate, we would like to get a sense of the degeneracy per area. Following [23], we first develop some intuition about the profile of our LLL wavefunctions (2.69). Due to the exponential factor they are localised in some finite region around the origin, and tend to zero as $|z| \to \infty$. Due to the monomial factor, they vanish at the origin. We expect them to take on a unique maximum value somewhere in between. To show this, we change to complex polar coordinates $z = \sqrt{B/2}e^{i\phi}r$ and solve for the radial derivative

$$\begin{aligned}\frac{\partial}{\partial r}\Psi_0^m &= (B/2)^{m/2}\frac{\partial}{\partial r}\big(e^{im\phi}r^m e^{-Br^2/4}\big) \\ &= \big(\frac{m}{r} - \frac{Br}{2}\big)\Psi_0^m\,.\end{aligned} \tag{2.70}$$

Setting this derivative to zero gives us the radial turning point

$$r_* = \sqrt{2m/B}\,. \tag{2.71}$$

Thus we see that our LLL wavefunctions in symmetric gauge are peaked on a ring of radius r_* surrounding the origin, where r_* increases with increasing angular momentum.

We can use this information to estimate the degeneracy of states in the LLL. In a disc shaped region of area $A = \pi R^2$, the number of states N can be estimated to be m_R, where $R = \sqrt{2m_R/B}$, so that

$$N = m_R = \frac{BR^2}{2} = \frac{AB}{2\pi} = \frac{\Phi}{\Phi_0} \equiv N_\phi\,, \tag{2.72}$$

where $\Phi = AB$ is the total flux through the disc shaped region and we have introduced the *flux quantum* $\Phi_0 \equiv 2\pi\hbar/e$. We have also briefly restored the fundamental constants e and $\hbar$ by dimensional analysis. We have thus shown that

the number of states N in the region is equal to the number of flux quanta N_ϕ through the region. Dividing through by the area of the region yields a result for the density of states, valid now for the entire infinite plane

$$\frac{N}{A} = \frac{Be}{2\pi\hbar} = \frac{1}{2\pi l^2}\,, \tag{2.73}$$

where we have introduced the *magnetic length* $l = \sqrt{\hbar/eB}$. Note that while the profiles of the wavefunctions we have found here are gauge dependent, our result for the density of states is not. The quick state-counting argument given here can be replicated in other gauges [23], with the same result. While we have not shown this, our result also holds for all Landau levels [22], and not merely the LLL.

2.2.3 Wavefunctions

Having solved for the entire single-particle state Hilbert space, we now seek to better understand the planar system by more closely examining the wavefunctions and analysing some representative plots.

We begin by rewriting our reduced eigenstates (2.38) as full eigenstates by restoring the exponential measure factor using (2.22), restoring the B dependence by rescaling $z \to \sqrt{B/2}z$ and changing to polar complex coordinates:

$$\begin{aligned}
\Psi_n^m(B;r,\phi) &= \sqrt{\frac{n!}{(n+m)!}}\Big(\frac{B}{2}\Big)^{\frac{m}{2}} r^m L_n^m\Big(\frac{B}{2}r^2\Big)e^{-Br^2/2}e^{im\phi} \\
&\equiv \psi_n^m(B;r)e^{im\phi} \\
E_{B,n} &= B\Big(n+\frac{1}{2}\Big) \\
n &= 0,1,2,... \\
m &= -n,-n+1,...
\end{aligned} \tag{2.74}$$

In the following we will plot $\psi_n^m(B;r)$ against r, ignoring the ϕ dependence which is not relevant to the probability distributions $|\Psi_n^m(r,\phi)|^2 = |\psi_n^m(r)|^2$ of the eigenstates.

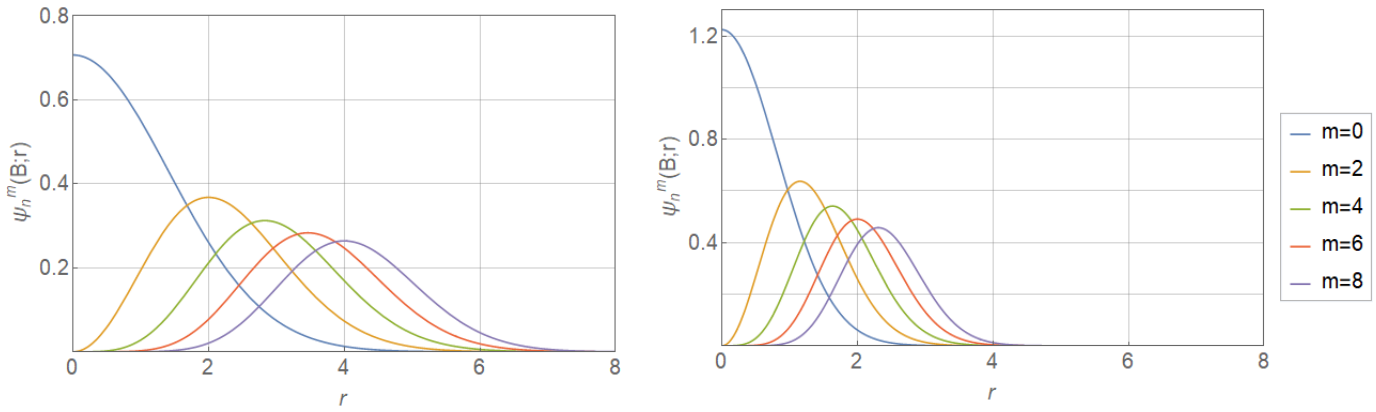

(a) $B = 1$ (b) $B = 3$

Figure 2.1: $\psi_n^m(B;r)$ for $n = 0$ and various m and B.

We begin with the LLL states, a representative selection of which are plotted in Figure 2.1. Recall that m takes integer values $m \geq 0$. All LLL states have no nodes. The lowest angular momentum $m = 0$ state is peaked at the origin and smoothly decays to zero as r increases. As m increases, the states become peaked at larger values of r, smoothly decaying to zero on both sides (they attain their maximum values at $r_* = \sqrt{2m/B}$). Comparing Figures 2.1a and 2.1b illustrates that the decay of the LLL states around the peak is faster for larger field strength B, meaning that the effect of a stronger field strength is to more sharply localise the particle (radially) on the plane. This statement is true for states in all Landau levels.

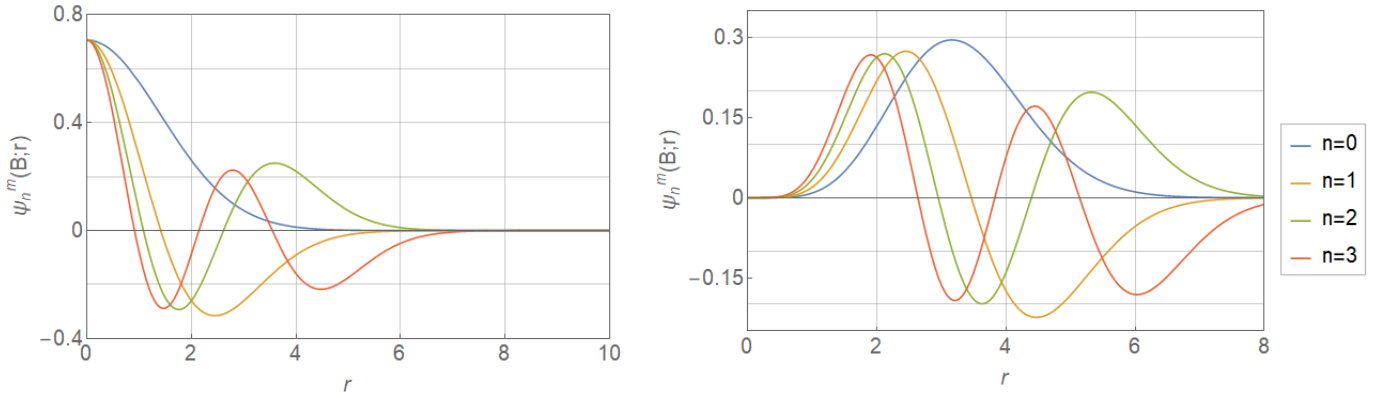

(a) $m = 0$ (b) $m = 5$

Figure 2.2: $\psi_n^m(B;r)$ for $B = 1$ and various n and m.

We next consider the higher Landau level states, a representative selection of which are plotted in Figure 2.2. The number of nodes (excluding the origin) of a state in the n^{th} Landau level is always n. Higher energy states are less spatially localised than their counterparts with the same m in lower Landau levels, as intuition would suggest. All $m = 0$ states take their maximum amplitude at the origin, and are the only states which have non-zero amplitude at the origin. Comparing Figure 2.2a and 2.2b we see that states which larger angular momentum m are radially localised at larger values of r.

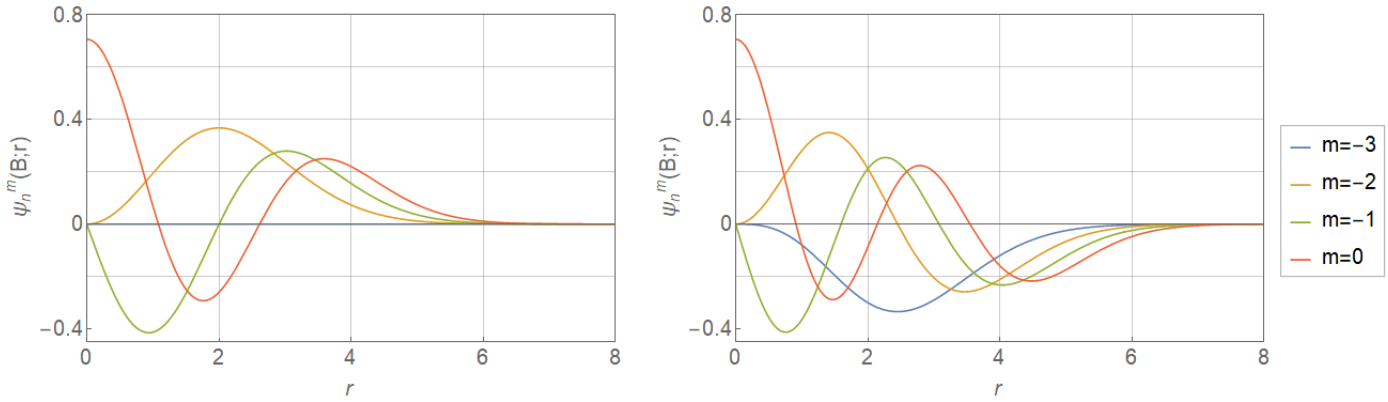

(a) $n = 2$ (b) $n = 3$

Figure 2.3: $\psi_n^m(B;r)$ for $B = 1$ and various n and $m \leq 0$.

Recall that in higher Landau levels, states can have negative angular momentum since m takes integer values starting at $m = -n$. In Figure 2.3 we illustrate that in general the $m = -n$ state has no nodes, while the $m = -n+1$ state has one, all the way up to the $m = 0$ state which has n nodes (we exclude nodes at the origin in each case). As m becomes positive, the number of nodes then remains constant but the overall distribution moves radially outwards as shown in Figure 2.2.

Chapter 3

The Spherical Monopole System

We now consider a geometrical variation of the planar system: charged particles moving on the surface of a sphere surrounding a magnetic monopole at its center. While 'unphysical' due to the magnetic monopole, the spherical monopole system replicates many of the key features of its planar counterpart. As with the perpendicular magnetic field in the planar system, the monopole field gives rise to a constant, perpendicular magnetic field through the surface of the sphere. We therefore expect the spectrum to exhibit a Landau level structure. While the translational symmetry of the planar geometry is replaced by the rotational symmetry of the sphere, in the large radius limit as the surface of the sphere becomes approximately flat, we expect the two descriptions to coincide. Whilst the planar system has an infinite surface area and therefore an infinite degeneracy per Landau level, the compact geometry of the sphere has finite area. We thus expect a finite degeneracy per Landau level. These expectations will be made precise in this section. We begin with a brief treatment of the classical problem.

3.1 Classical Dynamics

The Lagrangian for a particle of charge e and mass m moving in a background magnetic field $\mathbf{B} = \nabla \times \mathbf{A}$ is given, as before, by

$$L = \frac{1}{2} m \dot{\mathbf{x}}^2 + e \dot{\mathbf{x}} \cdot \mathbf{A} \,. \tag{3.1}$$

in units of $c = 1$. The magnetic monopole of charge g located at the origin gives rise to the radial magnetic field

$$B(r) = \frac{g}{r^2} \hat{r} \,. \tag{3.2}$$

We choose to express the corresponding magnetic vector potential in the *Dirac string gauge*

$$\mathbf{A}(\theta, \phi) = \frac{g}{r} \frac{1 - \cos\theta}{\sin\theta} (-\sin\phi, \cos\phi, 0) \,. \tag{3.3}$$

Constraining our particle to move on the surface of a sphere of radius R surrounding the origin,

$$\mathbf{x}(\theta, \phi) = R(\sin\theta\cos\phi, \sin\theta\sin\phi, \cos\theta) \,, \tag{3.4}$$

through which the magnetic field is constant and everywhere perpendicular with magnitude

$$B = \frac{g}{R^2} \,, \tag{3.5}$$

we recover the equations of motion

$$\theta'' = (B\sin\theta + \cos\theta\sin\theta\phi')\phi' \,, \tag{3.6}$$

$$\phi'' = -\csc\theta(B + 2\cos\theta\phi')\theta' \,. \tag{3.7}$$

The solutions correspond, as in the classical planar case, to closed circular orbits whose radius, center and phase are all a function of initial conditions. A number of representative trajectories are plotted in blue on the surface of the

sphere in Figure 3.1, where the magnetic vector field is illustrated in black.

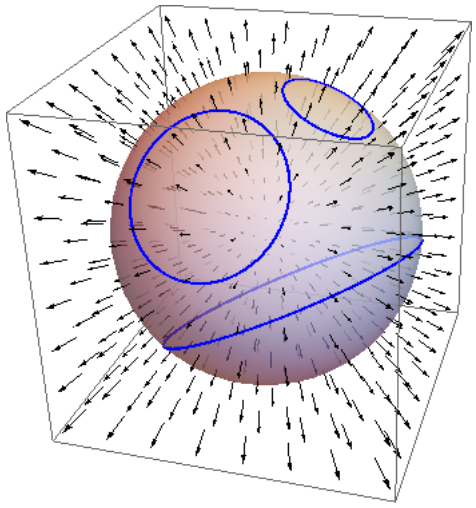

Figure 3.1: Classical trajectories for various initial conditions

3.2 Quantum Mechanics

3.2.1 Analytic Approach

Single-Particle States

We now consider the quantum problem, again following the treatment given in [17]. We work in spherical coordinates

$$\begin{aligned} x^1 &= r\sin\theta\cos\phi\,, \\ x^2 &= r\sin\theta\sin\phi\,, \\ x^3 &= r\cos\theta\,, \end{aligned} \tag{3.8}$$

where $0 < \theta < \pi$ and $0 \leq \phi < 2\pi$. We again write the magnetic vector potential corresponding to the monopole field in Dirac string gauge

$$\mathbf{A} = \Big(-\frac{gx^2}{r(r+x^3)}, \frac{gx^1}{r(r+x^3)}, 0 \Big)\,. \tag{3.9}$$

In spherical components and coordinates this becomes

$$A_r = A_\theta = 0\,, \qquad A_\phi = \frac{g}{r\sin\theta}(1-\cos\theta)\,. \tag{3.10}$$

Our gauge choice preserves azimuthal rotational symmetry, as did our gauge choice for the planar system. Note that the vector potential has a singularity along the negative x^3, axis where $r = -x_3$. We will return to this observation shortly.

There is an important constraint on the monopole charge g. We briefly outline one version of the argument here. Consider a particle with charge e that traverses a closed path $\mathcal{C}$ on the surface of the sphere surrounding the magnetic monopole. The path encloses a region Ω with area S_Ω. The phase shift $e^{i\gamma}$ experienced by the particle, as a result

of its motion in the presence of the gauge potential, is given by [23]

$$\begin{aligned} e^{i\gamma} &= \exp\Big(ie \oint_{\mathcal{C}} \boldsymbol{A}\cdot d\boldsymbol{x} \Big) \\ &= \exp\Big(ie \int_{\Omega} \boldsymbol{B}\cdot d\boldsymbol{S} \Big) \\ &= \exp\Big(ie \frac{g}{R^2} S_{\Omega} \Big) , \end{aligned} \tag{3.11}$$

where in the second equality we have used Stoke's theorem to convert the line integral into a surface integral, and we work in units of $\hbar = 1$. However, the path $\mathcal{C}$ also encloses the region Ω' which is the complement of Ω on the surface of the sphere. The area of this region is $S_{\Omega'} = 4\pi R^2 - S_{\Omega}$. Again using Stokes theorem, the phase shift is then given by

$$\begin{aligned} e^{i\gamma} &= \exp\Big(ie \oint_{\mathcal{C}} \boldsymbol{A}\cdot d\boldsymbol{x} \Big) \\ &= \exp\Big(-ie \int_{\Omega'} \boldsymbol{B}\cdot d\boldsymbol{S} \Big) \\ &= \exp\Big(-ie \frac{g}{R^2} (4\pi R^2 - S_{\Omega}) \Big) , \end{aligned} \tag{3.12}$$

where the minus sign is due to the surface Ω' having opposite orientation to Ω with respect to the path $\mathcal{C}$. As the phase shift $e^{i\gamma}$ is an observable quantity, consistency between (3.11) and (3.12) then requires that

$$\frac{eg}{R^2} S_{\Omega} + \frac{eg}{R^2} (4\pi R^2 - S_{\Omega}) = 2\pi n , \quad n \in \mathbb{Z} , \tag{3.13}$$

from which it follows that, in units of $e = 1$,

$$2g \in \mathbb{Z} . \tag{3.14}$$

This result is known as the *Dirac quantization condition* [41].

Returning to our problem, the Hamiltonian for the system (in units of $c = e = m = \hbar = 1$) is given by

$$\begin{aligned} H &= \frac{1}{2}(-i\nabla - A)^2 \\ &= -\frac{1}{2R^2 \sin\theta} \frac{\partial}{\partial\theta} \sin\theta \frac{\partial}{\partial\theta} + \frac{1}{2}\Big(-i \frac{1}{R\sin\theta} \frac{\partial}{\partial\phi} - g \frac{(1-\cos\theta)}{R\sin\theta} \Big)^2 \\ &= -\frac{1}{2R^2 \sin\theta} \frac{\partial}{\partial\theta} \sin\theta \frac{\partial}{\partial\theta} - \frac{1}{2R^2 \sin^2\theta} \frac{\partial^2}{\partial\phi^2} + \frac{ig}{R^2(1+\cos\theta)} \frac{\partial}{\partial\phi} + \frac{g^2}{2R^2} \Big(\frac{1-\cos\theta}{1+\cos\theta} \Big) , \end{aligned} \tag{3.15}$$

where we have restricted our particle motion to the surface of the sphere $r = R$.

We now perform a stereographic projection from the south pole of the sphere $(0, 0, -R)$ onto the complex plane tangent to the sphere at the north pole $(0, 0, R)$. Since the south pole itself is mapped to infinity under this transformation, we can think of excluding the south pole from our system, thus avoiding the aforementioned singularity of the Dirac string gauge at the south pole. This transformation is implemented via the coordinate transformation

$$z = \sqrt{\frac{B}{2}} 2R \tan\Big(\frac{\theta}{2}\Big) e^{i\phi} , \tag{3.16}$$

$$\bar{z} = \sqrt{\frac{B}{2}} 2R \tan\Big(\frac{\theta}{2}\Big) e^{-i\phi} . \tag{3.17}$$

Holomorophic and anti-holomorphic derivatives are then given by

$$\partial \equiv \frac{\partial}{\partial z} = \frac{1}{2R} \sqrt{\frac{2}{B}} e^{-i\phi} \left[\cos^2\Big(\frac{\theta}{2}\Big) \partial_\theta - \frac{i}{2} \cot\Big(\frac{\theta}{2}\Big) \partial_\phi \right] , \tag{3.18}$$

$$\bar{\partial} \equiv \frac{\partial}{\partial \bar{z}} = \frac{1}{2R} \sqrt{\frac{2}{B}} e^{i\phi} \left[\cos^2\Big(\frac{\theta}{2}\Big) \partial_\theta + \frac{i}{2} \cot\Big(\frac{\theta}{2}\Big) \partial_\phi \right] , \tag{3.19}$$

respectively.

Our Hamiltonian (3.15) in these coordinates is

$$H = B\bigg[-\Big(1+\frac{|z|^2}{2g}\Big)^2\partial\bar\partial - \frac{1}{2}\Big(1+\frac{|z|^2}{2g}\Big)(z\partial - \bar z\bar\partial) + \frac{|z|^2}{4}\bigg]\,. \tag{3.20}$$

Note what happens as we take the infinite radius limit $R\to\infty$ while keeping the magnetic field through the surface fixed. Since $B = g/R^2$, this requires $g\to\infty$. In this limit our Hamiltonian becomes

$$H \to B\Big(-\partial\bar\partial - \frac{1}{2}(z\partial - \bar z\bar\partial) + \frac{|z|^2}{4}\Big)\,, \tag{3.21}$$

which is precisely the full Hamiltonian for the planar system (2.19). We thus expect that as we proceed to solve for the eigenstates and energies of the spherical monopole system Hamiltonian (3.20) we should always recover the corresponding results for the planar system in the limit $g\to\infty$. We will hencforth refer to the limit $g\to\infty$ as the *planar limit*.

To determine the eigenstates for the spherical monopole system Hamiltonian (3.20) we proceed as we did for the planar system: we identify elements of the Hilbert space with the reduced wavefunction $\hat\Psi$, which are defined by factoring a measure factor out of the full eigenstates of (3.20)

$$\Psi(z,\bar z) \equiv \frac{1}{(1+|z|^2/2g)^g}\hat\Psi(z,\bar z)\,. \tag{3.22}$$

Note that the behaviour of the measure factor in the planar limit,

$$\lim_{g\to\infty}\frac{1}{(1+|z|^2/2g)^g} = e^{-|z|^2/2}\,, \tag{3.23}$$

recovers the measure factor for the planar system (2.22).

We define the Hilbert space inner product[1] as

$$\langle f|g\rangle \equiv \frac{2g+1}{4\pi i g}\int\frac{dzd\bar z}{(1+|z|^2/2g)^{2g+2}}\overline{f(z,\bar z)}g(z,\bar z)\,. \tag{3.24}$$

As before we must now work with reduced operators $\hat A$ which act directly on the Hilbert space, related to the full operators A by conjugation,

$$\hat A = \Big(1+\frac{|z|^2}{2g}\Big)^g A\Big(1+\frac{|z|^2}{2g}\Big)^{-g}\,. \tag{3.25}$$

The reduced Hamiltonian operator (3.20) is then

$$\hat H = B\Big[-\Big(1+\frac{|z|^2}{2g}\Big)^2\partial\bar\partial + \Big(1+\frac{|z|^2}{2g}\Big)\bar z\bar\partial + \frac{1}{2}\Big]\,, \tag{3.26}$$

which in the planar limit again reduces to the analogous result in the planar system (2.26).

The reduced angular momentum operator is

$$\hat J = z\partial - \bar z\bar\partial\,, \tag{3.27}$$

and can be written using (3.16) in our original spherical coordinates as

$$\hat J = -i\partial_\phi\,. \tag{3.28}$$

[1]The unusual measure is chosen here to ensure the correct orthogonality relations, as will become clearer when we consider normalisation in the next section.

Clearly J generates rotations about the x^3-axis on the sphere, or about the origin in the stereographical projection. Since $\hat{J}$ clearly commutes with the azimuthally symmetric $\hat{H}$ above, we now look for simultaneous eigenstates of energy and angular momentum. In the planar case we chose to express these eigenstates as $\hat{\Psi} = z^m P(|z|^2)$ in terms of some undetermined function P. However, noting that in terms of the coordinates (3.16) we have

$$|z|^2 = 2BR^2 \tan^2\Big(\frac{\theta}{2}\Big) = 2g\Big(\frac{1-\cos\theta}{1+\cos\theta}\Big) \quad \Rightarrow \quad \cos\theta = \frac{1-|z|^2/2g}{1+|z|^2/2g}\,, \tag{3.29}$$

we can choose to express P as a function of $\cos\theta$ instead,

$$\hat{\Psi} = z^m P\Big(\frac{1-|z|^2/2g}{1+|z|^2/2g}\Big)\,. \tag{3.30}$$

This will prove to be more convenient for our purposes. Clearly $\hat{\Psi}$ is again an angular momentum eigenstate, with angular momentum m. Requiring that $\hat{\Psi}$ also be an energy eigenstate allows us to impose the condition

$$\hat{H}\hat{\Psi} = E\hat{\Psi} \quad \Rightarrow \quad B\Big[-\Big(1+\frac{|z|^2}{2g}\Big)^2\partial\bar{\partial} + \Big(1+\frac{|z|^2}{2g}\Big)\bar{z}\bar{\partial} + \frac{1}{2}\Big]z^m P = Ez^m P\,, \tag{3.31}$$

which leads to the following differential equation for $P(x)$

$$(1-x^2)\frac{d^2P}{dx^2} + 2(g-j-(g+1)x)\frac{dP}{dx} + 2g\Big(\frac{E}{B}-\frac{1}{2}\Big)P = 0\,, \tag{3.32}$$

where we have defined $x \equiv \cos\theta$. We recognise this as having the form of a *Jacobi differential equation*

$$(1-x^2)f'' + (\beta-\alpha-(\alpha+\beta+2)x)f' + n(n+\alpha+\beta+1)f = 0\,, \tag{3.33}$$

which has as its regular solution on the interval $[-1,1]$ the *Jacobi polynomials*

$$P_n^{(\alpha,\beta)}(x) \equiv \frac{(-1)^n}{2^n n!}(1-x)^{-\alpha}(1-x)^{-\beta}\frac{d^n}{dx^n}\big[(1-x)^{\alpha+n}(1-x)^{\beta+n}\big] \tag{3.34}$$

$$= \frac{1}{2^n}\sum_{m=0}^{n}\binom{n+\alpha}{m}\binom{n+\beta}{n-m}(x-1)^{n-m}(x+1)^m\,. \tag{3.35}$$

which are defined for $\alpha, \beta \geq -n$. Comparing (3.32) with (3.33) we make the identifications

$$\alpha = m\,, \quad \beta = 2g-m\,, \tag{3.36}$$

$$E = B\Big(n+\frac{1}{2}+\frac{n(n+1)}{2g}\Big)\,. \tag{3.37}$$

Our reduced eigenstates are thus given by

$$\begin{aligned}\hat{\Psi}_n^m(g;z,\bar{z}) &= \mathcal{N}z^m P_n^{m,2g-m}\Big(\frac{1-|z|^2/2g}{1+|z|^2/2g}\Big)\\ E_{g,n} &= B\Big(n+\frac{1}{2}+\frac{n(n+1)}{2g}\Big)\\ n &= 0,1,2,...\\ m &= -n,-n+1,...,n+2g\,.\end{aligned} \tag{3.38}$$

Note the the Dirac quantization condition ensures that $2g$ is integer valued, while the conditions $\alpha, \beta \geq -n$ have led to the upper and lower bounds for m. As in the planar system the spectrum is independent of m, so we have degenerate Landau levels each labelled by the energy quantum number n. The n dependence of the energy is no longer linear as in the planar case, but has a quadratic part. As we would expect, in the planar limit $g \to \infty$ the quadratic part vanishes and the energy spectrum reduces to the planar result (2.38).

Using (3.38) and (3.22), we now write out the full unnormalised LLL eigenstates in the original spherical coordinates for future reference:

$$\Psi_0^m(\theta,\phi) = \tan^m\Big(\frac{\theta}{2}\Big)\cos^{2g}\Big(\frac{\theta}{2}\Big)e^{im\phi}\,. \tag{3.39}$$

Normalisation

$\mathcal{N}$ is a normalisation constant which can be determined by requiring that our reduced wavefunctions satisfy orthonormality with respect to the Hilbert space inner product (3.24),

$$\left\langle \hat{\Psi}_n^m \middle| \hat{\Psi}_{n'}^{m'} \right\rangle = \mathcal{N}^2 \frac{2g+1}{4\pi i g} \int \frac{dz d\bar{z}}{(1+|z|^2/2g)^{2g+2}} z^m \bar{z}^{m'} P_n^{(m,2g-m)}(x) P_{n'}^{(m',2g-m')}(x)\,, \tag{3.40}$$

where $x \equiv \frac{1-|z|^2/2g}{1+|z|^2/2g}$. Changing to complex polar coordinates (r,ϕ) yields

$$\begin{aligned}\left\langle \hat{\Psi}_n^m \middle| \hat{\Psi}_{n'}^{m'} \right\rangle &= \mathcal{N}^2 \frac{2g+1}{2\pi g} \int \frac{dr d\phi}{(1+r^2/2g)^{2g+2}} e^{i(m-m')\phi} r^{m+m'+1} P_n^{(m,2g-m)}(x) P_{n'}^{(m',2g-m')}(x) \\ &= \frac{2g+1}{g} \mathcal{N}^2 \delta_{m,m'} \int \frac{dr}{(1+r^2/2g)^{2g+2}} r^{2m+1} P_n^{(m,2g-m)}(x) P_{n'}^{(m,2g-m)}(x)\,, \end{aligned} \tag{3.41}$$

where in the second equality we have integrated over ϕ to obtain $2\pi\delta_{m,m'}$. Changing coordinates from r to $r^2 = |z|^2$, we obtain

$$\left\langle \hat{\Psi}_n^m \middle| \hat{\Psi}_{n'}^{m'} \right\rangle = \mathcal{N}^2 \frac{2g+1}{2g} \delta_{m,m'} \int \frac{d|z|^2}{(1+|z|^2/2g)^{2g+2}} |z|^{2m} P_n^{(m,2g-m)}(x) P_{n'}^{(m,2g-m)}(x)\,. \tag{3.42}$$

Consider now the following integral which expresses the orthogonality of the Jacobi polynomials on the interval $[-1,1]$ with respect to the weight $(1-x)^\alpha(1+x)^\beta$:

$$\int_1^{-1} dx (1-x)^\alpha (1+x)^\beta P_n^{(\alpha,\beta)}(x) P_{n'}^{(\alpha,\beta)}(x) = \delta_{n,n'} \frac{2^{\alpha+\beta}\Gamma(n+\alpha+1)\Gamma(n+\beta+1)}{n!(2n+\alpha+\beta+1)\Gamma(n+\alpha+\beta+1)}\,. \tag{3.43}$$

Implementing the change of variables $x = \frac{1-|z|^2/2g}{1+|z|^2/2g}$ and identifying $\alpha = m, \beta = 2g-m$ we find

$$(1-x)^\alpha (1+x)^\beta dx = \frac{2^{2g}}{g} \Big(\frac{1}{1+|z|^2/2g}\Big)^{2g+2} \Big(\frac{|z|^2}{2g}\Big)^m d|z|^2\,. \tag{3.44}$$

This allows us to rewrite (3.43) as

$$\frac{2^{2g-m}}{g^{m+1}} \int \frac{d|z|^2}{(1+|z|^2/2g)^{2g+2}} |z|^{2m} P_n^{(m,2g-m)}(x) P_{n'}^{(m,2g-m)}(x) = \delta_{n,n'} \frac{2^{2g}\Gamma(n+j+1)\Gamma(n+2g-j+1)}{n!(2n+2g+1)\Gamma(n+2g+1)}\,. \tag{3.45}$$

Comparison with (3.42) then fixes our normalisation to be

$$\mathcal{N} = \sqrt{\frac{n!(2n+2g+1)\Gamma(n+2g+1)}{(2g+1)(2g)^m \Gamma(n+m+1)\Gamma(n+2g-m+1)}}\,. \tag{3.46}$$

The wavefunctions (3.38) are now orthonormal with respect to both quantum numbers,

$$\left\langle \hat{\Psi}_n^m \middle| \hat{\Psi}_{n'}^{m'} \right\rangle = \delta_{m,m'}\delta_{n,n'}\,. \tag{3.47}$$

Degeneracy Counting

As in the planar system, degenerate states within a Landau level are distinguised by their angular momentum number m. The angular momentum has a lower bound of $-n$ as in the planar system, but now has the new feature of having an upper bound of $n+2g$ (note that as we would expect, this upper bound goes to infinity in the planar limit $g \to \infty$). Thus as opposed to the planar case where each Landau level is infinitely degenerate, the degeneracy for the spherical monopole system is finite.

The number of degenerate states per Landau level N is equal to the number of available momentum states, $N = 2g + 2n + 1$. The degeneracy per unit area is

$$\frac{N}{A} = \frac{2g+2n+1}{4\pi R^2} = \frac{B}{2\pi}\Big(1 + \frac{2n+1}{2g}\Big)\,, \tag{3.48}$$

where we have used $B = g/R^2$. In the planar limit, we recover our earlier standard planar result (2.73),

$$\frac{N}{A} = \frac{B}{2\pi}\,. \tag{3.49}$$

For the LLL, where $n = 0$, the number of available states is given by

$$N = 2g + 1 = 2BR^2 + 1 = \frac{AB}{2\pi} + 1 \tag{3.50}$$

$$= N_\phi + 1\,, \tag{3.51}$$

where as before $N_\phi = \Phi/\Phi_0$ denotes the number of flux quanta through the surface. Note that this differs by 1 from the planar degeneracy (2.72) result of $N = N_\phi$.

Comparison with Planar System

Let us now consider our results in comparison to the case of the planar system. We would expect that in the planar limit our states (3.38) reduce to the planar states (2.38). This is seen by considering the following limiting relation between Jacobi and Laguerre polynomials [17],

$$\lim_{\beta\to\infty} P_n^{(\alpha,\beta)}\Big(1 - \frac{2x}{\beta}\Big) = L_n^\alpha(x)\,. \tag{3.52}$$

Note that

$$\lim_{g\to\infty}\Big(\frac{1-|z|^2/2g}{1+|z|^2/2g}\Big) \approx 1 - \frac{|z|^2}{g}\,, \tag{3.53}$$

so, using the relation $\beta = 2g - m$,

$$\lim_{\beta\to\infty}\Big(\frac{1-|z|^2/2g}{1+|z|^2/2g}\Big) \approx 1 - \frac{2|z|^2}{\beta+m} \approx 1 - \frac{2|z|^2}{\beta}\,. \tag{3.54}$$

It follows that

$$\begin{aligned}\lim_{g\to\infty}\Big[z^m P_n^{(m,2g-m)}\Big(\frac{1-|z|^2/2g}{1+|z|^2/2g}\Big)\Big] &= z^m \lim_{\beta\to\infty} P_n^{(m,\beta)}\Big(1 - \frac{2|z|^2}{\beta}\Big) \\ &= z^m L_n^m(|z|^2)\,,\end{aligned} \tag{3.55}$$

where in the last equality we have used (3.52). As expected, our spherical monopole wavefunctions indeed reduce to the planar wavefunctions (2.38) in the limit $g \to \infty$.

3.2.2 Algebraic Approach

Single-Particle States

We now seek an algebraic formulation of the spherical monopole system, as we did for the planar system. Additionally we hope that in the planar limit $g \to \infty$, the algebraic formulation here will reduce to that of the planar system.

We begin by defining the differential operators [17]

$$\begin{aligned} L_+ &\equiv -\frac{1}{\sqrt{2g}} z^2\partial - \sqrt{2g}\bar\partial + \sqrt{g/2}\, z\,, \\ L_- &\equiv \sqrt{2g}\partial + \frac{1}{\sqrt{2g}}\bar z^2\bar\partial + \sqrt{g/2}\,\bar z\,, \\ L_3 &\equiv z\partial - \bar z\bar\partial - g\,. \end{aligned} \tag{3.56}$$

These can be shown to satisfy the commutation relations

$$\begin{aligned}[L_+, L_-] &= 2L_3\,,\\ [L_3, L_\pm] &= \pm L_\pm\,.\end{aligned} \tag{3.57}$$

These are just the commutation relations of the generators of the Lie algebra of $SU(2)$. We thus see that our differential operators furnish a representation of this Lie algebra. $L_{+/-}$ act as raising/lowering operators for the eigenvalue of L_3. Noting that the angular momentum operator J is given by

$$J = L_3 + g\,, \tag{3.58}$$

we see that $L_{+/-}$ are in fact raising/lowering operators for angular momentum, analogous to b and $b^\dagger$ in (2.46).

We rewrite the full Hamiltonian (3.20) as

$$\begin{aligned}H &= \frac{B}{2g}\Big(\frac{1}{2}(L_+L_- + L_-L_+) + L_3^2 - g^2\Big)\\ &= \frac{B}{2g}\Big(L_+L_- + L_3(L_3-1) - g^2\Big)\,,\end{aligned} \tag{3.59}$$

where in the second equality we have used (3.57). Note that, introducing the quadratic Casimir operator for $SU(2)$,

$$\mathbf{L}^2 = \frac{1}{2}(L_+L_- + L_-L_+) + L_3^2\,, \tag{3.60}$$

we can also write our Hamiltonian in the alternative form

$$H = \frac{B}{2g}\Big(\mathbf{L}^2 - g^2\Big)\,. \tag{3.61}$$

It is then clear that $L_{+/-}$ commutes with our Hamiltonian, so we expect to be able to act with these operators on any angular momentum state of a given energy to generate all other angular momentum states of that energy.

Finding simultaneous eigenstates for H and J entails simultaneously diagonalizing the operators L_+L_- and L_3. This can be done by finding the eigenstate Ψ_0 of lowest angular momentum, which must satisfy

$$L_-\Psi_0 = 0\,. \tag{3.62}$$

We expect that there will be one such lowest angular momentum state in each Landau level. It can be simply verified that regular solutions to (3.62) are given by

$$\Psi_0 = \frac{\bar{z}^n}{(1+|z|^2/2g)^{g+n}}\,, \quad n = 0, 1, 2, ... \tag{3.63}$$

We can compare these states to the states of lowest angular momentum $m = -n$ found previously using the analytic approach (2.38), given by

$$\hat{\Psi}_n^{-n} = z^{-n} P_n^{(-n,2g+n)}\Big(\frac{1-|z|^2/2g}{1+|z|^2/2g}\Big)\,, \tag{3.64}$$

where we have ignored the normalisation constant for simplicity. Using the explicit form of the Jacobi polynomials (3.35), we find

$$P_n^{(-n,2g+n)}(x) = \frac{1}{2^n}\sum_{m=0}^{n}\binom{0}{m}\binom{2n+2g}{n-m}(x-1)^{n-m}(x+1)^m \tag{3.65}$$

$$= \frac{1}{2^n}\binom{2n+2g}{n}(x-1)^n\,, \tag{3.66}$$

where the $\binom{0}{m}$ factor in the first line ensures that only the $m = 0$ term will contribute in the sum. Substituting in $x = \frac{1-|z|^2/2g}{1+|z|^2/2g}$ and simplifying, we find

$$\hat{\Psi}_n^{-n} \propto z^{-n} \frac{|z|^{2n}}{(1+|z|^2/2g)^n}\,, \tag{3.67}$$

where we have ignored all constant prefactors. Finally, we include the measure factor to obtain the full states

$$\Psi_n^{-n} = \frac{\hat{\Psi}_n^{-n}}{(1+|z|^2/2g)} \propto \frac{\bar{z}^n}{(1+|z|^2/2g)^{g+n}}\,. \tag{3.68}$$

These are precisely the states (3.63) found using our algebraic approach. We thus identify the state of lowest angular momentum Ψ_0 in Landau level n with Ψ_n^{-n}.

We can also find an explicit expression for the spectrum. Having verified that the lowest angular momentum state Ψ_0 has angular momentum $j = -n$, it follows that

$$L_3\Psi_0 = (J-g)\Psi_0 = (-n-g)\Psi_0\,. \tag{3.69}$$

Therefore

$$\begin{aligned} H\Psi_0 &= \frac{B}{2g}\Big(L_+L_- + L_3(L_3-1) - g^2\Big)\Psi_0 \\ &= \frac{B}{2g}\Big(0 + (-n-g)(-n-g-1) - g^2\Big)\Psi_0 \\ &\Rightarrow E_{g,n} = B\Big(n + \frac{1}{2} + \frac{n(n+1)}{2g}\Big)\,, \end{aligned} \tag{3.70}$$

which agrees with the energy spectrum (3.38) found using the analytic approach. Note that since each Landau level is degenerate in energy, finding the energy of the state of lowest angular momentum is sufficient to determine the energy of every state in the Landua level.

As mentioned above, all other states in Landau level n can be obtained by acting on $\Psi_0 = \Psi_n^{-n}$ with the raising operator L_+. Noting that

$$(L_+)^{2g+2n+1} \frac{\bar{z}^n}{(1+|z|^2/2g)^{g+n}} = 0\,, \tag{3.71}$$

we recover the earlier result that each Landau level a finite degeneracy of $2g + 2n + 1$.

We have so far considered full operators acting on full eigenstates, as opposed to Hilbert space operators acting on the reduced wavefunctions. Using the prescription (3.25) we find these Hilbert space operators to be given by

$$\begin{aligned} \hat{\mathcal{L}}_+ &= -\frac{z^2}{2g}\partial - \bar{\partial} + z\,, \\ \hat{\mathcal{L}}_- &= \partial + \frac{\bar{z}^2}{2g}\bar{\partial}\,, \\ \hat{\mathcal{L}}_3 &= \mathcal{L}_3\,. \end{aligned} \tag{3.72}$$

It can be verified that $\hat{\mathcal{L}}_+$ and $\hat{\mathcal{L}}_-$ are adjoints with respect to the Hilbert space inner product (3.24), whilst $\hat{\mathcal{L}}_3$ is self-adjoint.

The difference and differential-difference relations for the Jacobi polynomials in Appendix A can be used to verify the following actions of our operators on the wavefunctions

$$\hat{\mathcal{L}}_+(\hat{\Psi}_n^m) = \sqrt{(2g+n-j)(j+n+1)/2g}(\hat{\Psi}_n^{m+1}) \tag{3.73}$$

$$\hat{\mathcal{L}}_-(\hat{\Psi}_n^m) = \sqrt{(2g+n-j+1)(j+n)/2g}(\hat{\Psi}_n^{m-1}) \tag{3.74}$$

$$\hat{\mathcal{L}}_3(\hat{\Psi}_n^m) = \Big(\frac{j-g}{g}\Big)(\hat{\Psi}_n^m) \tag{3.75}$$

confirming the $\hat{\mathcal{L}}_\pm$ operators as step operators for angular momentum.

Comparison with Planar System

Let us now investigate the relationship between the algebraic formulation of the spherical monopole system and that of the planar system. Rescaling our generators (3.56) as

$$\begin{aligned}\mathcal{L}_+ &\equiv \frac{1}{\sqrt{2g}}L_+ = -z^2\partial - \bar{\partial} + \frac{1}{2}z\,,\\ \mathcal{L}_- &\equiv \frac{1}{\sqrt{2g}}L_- = \partial + \frac{1}{2g}\bar{z}^2\bar{\partial} + \frac{1}{2}\bar{z}\,,\\ \mathcal{L}_3 &\equiv \frac{1}{g}L_3 = \frac{1}{g}(z\partial - \bar{z}\bar{\partial}) - 1\,,\end{aligned} \tag{3.76}$$

the commutation relations (3.57) are now

$$\begin{aligned}[\mathcal{L}_+, \mathcal{L}_-] &= \mathcal{L}_3\,,\\ [\mathcal{L}_3, \mathcal{L}_\pm] &= \pm\frac{1}{g}\mathcal{L}_\pm\,,\end{aligned} \tag{3.77}$$

whilst our Hamiltonian (3.59) becomes

$$\begin{aligned}H &= B\Big(\mathcal{L}_+\mathcal{L}_- + \frac{1}{2}\mathcal{L}_3(g\mathcal{L}_3 - 1) - \frac{g}{2}\Big)\\ &= B\Big(\mathcal{L}_+\mathcal{L}_- - J + \frac{1}{2} + \frac{1}{2g}J(J-1)\Big)\,.\end{aligned} \tag{3.78}$$

In the planar limit, our rescaled operators reduce to

$$\begin{aligned}\mathcal{L}_+ &\to b^\dagger\,,\\ \mathcal{L}_- &\to b\,,\\ \mathcal{L}_3 &\to -1\,.\end{aligned} \tag{3.79}$$

which are, as we would expect, the momentum raising and lowering operators for the planar system. The commutation relations (3.77) reduce to

$$\begin{aligned}[b, b^\dagger] &= 1\,,\\ [1, b] = [1, b^\dagger] &= 0\,.\end{aligned} \tag{3.80}$$

The second of these is trivial, whilst the first is the commutation relation for the angular momentum raising and lowering operators in the planar system. We thus see that the relation of the spherical monopole system to the planar system is, in group theoretic terms, one of contraction of Lie algebras [33]: the $SU(2)$ commutation relations (3.77) contract to the Heisenberg algebra commutation relations (2.47).

The Hamiltonian reduces to

$$\begin{aligned}H &= B\Big(b^\dagger b - J + \frac{1}{2}\Big)\\ &= B\Big(a^\dagger a + \frac{1}{2}\Big)\,,\end{aligned} \tag{3.81}$$

where in the second equality we have used (2.49). This is the planar system Hamiltonian (2.48). We note here that since the quantum number associated with energy n appears in the energy spectrum nonlinearly, it is tricky to define analogues of the energy raising and lowering operators $a^\dagger$ and a, and we will not be attempting to do so here[2].

[2]See [32] for a formulation of energy raising and lowering operators for the spherical monopole system.

3.2.3 Wavefunctions

Having solved for the full single particle state Hilbert space, we now proceed to plot some representative wavefunctions to better understand the spherical monopole system.

We first rewrite our solutions (3.38) as full solutions by restoring the exponential measure factor and changing to the original spherical coordinates on the sphere

$$\begin{aligned}
\Psi_n^m(g;\theta,\phi) &= \mathcal{N}(2g)^{m/2}\tan^m\left(\frac{\theta}{2}\right)\cos^{2g}\left(\frac{\theta}{2}\right)P_n^{m,2g-m}(\cos\theta)e^{im\phi} \\
&\equiv \psi_n^m(g;\theta)e^{im\phi} \\
E_{g,n} &= B\Big(n+\frac{1}{2}+\frac{n(n+1)}{2g}\Big) \\
n &= 0,1,2,... \\
m &= -n,-n+1,...,n+2g
\end{aligned} \tag{3.82}$$

where the normalisation constant $\mathcal{N}$ is given by (3.46). In the following we will plot $\psi_n^m(g;\theta,\phi)$ against θ, ignoring the ϕ dependence which is not relevant to the probability distributions $|\Psi_n^m(\theta,\phi)|^2 = |\psi_n^m(\theta)|^2$ of the eigenstates.

Note that our states are independent of the radius R of the sphere and depend only on the monopole strength g. The energy spectrum on the other hand, depends on the magnetic field strength B at the sphere's surface. Equivalently, for fixed monopole strength g, the spacing between our Landau levels goes as the inverse square of the radius R.

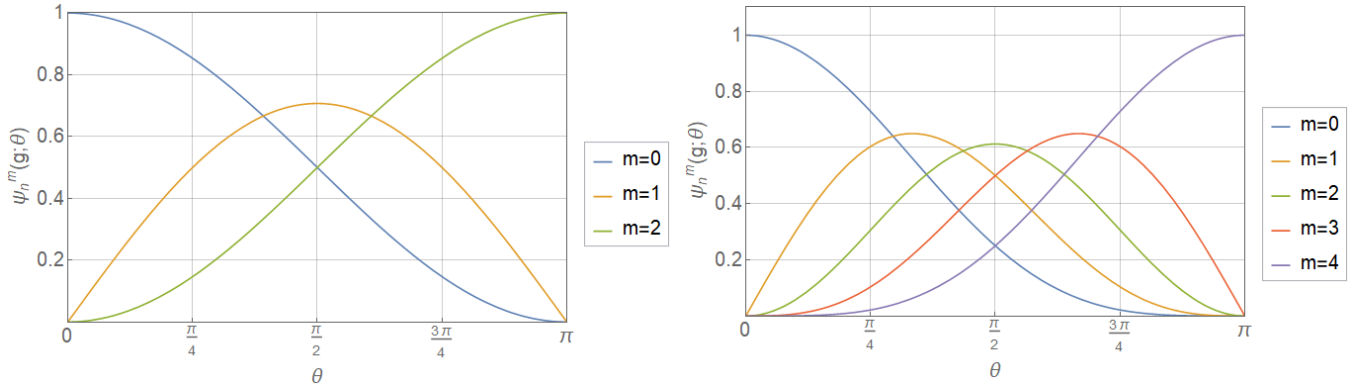

(a) $g = 1$ (b) $g = 2$

Figure 3.2: $\psi_n^m(g;\theta)$ for $n = 0$ and various m and g.

We first plot a selection of LLL states in Figure 3.2. Note that m takes integer values $0 \leq m \leq 2g$, where $2g$ must take integer values by the Dirac quantization condition. As in the planar system, all LLL states have no nodes. For any value of g, the $m = 0$ state is peaked at the north pole $\theta = 0$ and smoothly decays to zero as θ increases. As m increases, the states become peaked at larger values of θ, smoothly decaying to zero on both sides. For $g \in \mathbb{Z}$, the $m = g$ state is always peaked at the equator $\theta = \pi/2$. The $m > g$ states are then simply reflections about the equator of their counterparts with angular momentum $m - g$.

Note that, as in the planar system, the decay of the LLL states around the peak is faster for larger g, meaning that larger g states are more sharply localised (with respect to the polar angle) on the sphere. This behaviour holds for states in all Landau levels.

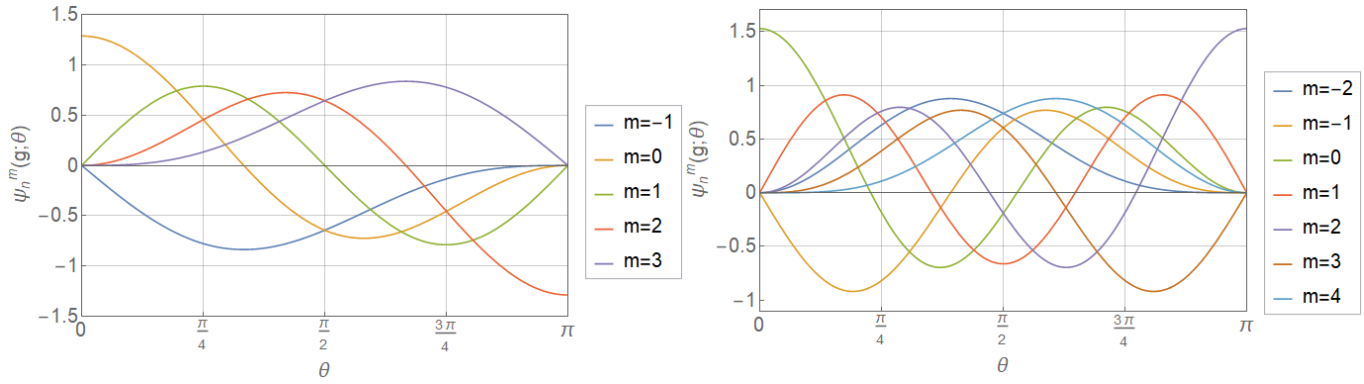

(a) $n = 1$

(b) $n = 2$

Figure 3.3: $\psi_n^m(g;\theta)$ for $g = 1$ and various m and n.

We now plot higher Landau level states $n > 0$ in Figure 3.3, where the angular momentum now takes integer values $-n \leq m \leq n + 2g$. The highest and lowest m states always have no nodes. For n even, states with $m > g$ are reflections about the equator of their counterparts with angular momentum $m - g$ (see Figure 3.3a). For n odd, the $m > g$ states are the negative of the reflection about the equator of their counterparts with angular momentum $m - g$ (see Figure 3.3b). Figure 3.4 illustrates that higher energy states are less spatially localised than their counterparts with the same m in lower Landau levels, as intuition would suggest (see the similarities with the $m = 0$ planar states in Figure 2.2a).

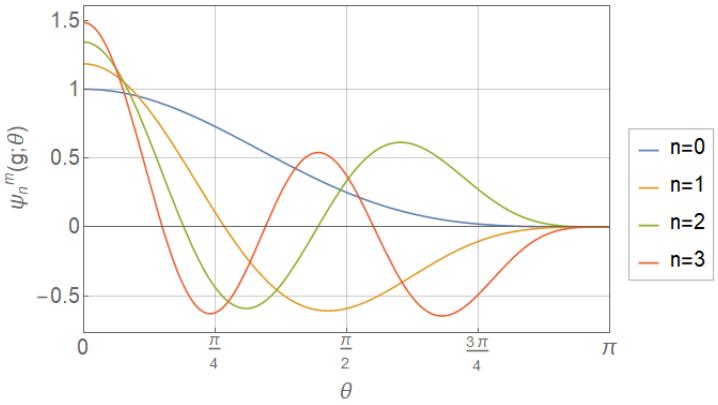

Figure 3.4: $\psi_n^m(g;\theta)$ for $g = 2, m = 0$ and various n.

Chapter 4

The General Framework

In this Chapter we present the framework, also developed in [17], for treating the general system of charged particles constrained to the surface of any two-dimensional Kähler manifold in a constant, perpendicular magnetic field. Our results for the planar and spherical monopole system then emerge as special cases of this general framework. Following [4], we then extend this framework to allow us to solve for the lowest Landau level states on a two dimensional compact Kähler manifold in the case of a *non-constant, non-perpendicular* magnetic field.

4.1 Single-Particle States

We work in isothermal complex coordinates $z = x_1 + ix_2$, $\bar{z} = x_1 - ix_2$ with holomorphic and anti-holomorphic derivatives $\partial = \frac{1}{2}(\partial_1 - i\partial_2)$ and $\bar{\partial} = \frac{1}{2}(\partial_1 + i\partial_2)$ respectively. Our particle will be confined to a Riemann surface with line element

$$ds^2 = g_{z\bar{z}} dz d\bar{z} \equiv \sqrt{g} dz d\bar{z} \,. \tag{4.1}$$

The volume form is given by

$$dV = \frac{\sqrt{g}}{2i} dz \wedge d\bar{z} \,, \tag{4.2}$$

while the Ricci scalar curvature is

$$\mathrm{Ric} = -\Delta_g \log \sqrt{g} \,, \tag{4.3}$$

where we have defined the Laplace-Beltrami operator

$$\Delta_g \equiv \frac{4}{\sqrt{g}} \partial\bar{\partial} \,. \tag{4.4}$$

In the cases of interest to us, the metric of the surface may be expressible in terms of a Kähler potential K, defined via

$$\partial\bar{\partial} K = \sqrt{g} \,. \tag{4.5}$$

To define the magnetic field in which our particle moves, we need some notion of *orthogonality* in the intrinsically two-dimensional geometric framework we are working in. To this end, the most natural definition of the constant, perpendicular gauge field is a field strength two-form which is proportional to the volume form [9]

$$F = B dV \,. \tag{4.6}$$

We also know the gauge field can be written in terms of the gauge potential

$$F = (\partial \bar{A} - \bar{\partial} A) dz \wedge d\bar{z} \,, \tag{4.7}$$

where in complex coordinates our gauge potential has holomorphic and anti-holomorphic components $A \equiv A_z$ and $\bar{A} \equiv A_{\bar{z}}$ respectively. It follows that

$$\partial \bar{A} - \bar{\partial} A = i\sqrt{g} B/2 \,. \tag{4.8}$$

Choosing to work in *covariant Coulomb gauge*,

$$\bar{\partial}A + \partial\bar{A} = 0\,, \tag{4.9}$$

we can rewrite (4.8) as

$$B = \frac{4i}{\sqrt{g}}\bar{\partial}A\,. \tag{4.10}$$

We now introduce a real *magnetic potential* Q defined by

$$i\hbar\partial Q = 2eA\,, \qquad -i\hbar\bar{\partial}Q = 2e\bar{A}\,. \tag{4.11}$$

Combining (4.12) with (4.10) we arrive at the following differential equation for Q

$$\Delta_g Q \equiv \frac{4}{\sqrt{g}}\partial\bar{\partial}Q = -\frac{2eB}{\hbar}\,. \tag{4.12}$$

In the case of a constant magnetic flux density through the surface (constant B), it is easily verified that the magnetic potential Q can be chosen to be proportional to the Kähler potential of the surface

$$Q = -\frac{K}{2l^2}\,, \tag{4.13}$$

where $l \equiv \sqrt{\hbar/eB}$ is the magnetic length.

With all geometric objects defined, we now turn to the physics. The Pauli Hamiltonian for spin polarized electrons appropriate for modelling free electrons on a Riemann surface [9] is

$$H = \frac{1}{2m}\Big(\frac{1}{\sqrt{g}}\pi_i\sqrt{g}g^{ij}\pi_j - \frac{g_s}{2}e\hbar B\Big)\,, \tag{4.14}$$

where $\pi_i = -i\hbar\partial_i - eA_i$ is the kinetic momentum with $i,j = 1,2$, and g_s is the Landè g-factor. Changing to complex coordinates and using the commutation relations[1]

$$[\bar{\pi},\pi] = \sqrt{g}\frac{e\hbar B}{2}\,, \tag{4.15}$$

yields

$$H = \frac{2}{m}\Big(\frac{1}{\sqrt{g}}\pi\bar{\pi} + \frac{2-g_s}{8}e\hbar B\Big)\,, \tag{4.16}$$

where

$$\pi = -i\hbar\partial - eA\,, \qquad \bar{\pi} = -i\hbar\bar{\partial} - e\bar{A}\,, \tag{4.17}$$

are the holomorphic and anti-holomorphic components of the momentum respectively.

4.1.1 Uniform Magnetic Flux

We now seek to make contact with our earlier descriptions of the planar and spherical monopole systems. Setting $\hbar = m = e = 1$ and restricting our attention to the case of uniform magnetic flux, where B is constant and (4.13) holds, the Hamiltonian (4.16) can be written as

$$H = -\frac{2}{\partial\bar{\partial}K}\Big(\partial - \frac{1}{4l^2}\partial K\Big)\Big(\bar{\partial} + \frac{1}{4l^2}\bar{\partial}K\Big) + \frac{2-g_s}{4}B\,, \tag{4.18}$$

[1] These are the appropriate generalisation of the commutation relations in flat space given by (2.14).

where we have used (4.11). For $g_s = 2$, this is precisely the form of our Hamiltonian for the planar (2.19) and spherical monopole (3.20) systems, under a rescaling of coordinates by $\sqrt{2/B}$ (to match with our earlier coordinate choice (2.17)) and once substituted in for the respective Kähler potentials of the plane and the sphere

$$K = \begin{cases} |z|^2 & \text{plane} \\ 4R^2 \log\big(1 + |z|^2/4R^2\big) & \text{sphere of radius } R. \end{cases} \tag{4.19}$$

Given the form of the Hamiltonian (4.18), it is natural to redefine our wavefunctions as

$$\psi(z, \bar{z}) = e^{-K/4l^2} \hat{\psi}(z, \bar{z}) \,. \tag{4.20}$$

The $\hat{\psi}$'s are now our Hilbert space elements, with inner product

$$\langle f|g\rangle = \mathcal{N} \int dV e^{-K/2l^2} \overline{f(z,\bar{z})} g(z, \bar{z}) \,, \tag{4.21}$$

which is the appropriate generalisation of the inner products (2.23) and (3.24). $\mathcal{N}$ is chosen such that $\langle 1|1\rangle = 1$. This motivates our seemingly arbitrary Hilbert space element definitions (2.22) and (3.22), which after a rescaling of coordinates by $\sqrt{2/B}$ are of precisely the form (4.20).

The reduced Hamiltonian corresponding to (4.18) is then given by

$$\begin{aligned} \hat{H} &= e^{K/4l^2} H e^{-K/4l^2} \\ &= -\frac{2}{\partial\bar{\partial}K}\Big(\partial - \frac{1}{2l^2}\partial K\Big)\bar{\partial} + \frac{2 - g_s}{4} B \,. \end{aligned} \tag{4.22}$$

Our treatment here has been general and applies to any system of charged particles confined to a two-dimensional Kähler Riemann surface in a constant and perpendicular magnetic field. Clearly any holomorphic function will be annihilated by the first term in the Hamiltonian (4.22). Restricting now to the particular case where $g_s = 2$, such states will all be degenerate with energy $B/2$, and will constitute a lowest Landau level. The full LLL states in such a case will be given by

$$\psi_{LLL,m}(z, \bar{z}) = s_m(z) e^{-K/4l^2} \,, \tag{4.23}$$

where the holomorphic functions $\{s_m\}$ satisfy $\bar{\partial} s_m = 0$ such that ψ_m is normalisable under the inner product (4.21)

$$\langle \psi_n | \psi_m \rangle \equiv \int s_n \bar{s}_m e^{-K/2l^2} dV = \delta_{mn} \,. \tag{4.24}$$

Note that the form of the exponential measure factor of our LLL states is entirely determined by the underlying geometry of the Riemann surface (via the Kähler potential). In the mathematical literature, $\{s_n\}$ are called sections of the holomorphic line bundle equipped with the hermitian metric $e^{-K/2l^2}$. Holomorphic sections defined in the conformal class of a sphere are polynomials, whose degree cannot exceed N_ϕ [4]. It follows from the Riemann-Roch theorem [9] that the number of such holomorphic sections on a manifold of genus G is given by

$$N = N_\phi - G + 1 \,. \tag{4.25}$$

Our result for the degeneracy of the LLL on the sphere (3.50) follows from this formula by setting $G = 0$ as appropriate for the sphere.

Any $N_\phi + 1$ linearly independent holomorphic polynomials of degree less that N_ϕ will thus constitute a basis for the LLL. The simplest choice is

$$s_m(z) = z^m \quad \text{where} \quad m = 0, 1, ..., N_\phi \,, \tag{4.26}$$

which coincides with the angular momentum eigenstates we have been working with thus far.

Any Kähler Riemann surface which additionally possesses azimuthal rotational symmetry will have a Kähler potential depending only on $|z|^2$. In such a case, the angular momentum operator $J = z\partial - \bar{z}\bar{\partial}$ commutes with the reduced Hamiltonian (4.22). We may therefore look for simultaneous eigenstates of the form

$$\hat{\psi} = z^m P(|z|^2)\,. \tag{4.27}$$

Imposing that this state be an energy eigenstate leads to the following differential equation for P

$$\Big(\frac{x}{K' + xK''}\Big)P'' + \frac{(m+1-x)K'}{(K'+xK'')}P' + \Big(\frac{E}{B} - \frac{1}{2}\Big)P = 0\,, \tag{4.28}$$

where $x \equiv |z|^2$ and primes denote derivatives with respect to x. For choices of K for which this differential equation is solvable for P, we here have a prescription for finding the higher Landau level states. Indeed, substituting in for the Kähler potentials of the plane (4.19) yields the Laguerre equation of the planar system (2.33). Substituting in the Kähler potentials of the sphere (4.19) and redefining the argument of P appropriately yields the Jacobi equation of the spherical monopole system (3.33)[2].

4.1.2 Non-Uniform Magnetic Flux

We now turn to the more general case in which the magnetic field through the surface is non-uniform (non-constant and/or non-perpendicular). We assume small variations over a large constant background [4]. Due to the term proportional to $B = B(z, \bar{z})$ in the Hamiltonian (4.16), the degeneracy of the LLL is broken for general g_s. However, for $g_s = 2$, the degeneracy remains and the LLL eigenstates states then satisfy [26]

$$\bar{\pi}\psi = 0\,, \tag{4.29}$$

as before. The solutions are now given by

$$\psi_m(z, \bar{z}) = s_m(z)e^{Q/2}\,, \tag{4.30}$$

where Q is the magnetic potential satifsying (4.12) and the holomorphic functions s_m satisfy $\bar{\partial}s_m = 0$ such that ψ_m is normalisable under the inner product

$$\langle\psi_n|\psi_m\rangle \equiv \int s_n\bar{s}_m e^Q dV \tag{4.31}$$

Note that the magnetic potential Q appears here instead of the Kähler potential K because the two are not necessarily proportional in the case of non-uniform magnetic flux. The maximal degeneracy is still

$$N = N_\phi + 1\,. \tag{4.32}$$

For an LLL basis of states we choose $s_m(z) = z^m$ where $m = 0, 1, ..., N_\phi$.

4.1.3 Zero Flux Case

We now wish to consider a particular case of the above class of systems, in which there is a vanishing net flux ($\Phi = 0$) through our compact Riemann surface. We follow the treatment given in [25] and prove that in such a case there is either a unique LLL state, or none.

We know that for the case of $g_s = 2$, the LLL states are solutions of

$$\bar{\pi}\psi = -i\hbar\bar{\partial}\psi - e\bar{A}\psi = 0\,. \tag{4.33}$$

Suppose that another state ψ' solves this equation for the same vector potential A. It necessarily follows that

$$\psi' = f(z)\psi\,. \tag{4.34}$$

However, the only holomorphic functions $f(z)$ on a compact surface are constant functions. In this case ψ and ψ' are identical up to normalisation, and we are done.

[2] See [17] for the application of this framework to the *hyperbolic monopole* system.

It is however possible that f could have a pole at some point z_0 if ψ has a zero at z_0 to compensate. We rule this case out as follows. We know that $\psi = g(z)e^{Q/2}$ for some holomorphic function $g(z)$. Since the exponential factor has no zeros, it follows that any zero of ψ is necessarily a zero of the holomorphic function, and therefore has the form $(z - z_0)^p$. We now use a formula [25] expressing the magnetic flux Φ in terms of the zeros z_{0i} of ψ and their orders p_i:

$$\Phi = 2\pi \sum_i p_i \tag{4.35}$$

where the summation is over all zeros. In our case where $\Phi = 0$, it follows that $p_i = 0$ for all i. Thus ψ can have no zeros.

We have thus shown that in the case where $g_s = 2$ and the net flux through our surface vanishes, there is either a unique LLL state, or none.

4.2 Multi-Particle States

Up until this point we have only considered single-particle states. We now give a prescription for constructing the multi-particle ground states in terms of our single-particle eigenstates.

To construct the N_p-particle ground state wavefunction for free fermions, we take the Slater determinant of the single particle states [24],

$$\Psi(\xi_1, ..., \xi_{N_p}) = \frac{1}{\sqrt{N!}} e^{-\sum_i^{N_p} K(\xi_i)/4l^2} \det[s_m(z_i)]\,, \tag{4.36}$$

where N_p cannot exceed the maximal degeneracy N, and $\xi_i = (z_i, \bar{z}_i)$ is used to indicate that the argument is not holomorphic. For a fully filled Landau level, the Vandermonde identity implies that

$$\det[s_m(z_i)] = \mathcal{N}\sqrt{N!} \prod_{i<j}^{N} (z_i - z_j)\,, \tag{4.37}$$

which is valid for spherical, conical and planar geometries [4]. The maximally degenerate N-particle state is then given by

$$\Psi = \mathcal{N} \prod_{i<j}^{N} (z_i - z_j) e^{-\frac{1}{4l^2}\sum_i^{N_p} K(\xi_i)}\,, \tag{4.38}$$

where $\mathcal{N}$ is chosen such that $\langle\Psi|\Psi\rangle = 1$.

In the non-uniform magnetic flux case, The N-particle state is given by

$$\Psi = \mathcal{N} \prod_{i<j}^{N} (z_i - z_j) e^{\frac{1}{2}\sum_i Q(\xi_i)} \tag{4.39}$$

where $\mathcal{N}$ is chosen such that $\langle\Psi|\Psi\rangle = 1$.

Chapter 5

The 'Squashed Sphere' System

In this chapter we will be considering a variant of the spherical monopole system in which the sphere is 'squashed' into a spheroid. We will consider two cases of the field configuration: firstly, where the monopole field is deformed along with the sphere so as to remain perpendicular to the surface of the resultant spheroid; and secondly, where a background monopole-like field $\vec{B} = B_0\hat{r}$ remains static as the sphere is deformed. Although neither of these cases are equivalent to studying the more difficult problem of squashing the sphere in the presence of a static background monopole field, they better suit the purpose of applying the framework developed in Chapter 4 to see what we can learn about the effects that perturbing the geometry of the system has on the LLL states, as well as the difference between the uniform and non-uniform flux cases. That will be our aim here.

We begin by deriving the conformal map from the spheroid to the sphere, as required for the application of the general framework outlined in Chapter 4. We then apply the framework and derive a perturbative result for the single particle LLL states in both cases. Finally, we compare the two results and analyse the effect of 'squashing' on the states. The work presented in this chapter is original, but has not been submitted for publication elsewhere.

5.1 Application of the General Framework

We now outline the strategy for finding the LLL states for surfaces whose metrics are conformally related to that of the sphere of radius R with metric

$$\sqrt{g_0} = \frac{1}{(1+|z|^2/4R^2)^2}\,, \tag{5.1}$$

and Kähler potential

$$K_0 = 4R^2\log\big(1+|z|^2/4R^2\big)\,. \tag{5.2}$$

This metric corresponds to the standard stereographic projection from the north pole of the sphere onto the complex plane tangent to the sphere at the south pole[1]. The corresponding line element in polar coordinates is

$$ds^2_{sphere} = \frac{1}{(1+r^2/4R^2)^2}(dr^2 + r^2 d\phi^2)\,. \tag{5.3}$$

A metric $\sqrt{g}$ with Kähler potential K is said to be conformally related to the metric $\sqrt{g_0}$ if

$$\sqrt{g} = e^{2\sigma}\sqrt{g_0}\,, \tag{5.4}$$

for some conformal factor $e^{2\sigma}$ which will in general be a function of coordinates. The Kähler potentials of the two metrics are then related by

$$K = K_0 + u\,. \tag{5.5}$$

[1]Note that for the spherical monopole system we stereographically projected from the north pole, not the south pole. Our results here will thus be related to our results in Chapter 3.2 by the transformation $\theta \to \pi - \theta$.

where the *deformed* part of the Kahler potential u satisfies

$$\Delta_0 u \equiv \frac{4}{\sqrt{g_0}}\partial\bar{\partial}u = 2(e^{2\sigma}-1)\,. \tag{5.6}$$

In the uniform field case, a basis for the LLL eigenstates on the surface with metric $\sqrt{g}$ is then given by

$$\psi_m(z,\bar{z}) = z^m e^{-(K_0+u)/4l^2}, \quad m = 0,1,...,N_\phi\,. \tag{5.7}$$

Note that in the limit $u \to 0$ these states reduce to the LLL states in the spherical monopole system.

In the non-uniform field case, the LLL eigenstates are given as before by

$$\psi_m(z,\bar{z}) = z^m e^{Q/2}, \quad m = 0,1,...,N_\phi\,, \tag{5.8}$$

where Q satisfies (4.12).

We now seek to write down the LLL states on the surface of the oblate spheroid, referred to as the 'squashed sphere'. This requires us to write down the conformal factor relating the metric of the spheroid to that of the sphere, and solve (5.6) to find the Kähler potential of the spheroid, from which we can calculate the LLL states via the above prescriptions (5.7) and (5.8).

Conformal Map from the Spheroid to the Sphere

We begin by constructing the conformal factor. We know that the metric of the sphere g^S_{ab} of radius R and that of the plane g^P_{ab} are related via stereographic projection as

$$g^S_{ab}(r,\phi) = \frac{1}{(1+r^2/4R^2)^2} g^P_{ab}(r,\phi)\,, \tag{5.9}$$

where

$$g^P_{ab}(r,\phi) = \begin{bmatrix} 1 & 0 \\ 0 & r^2 \end{bmatrix} \tag{5.10}$$

is the usual metric of the plane in polar coordinates and our stereographic projection is given by

$$r(\theta) = 2R\cot(\theta/2)\,, \tag{5.11}$$

where $0 < \theta < \pi$ is the polar angle on the sphere.

We now seek the conformal factor relating the metric of the spheroid g^E_{ab} to that of the plane. The spheroid is defined in three-dimensional Cartesian coordinates by

$$\frac{x^2+y^2}{a^2} + \frac{z^2}{b^2} = 1\,, \tag{5.12}$$

where a and b are the equatorial and polar radii respectively. The parametric equations are

$$\begin{aligned} x &= a\sin\theta\cos\psi\,, \\ y &= a\sin\theta\sin\psi\,, \\ z &= b\cos\theta\,, \end{aligned} \tag{5.13}$$

where $0 \le \theta \le \pi$ is the polar angle and $0 < \psi \le 2\pi$ is the azimuthal angle. The line element is given by

$$ds^2_E = (a^2\cos^2\theta + b^2\sin^2\theta)d\theta^2 + a^2\sin^2\theta d\psi^2\,. \tag{5.14}$$

We now consider the following coordinate transformation [10] derived in Appendix B[2]:

$$r(\theta) = 2Re^{-h(\theta)}\,, \qquad \phi(\psi) = \psi\,, \tag{5.15}$$

where

$$h(\theta) = \int_{\pi/2}^{\theta} \sqrt{\Big(\frac{b}{a}\Big)^2 + \cot^2 v}\, dv\,. \tag{5.16}$$

It follows that

$$\begin{aligned} \frac{dr}{d\theta} &= -2Re^{-h}\frac{dh}{d\theta} \\ \Rightarrow dr^2 &= 4R^2e^{-2h}\big[(b/a)^2 + \cot^2\theta\big]d\theta^2\,, \end{aligned} \tag{5.17}$$

allowing us to rewrite the spheroidal line element (5.14) as

$$ds_E^2 = \Big(\frac{a}{r}\sin\theta\Big)^2\big(dr^2 + r^2 d\phi^2\big)\,, \tag{5.18}$$

where we bear in mind that r here is given by $r(\theta) = 2Re^{-h(\theta)}$. We thus recognise the coordinate transformation (5.15) as conformally mapping the spheroid of equatorial radius a and polar radius b to the plane.

The metric of the spheroid g^E_{ab} and the metric of the plane g^P_{ab} are then related by

$$g^E_{ab}(r,\phi) = \Big(\frac{a}{r}\sin\theta\Big)^2 g^P_{ab}(r,\phi)\,. \tag{5.19}$$

Note that this metric transformation from the plane to the spheroid should have the metric transformation from the plane to the sphere (5.9) as a special case when $a = b = R$. Indeed, in this case we have

$$h(\theta)|_{a=b=R} = \int_{\pi/2}^{\theta} \sqrt{1+\cot^2 v}\, dv = \int_{\pi/2}^{\theta} \frac{1}{\sin v}\, dv = -\log\Big(\frac{\sin\theta}{1-\cos\theta}\Big) \tag{5.20}$$

$$\Rightarrow r|_{a=b=R} = 2Re^{-h} = 2R\frac{\sin\theta}{1-\cos\theta} = 2R\cot(\theta/2)\,. \tag{5.21}$$

We now combine (5.19) with (5.9) to recover the conformal relation between the metric of the sphere and the metric of the spheroid:

$$g^E_{ab}(r,\phi) = \Big(\frac{a}{r}\sin\theta\Big)^2\Big(1+\frac{r^2}{4R^2}\Big)^2 g^S_{ab}(r,\phi)\,. \tag{5.22}$$

Changing coordinates from r to θ, the conformal factor relating the sphere and the spheroid is thus

$$e^{2\sigma} = \Big(\frac{a}{2R}e^{h(\theta)}\sin\theta\Big)^2\Big(1+e^{-h(\theta)}\Big)^2\,. \tag{5.23}$$

It is straight forward to show that in the case where $a = b = R$, this conformal factor reduces to unity, as we would expect.

Note that in our coordinates,

$$z = 2Re^{-h(\theta)}e^{i\phi}\,, \qquad \bar{z} = 2Re^{-h(\theta)}e^{-i\phi}\,, \tag{5.24}$$

the Jacobian is given by

$$dzd\bar{z} = 8iR^2e^{-2h(\theta)}\sqrt{(b/a)^2+\cot^2\theta}\, d\phi d\theta\,. \tag{5.25}$$

[2]Note that, as explained in Appendix B, the map (5.15) is constructed using a map to the sphere of radius R as an intermediary step. This has introduced the free parameter R, which is not fixed by the geometry of the spheroid, into the map. In our case we are subsequently mapping back to the sphere, so we of course identify this free parameter with the radius of this sphere.

The metric becomes

$$\sqrt{g} = \frac{1}{(1 + r^2/4R^2)^2} = \frac{1}{(1 + e^{-2h(\theta)})^2} \,. \tag{5.26}$$

which, using (4.2), yields the volume element

$$dV = 4R^2 \frac{e^{-2h(\theta)}}{(1 + e^{-2h(\theta)})^2} \sqrt{(b/a)^2 + \cot^2\theta} d\phi d\theta \,. \tag{5.27}$$

Note that in the limit $a = b = R$ our volume element reduces to the volume element of the sphere $dV = R^2 \sin\theta d\phi d\theta$ as required.

We now proceed to solve for the single particle LLL states on the surface of the deformed sphere. We will consider two cases: first, the case in which as we deform the sphere, the flux density of magnetic field lines through the surface remains uniform (we can think of this as the magnetic monopole field lines deforming appropriately, so as to remain perpendicular to the sphere's surface, as the sphere is deformed). Secondly, we consider the case in which a monopole-like field, given by

$$\vec{B} = B_0 \hat{r} \tag{5.28}$$

remains static as we deform the sphere. This results in the density of field lines through the surface of the deformed sphere becoming non-uniform. Note that the field (5.28) that we are considering differs from the standard monopole field (3.2) in that it has no $1/r^2$ dependence. It is however equal to the standard monopole field at the surface of the unsquashed unit sphere where $r = R = 1$. In this limit we therefore still recover the spherical monopole system studied in Chapter 3, and the results derived there remain applicable.

5.2 Uniform Magnetic Flux

5.2.1 Single Particle States

In the case of uniform flux density through the surface, our LLL states depend only on the Kähler potential of the surface. We rewrite the differential equation (5.6) for the 'deformed' part of the Kähler potential u as

$$\frac{1}{r}\frac{\partial}{\partial r}\Big(r\frac{\partial u}{\partial r}\Big) = \frac{4(e^{2\sigma} - 1)}{(1 + r^2/4R^2)^2} \,, \tag{5.29}$$

where we have written the Laplacian in polar coordinates and assumed that $u = u(r)$ is independent of ϕ, motivated by the azimuthal symmetry of the problem. At this point we introduce the *deformation parameter* ϵ by setting $a = 1 + \epsilon$ and $b = 1$. Fixing $R = 1$, we interpret our deformation of the sphere as follows: for $\epsilon = 0$ we recover our spherical monopole system studied earlier, and increasing ϵ corresponds to stretching the equatorial radius whilst holding the polar radius fixed.

Now substituting in for the conformal factor $e^{2\sigma}$ and changing coordinates from r to θ, we recover after some manipulation the following differential equation for u,

$$\begin{aligned}\frac{\partial}{\partial\theta}\left(\Big[\frac{1}{(1+\epsilon)^2} + \cot^2\theta\Big]^{-1/2}\frac{\partial u}{\partial\theta}\right) &= 16e^{-2h}\sqrt{\frac{1}{(1+\epsilon)^2} + \cot^2\theta} \\ &\quad \times \left(\Big(\frac{1+\epsilon}{2}e^h \sin\theta\Big)^2 - \Big(1 + e^{-h}\Big)^{-2}\right). \end{aligned} \tag{5.30}$$

We now seek to integrate with respect to θ. Failing to find a closed form of the integral, we first Taylor expand the

right hand side in ϵ about $\epsilon = 0$, to order ϵ^5, yielding

$$\begin{aligned}\frac{\partial u}{\partial\theta} = 2\sqrt{\frac{1}{(1+\epsilon)^2}+\cot^2\theta}\Bigg[&\frac{1}{3}\Big(-9\cos\theta+\cos 3\theta\Big)\epsilon\\ &+\frac{1}{60}\Big(-20\cos\theta-35\cos 3\theta+7\cos 5\theta\Big)\epsilon^2\\ &+\frac{1}{3360}\Big(-525\cos\theta+833\cos 3\theta-637\cos 5\theta+73\cos 7\theta\Big)\epsilon^3\\ &+\frac{1}{40320}\Big(-1792\cos\theta-4242\cos 3\theta+9778\cos 5\theta-2687\cos 7\theta+223\cos 9\theta\Big)\epsilon^4\\ &+\frac{1}{7096320}\Big(950950\cos\theta-72006\cos 3\theta-1662067\cos 5\theta+816739\cos 7\theta\\ &-139161\cos 9\theta+7241\cos 11\theta\Big)\epsilon^5\Bigg]+\mathcal{O}(\epsilon^6)\,.\end{aligned} \tag{5.31}$$

Taylor expanding the right hand side again to the order ϵ^5 and integrating, we obtain the result

$$\begin{aligned}u(\epsilon;\theta) =&\frac{2}{3}\Big(\cos 2\theta-8\log(\sin\theta)\Big)\epsilon+\frac{1}{5}\Big(-13\cos 2\theta+\cos 4\theta-8\log(\sin\theta)\Big)\epsilon^2\\ &+\frac{1}{630}\Big(1479\cos 2\theta-216\cos 4\theta+17\cos 6\theta-96\log(\sin\theta)\Big)\epsilon^3\\ &+\frac{1}{15120}\Big(-37260\cos 2\theta+6192\cos 4\theta-1348\cos 6\theta+75\cos 8\theta+960\log(\sin\theta)\Big)\epsilon^4\\ &+\frac{1}{138600}\Big(346125\cos 2\theta-56370\cos 4\theta+24350\cos 6\theta-2335\cos 8\theta\\ &+101\cos 10\theta-3840\log(\sin\theta)\Big)\epsilon^5+\mathcal{O}(\epsilon^6)\,.\end{aligned} \tag{5.32}$$

Substituting into (5.7) we obtain the LLL solutions

$$\begin{aligned}\psi_m(B,\epsilon;\theta,\phi) = \mathcal{N}\exp\!\left(-\frac{K_0+u(\epsilon;\theta)}{4l^2}-mh(\theta)\right)e^{im\phi}\,,\\ m=0,1,2,...,2/l^2\,,\end{aligned} \tag{5.33}$$

where we have substituted in for $r = 2Re^{-h(\theta)}$.

Normalisation

$\mathcal{N}$ is a normalisation constant, chosen such that $\langle\psi_m|\psi_m\rangle = 1$ with respect to the inner product (4.31),

$$\langle\psi_n|\psi_m\rangle = \int\psi_n\bar{\psi}_m dV \tag{5.34}$$

$$= 4R^2\mathcal{N}^2\int d\phi d\theta\frac{e^{-2h(\theta)}}{(1+e^{-2h(\theta)})^2}\sqrt{(b/a)^2+\cot^2\theta}e^{-(K_0+u)/2l^2-(n+m)h(\theta)}e^{i(n-m)\phi}\,, \tag{5.35}$$

where in the second equality we have used the volume element (5.27) and the explicit form of our states (5.33). Doing the ϕ integral, we obtain

$$\langle\psi_n|\psi_m\rangle = 8\pi R^2\mathcal{N}^2\delta_{m,n}\int d\theta\frac{e^{-2(n+1)h(\theta)}}{(1+e^{-2h(\theta)})^2}\sqrt{(b/a)^2+\cot^2\theta}e^{-(K_0+u)/2l^2}\,. \tag{5.36}$$

Substituting in for the Kähler potential of the sphere in (4.19),

$$e^{-K_0/2l^2} = \sin^{\frac{4R^2}{l^2}}\left(\frac{\theta}{2}\right), \tag{5.37}$$

we obtain

$$\langle\psi_n|\psi_m\rangle = 8\pi R^2\mathcal{N}^2\delta_{m,n}\int d\theta\frac{e^{-2(n+1)h(\theta)}}{(1+e^{-2h(\theta)})^2}\sqrt{(b/a)^2+\cot^2\theta}\sin^{\frac{4R^2}{l^2}}\left(\frac{\theta}{2}\right)e^{-u/2l^2}\,. \tag{5.38}$$

Requiring our states to be orthonormal with respect to this inner product then requires

$$\mathcal{N}^{-2} = 8\pi R^2\int d\theta\frac{e^{-2(n+1)h(\theta)}}{(1+e^{-2h(\theta)})^2}\sqrt{(b/a)^2+\cot^2\theta}\sin^{\frac{4R^2}{l^2}}\left(\frac{\theta}{2}\right)e^{-u/2l^2}\,. \tag{5.39}$$

Unable to find a closed form for this integral in general, $\mathcal{N}$ must be evaluated numerically on a case by case basis.

5.3 Non-Uniform Magnetic Flux

We now consider the case where as we deform the sphere, the monopole-like field $\vec{B} = B_0\hat{r}$ remains static. We will take this modification to the standard monopole field as understood and henceforth refer to it simply as the monopole field. The magnetic flux density $B(z,\bar{z})$ through the surface will thus depend on the deformation parameter ϵ and the coordinates on the spheroid.

5.3.1 Single Particle States

Recall that for general g_s, the term proportional to $B(z,\bar{z})$ in the Hamiltonian (4.16) breaks the degeneracy of the LLL and our solutions derived thus far are not applicable. In the special case $g_s = 2$ however, our LLL states ψ must simply satisfy $\bar{\pi}\psi = 0$ as before. Our basis of LLL states are then given by (5.8).

To solve for the flux $B(z,\bar{z})$ of the magnetic monopole field through the deformed sphere, we simply take the dot product between the monopole-like field $\vec{B}$ and the unit normal field $\hat{n}$ of the spheroid. We are here assuming that the sphere is deformed such that the monopole remains at the centre of the resultant spheroid: if we parameterize the spheroid as in (5.13), the magnetic monopole sits at the origin. A quick calculation yields

$$\vec{B} = B_0(\sin\theta\cos\phi, \sin\theta\sin\phi, \cos\theta)\,, \tag{5.40}$$

$$\hat{n} = \frac{1}{\sqrt{b^2\sin^2\theta + a^2\cos^2\theta}}(b\sin\theta\cos\phi, b\sin\theta\sin\phi, a\cos\theta)\,, \tag{5.41}$$

$$\begin{aligned}\Rightarrow\quad B(\theta) &= \vec{B}\cdot\hat{n}\\ &\equiv B_0\hat{B}(\theta)\,,\end{aligned} \tag{5.42}$$

where

$$\hat{B}(\theta) \equiv \frac{\sin^2\theta + (1+\epsilon)\cos^2\theta}{\sqrt{\sin^2\theta + (1+\epsilon)^2\cos^2\theta}}\,. \tag{5.43}$$

Note that we have introduced the deformation parameter ϵ by fixing $a = 1+\epsilon$ and $b = 1$, as before. As one would expect, the magnetic flux of the monopole through the spheroid is azimuthal rotationally symmmetric. We also have that $B(\theta) = B_0$ at the equator ($\theta = \pi/2$) and the poles ($\theta = 0, \pi$), the points where the monopole field remains perpendicular to the spheroid. At all other points, where the field lines are not perpendicular to the surface, we have $B(\theta) < B_0$.

We will now solve the differential equation (4.12)

$$\frac{4}{\sqrt{g}}\partial\bar{\partial}Q(z,\bar{z}) = -\frac{2e}{\hbar}B(z,\bar{z}) \tag{5.44}$$

for Q. Changing to polar coordinates yields

$$\frac{1}{r}\frac{\partial}{\partial r}\Big(r\frac{\partial Q(r)}{\partial r}\Big) = -\frac{2e}{\hbar}\sqrt{g}B(r)\,, \tag{5.45}$$

where we have made the assumption that Q respects the azimuthal symmetry of the problem and has no ϕ dependence.

Substituting in for the metric (5.26) and changing coordinates from r to θ, (5.45) becomes

$$\frac{\partial}{\partial\theta}\left(\Big[\frac{1}{(1+\epsilon)^2}+\cot^2\theta\Big]^{-1/2}\frac{\partial Q}{\partial\theta}\right)=-\frac{2}{l^2}\hat{B}(\theta)\Big[\frac{1}{(1+\epsilon)^2}+\cot^2\theta\Big]^{1/2}(1+\epsilon)^2\sin^2\theta\,, \tag{5.46}$$

where we have defined an analogue of the magnetic length for this system $l=\sqrt{\hbar/eB_0}$. We integrate by θ once and rearrange, to obtain

$$\frac{\partial Q}{\partial\theta}=\frac{1}{3l^2}\big[1+(1+\epsilon)^2\cot^2\theta\big]^{1/2}\big(6+\epsilon+\epsilon\cos 2\theta\big)\cos\theta\,. \tag{5.47}$$

Unable to find a closed form solution to this integral, we Taylor expand the right hand side about about $\epsilon=0$ to order ϵ^5. Integrating again, we then obtain

$$\begin{aligned}l^2Q(\epsilon;\theta)=&2\log(\sin\theta)+\frac{2}{3}\Big(\cos 2\theta+4\log(\sin\theta)\Big)\epsilon\\&+\frac{1}{96}\Big(12\cos 2\theta-\cos 4\theta+64\log(\sin\theta)\Big)\epsilon^2+\frac{1}{9}\cos^6\theta\epsilon^3\\&+\frac{1}{12288}\Big(-176-376\cos 2\theta-212\cos 4\theta-72\cos 6\theta-11\cos 8\theta\Big)\epsilon^4\\&+\frac{1}{7680}\Big(140+140\cos 2\theta+100\cos 4\theta+50\cos 6\theta+15\cos 8\theta+2\cos 10\theta\Big)\epsilon^5\\&+\mathcal{O}(\epsilon^6)\,.\end{aligned} \tag{5.48}$$

We would like this expression for Q to be such that in the limit $\epsilon\to 0$, our LLL states $\psi_m=z^m e^{Q/2}$ reduce to those of the spherical monopole system (3.39). For comparison we reproduce the result for spherical monopole LLL states here. Restoring dimensionful constants so that $g=eB/\hbar=1/l^2$, ignoring the constant prefactor and making the change of coordinates $\theta\to\pi-\theta$ to account for the differing choices of stereographic projection, we obtain the expression for LLL spherical monopole states

$$\psi_m(\theta,\phi)=\cot^m\left(\frac{\theta}{2}\right)\sin^{2/l^2}\left(\frac{\theta}{2}\right)e^{im\phi}\,. \tag{5.49}$$

In the $\epsilon\to 0$ limit, we find that

$$e^{Q/2}\to\sin^{1/l^2}\theta\,, \tag{5.50}$$

which is not consistent with the spherical monopole states. We remedy this by noting that if Q solves the differential equation (5.45), then so does $Q+C\log r$ where C is a constant (this is simply a choice of integration constant). Making the choice $C=2/l^2$ so that $Q\to Q-\frac{2\log r}{l^2}$, we recover

$$\lim_{\epsilon\to 0}e^{Q/2-\log r/l^2}=\left(\frac{\sin\theta}{r|_{\epsilon=0}}\right)^{1/l^2}=\left(\frac{\sin\theta}{2\cot(\theta/2)}\right)^{1/l^2}=\sin^{2/l^2}\left(\frac{\theta}{2}\right) \tag{5.51}$$

where in the second equality we have used (5.21). With this choice of integration constant we are thus assured that our states reduce to the spherical monopole system LLL states in the spherical limit. Our squashed sphere LLL states are then given by

$$\begin{aligned}\psi_m(B_0,\epsilon;\theta,\phi)&=\mathcal{N}\exp\left(\frac{Q(\epsilon;\theta)}{2}-mh(\theta)\right)e^{im\phi}\\m&=0,1,2,...,2/l^2\,.\end{aligned} \tag{5.52}$$

Normalisation

$\mathcal{N}$ is the normalisation constant, chosen such that $\langle\psi_m|\psi_m\rangle = 1$ with respect to the inner product (4.31). We now write this inner product in our coordinates:

$$\langle\psi_n|\psi_m\rangle = \int \psi_n\bar{\psi}_m dV \tag{5.53}$$

$$= 4R^2\mathcal{N}^2 \int d\phi d\theta \frac{e^{-2h(\theta)}}{(1+e^{-2h(\theta)})^2}\sqrt{(b/a)^2+\cot^2\theta}\, e^{Q/l^2-(n+m)h(\theta)} e^{i(n-m)\phi}\,, \tag{5.54}$$

where in the second equality we have used the volume element (5.27) and the explicit form of our states (5.52). Doing the ϕ integral, we obtain

$$\langle\psi_n|\psi_m\rangle = 8\pi R^2\mathcal{N}^2\delta_{m,n}\int d\theta \frac{e^{-2(n+1)h(\theta)}}{(1+e^{-2h(\theta)})^2}\sqrt{(b/a)^2+\cot^2\theta}\, e^{Q/l^2} \tag{5.55}$$

Requiring our states to be orthonormal with respect to this inner product then requires

$$\mathcal{N}^{-2} = 8\pi R^2 \int d\theta \frac{e^{-2(n+1)h(\theta)}}{(1+e^{-2h(\theta)})^2}\sqrt{(b/a)^2+\cot^2\theta}\, e^{Q/l^2} \tag{5.56}$$

Unable to find a closed form for this integral in general, in the following we calculate $\mathcal{N}$ numerically on a case by case basis.

5.4 Comparison

Having derived the single particle states for both the uniform and non-uniform flux cases of the squashed sphere, we analyse and compare our results. Knowing that in both cases we recover the spherical monopole LLL states in the limit $\epsilon \to 0$, we need only compare the ϵ dependent part of our expressions. For the uniform flux case, all ϵ dependence in the LLL states is given by

$$\psi_m(B,\epsilon;\theta,\phi) \sim \mathcal{N}_1(\epsilon)\exp\left(\frac{u'(\epsilon;\theta)}{l^2}\right), \tag{5.57}$$

where in general the normalisation constant $\mathcal{N}_1$ depends on ϵ, and for ease of comparison we have defined

$$\begin{aligned} u'(\epsilon;\theta) =& \frac{1}{6}\Big(8\log(\sin\theta)-\cos 2\theta\Big)\epsilon - \frac{1}{20}\Big(-13\cos 2\theta+\cos 4\theta-8\log(\sin\theta)\Big)\epsilon^2 \\ &- \frac{1}{2520}\Big(1479\cos 2\theta-216\cos 4\theta+17\cos 6\theta-96\log(\sin\theta)\Big)\epsilon^3 \\ &- \frac{1}{60480}\Big(-37260\cos 2\theta+6192\cos 4\theta-1348\cos 6\theta+75\cos 8\theta+960\log(\sin\theta)\Big)\epsilon^4 \\ &- \frac{1}{554400}\Big(346125\cos 2\theta-56370\cos 4\theta+24350\cos 6\theta-2335\cos 8\theta \\ &+101\cos 10\theta-3840\log(\sin\theta)\Big)\epsilon^5+\mathcal{O}(\epsilon^6)\,. \end{aligned} \tag{5.58}$$

For the non-uniform flux case, all ϵ dependence in the LLL states is given by

$$\psi_m(B_0,\epsilon;\theta,\phi) \sim \mathcal{N}_2(\epsilon)\exp\left(\frac{Q'(\epsilon;\theta)}{l^2}\right), \tag{5.59}$$

where in general the normalisation constant $\mathcal{N}_2$ depends on ϵ, and for ease of comparison we have defined

$$\begin{aligned} Q'(\epsilon;\theta) =& \frac{1}{6}\Big(8\log(\sin\theta)+2\cos 2\theta\Big)\epsilon \\ &+\frac{1}{192}\Big(12\cos 2\theta-\cos 4\theta+64\log(\sin\theta)\Big)\epsilon^2+\frac{1}{9}\cos^6\theta\epsilon^3 \\ &+\frac{1}{24576}\Big(-176-376\cos 2\theta-212\cos 4\theta-72\cos 6\theta-11\cos 8\theta\Big)\epsilon^4 \\ &+\frac{1}{15360}\Big(140+140\cos 2\theta+100\cos 4\theta+50\cos 6\theta+15\cos 8\theta+2\cos 10\theta\Big)\epsilon^5 \\ &+\mathcal{O}(\epsilon^6)\,. \end{aligned} \tag{5.60}$$

Firstly, note that in the expressions for both u' and Q', for $\epsilon < 1$ the only term of magnitude greater than unity is $\log(\sin\theta)$, which diverges to negative infinity when $\theta \to 0$ and $\theta \to \pi$. The effect of this is that the ϵ dependent factors (5.57) and (5.59) tend towards zero at the poles. This suppresses the amplitude of the wavefunctions around the poles, and ensures that the amplitude at the poles become effectively zero as soon as the sphere is even slightly deformed.

Secondly, note that in (5.58), at each order in ϵ the first term in the brackets is of the same order of magnitude as the denominator of the coefficient of the brackets. This means that for values $\epsilon \approx 1$ we expect a non-negligible contribution to the expression even at order ϵ^5. However, for values of $\epsilon \ll 1$ we expect our perturbative result to be valid. This expectation is verified by a numerical approach, where we see that for field strengths in the range $0 < B < 50$ our perturbative result is valid only up to $\epsilon \approx 0.3$, after which the states plotted using the $\mathcal{O}(\epsilon^4)$ and $\mathcal{O}(\epsilon^5)$ results begin to differ. This is illustrated for $B = 5$ in Figure 5.1, where we have zoomed into the interval $\pi/4 \leq \theta \leq \pi$ for a clearer image.

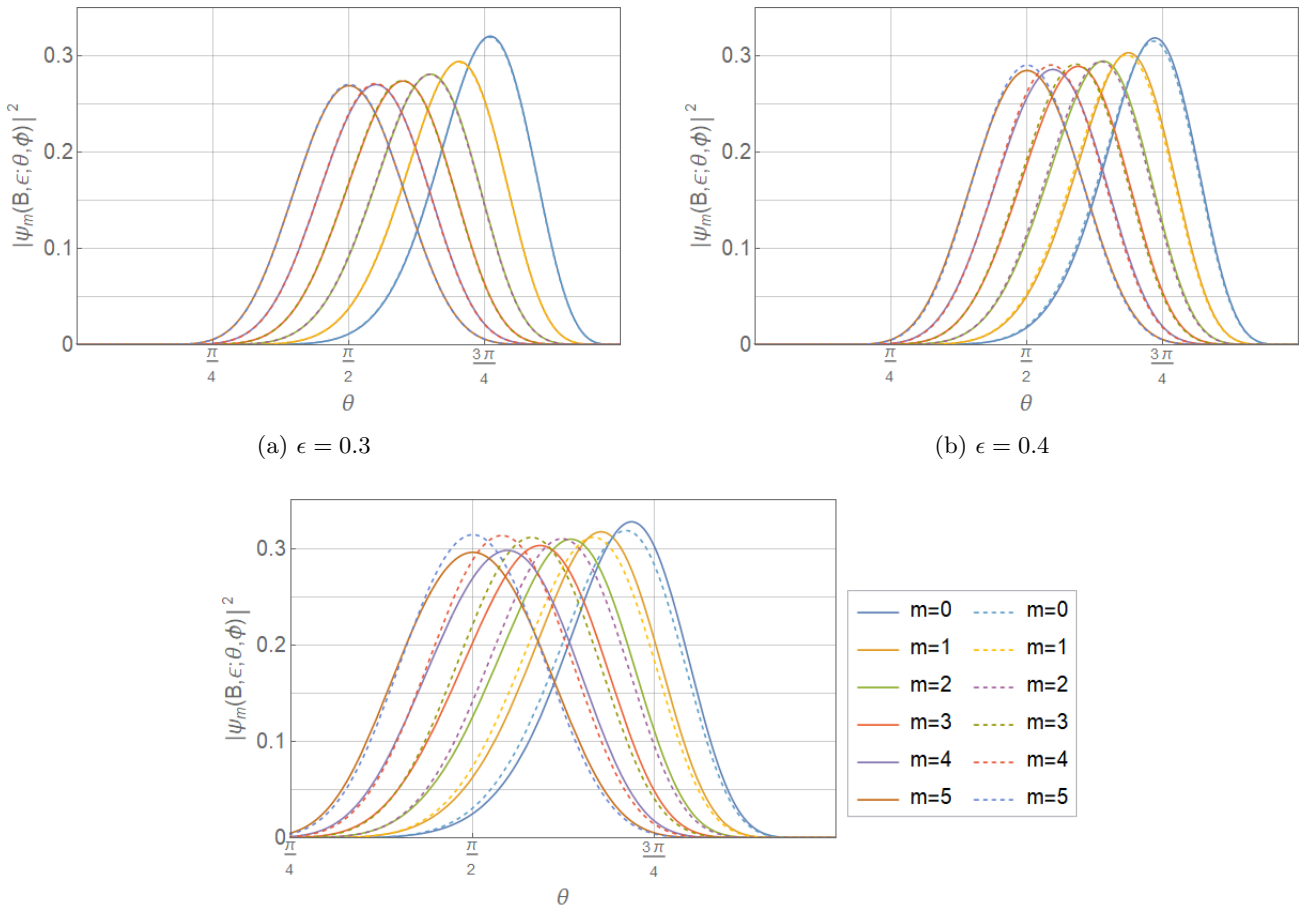

(a) $\epsilon = 0.3$

(b) $\epsilon = 0.4$

(c) $\epsilon = 0.5$

Figure 5.1: $|\psi_m(B, \epsilon; r, \phi)|^2$ for $R = 1$, $B = 5$ and various m and ϵ. The $\mathcal{O}(\epsilon^4)$ results are plotted in solid lines and the $\mathcal{O}(\epsilon^5)$ results in dashed lines.

In (5.60) however, note that at each order in ϵ all terms in the brackets are orders of magnitude smaller than the denominator of the coefficient of the brackets. This means that we expect our perturbative result to be valid up to values $\epsilon \approx 1$. This is verified by the numerics, where we see that for field strengths in the range $0 < B < 50$ our perturbative result is valid up to $\epsilon \approx 1$, at which the $\mathcal{O}(\epsilon^4)$ and $\mathcal{O}(\epsilon^5)$ results still coincide. This is illustrated in Figure 5.2 for $B = 5$, where we have zoomed into the interval $\pi/4 \leq \theta \leq \pi$ for a clearer image.

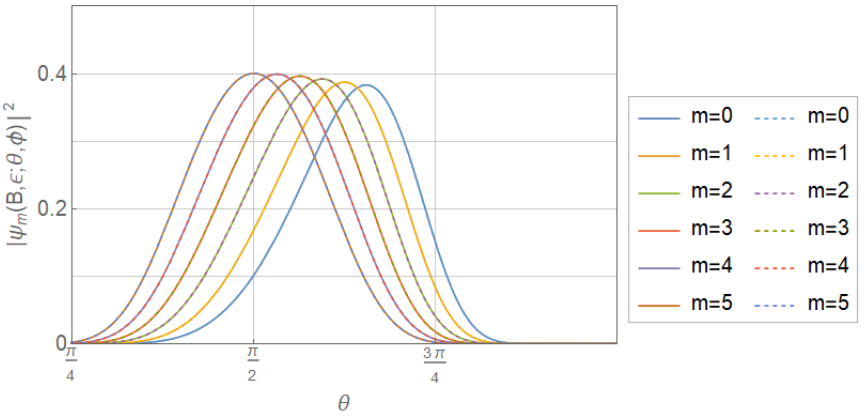

Figure 5.2: $|\psi_m(B,\epsilon;r,\phi)|^2$ for $B = 5$, $\epsilon = 1$ and various m. The $\mathcal{O}(\epsilon^4)$ results are plotted in solid lines and the $\mathcal{O}(\epsilon^5)$ results in dashed lines.

We would now like to compare our states for the constant and non-constant flux cases to see to what extent and in which parameter regimes they differ from each other. Unfortunately, without having a general form for the overall normalisation factors $\mathcal{N}_i(\epsilon)$, (5.39) and (5.56), it is difficult to address this from an analytic perspective. Taking a numerical approach, we find that within the range of validity of the constant flux solutions $0 \leq \epsilon \leq 0.3$ and for field strengths $0 < B < 50$, both cases of solutions agree with negligible difference.

As $0 < B < 50$ is the only regime of field strength values numerically available to us for study, from now on we therefore deal only with the non-constant flux states (5.52).

5.5 Non-Uniform Magnetix Flux Wavefunctions

We now perform a qualitative analysis of the effects of squashing on our basis of LLL states (5.52). We plot the probability distributions $|\psi|^2$ for a representative selection of these states as a function of the polar angle $0 \leq \theta \leq \pi$. We do so for various values of squashing parameter ϵ, angular momentum m and field strength $B = 1/l^2$ (in units of $e = \hbar = 1$). In all of the following we set $R = 1$. Recall that the field strength B takes positive values, while the angular momentum takes integer values such that $0 \leq m \leq 2B$.

Let us briefly discuss what happens to the geometry of the system as we increase ϵ from zero. This corresponds to squashing the sphere oblately, breaking the polar angle rotational symmetry of the system. The poles of the sphere, previously indistinguishable from any other point on the sphere, now become distinguished as the two points of minimum scalar curvature. Similarly, the set of points on the equator now become the set of points of maximum curvature on the spheroid.

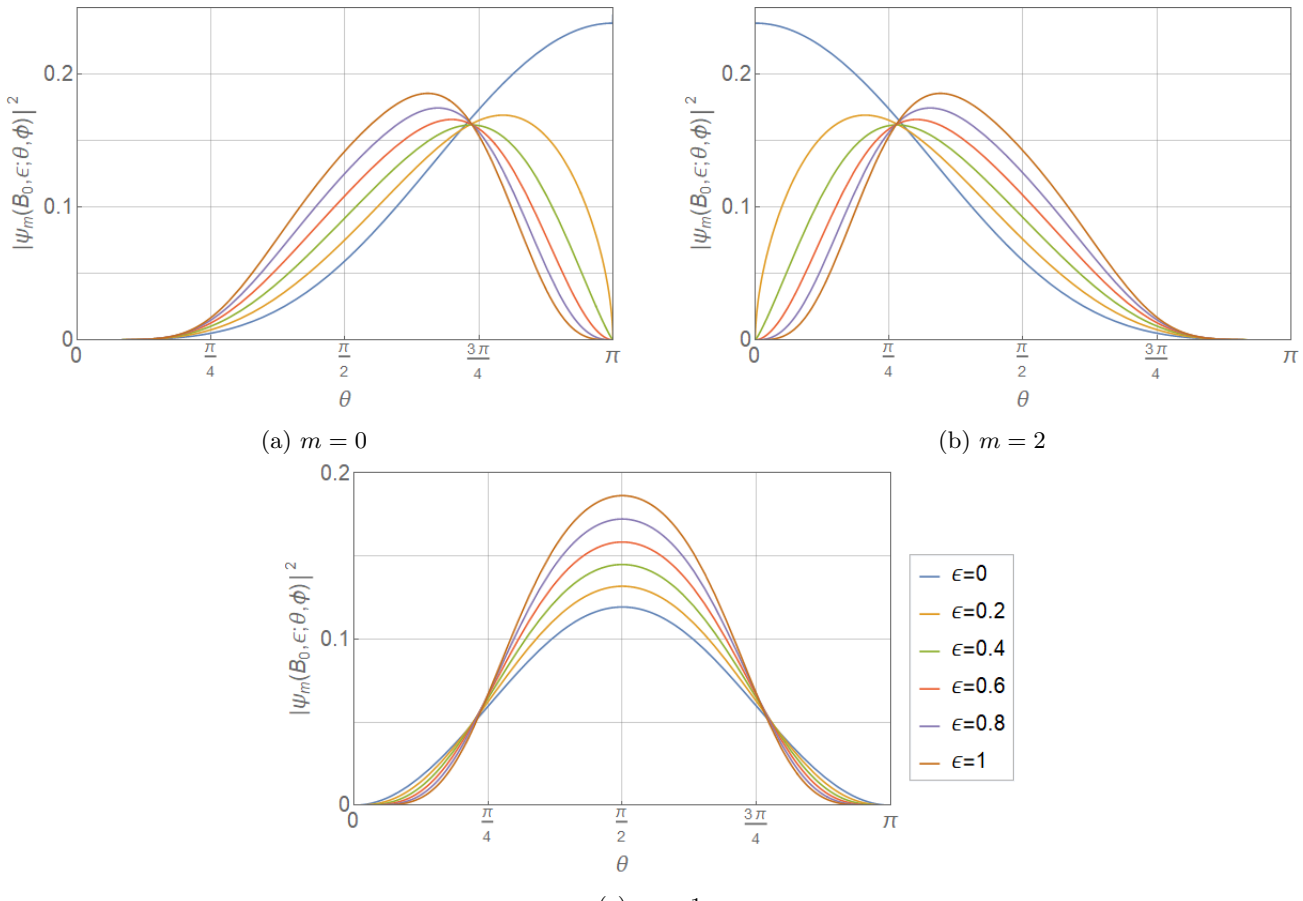

(a) $m = 0$

(b) $m = 2$

(c) $m = 1$

Figure 5.3: $|\psi_m(B, \epsilon; r, \phi)|^2$ for $B = 1$ and various m and ϵ.

We begin by plotting the entire set of state distributions for $B = 1$ for a range of ϵ values in Figure 5.3. For $\epsilon = 0$ we of course recover the spherical monopole distribution, peaked at the south pole ($m = 0$), the north pole ($m = 2$) and the equator ($m = 1$). We see that in Figures 5.3a and 5.3b as soon as ϵ becomes non-zero, the probability distributions drop to zero at the poles, as we predicted analytically. Furthermore, the peaks of the distributions move gradually towards the equator for increasing values of ϵ. These two plots are related to each other by a reflection about the equator; as expected given the symmetry of the squashed sphere about the equator. In Figure 5.3c we see that the $m = B$ state, which is as usual peaked at the equator, respects this symmetry as well, remaining peaked at and symmetrical about the equator as the sphere is squashed. This symmetry is respected by all LLL states and will not be illustrated further for other B.

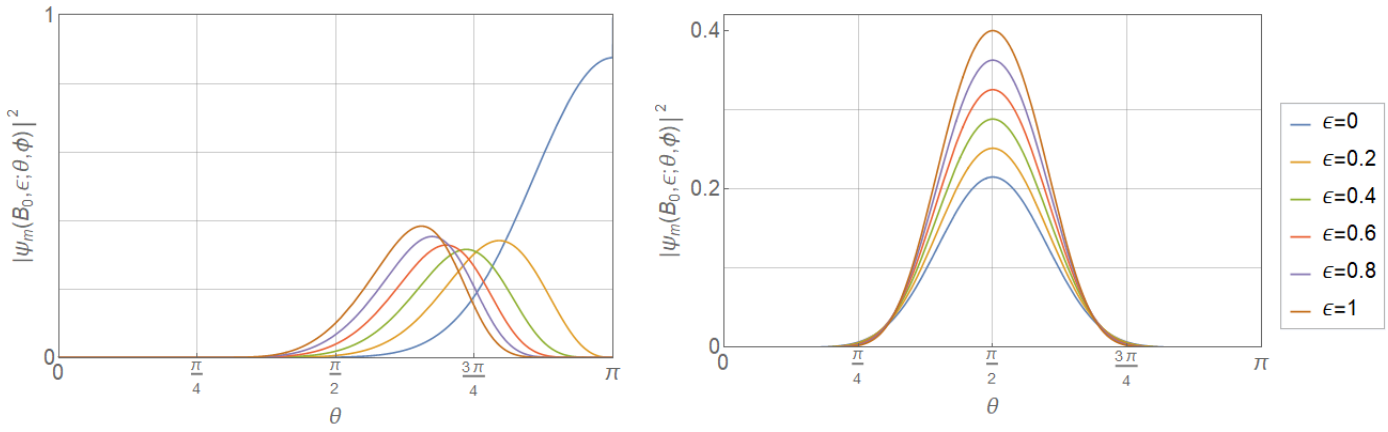

(a) $m = 0$ (b) $m = 5$

Figure 5.4: $|\psi_m(B, \epsilon; r, \phi)|^2$ for $B = 5$ and various m and ϵ.

In Figure 5.4 we again plot the $m = 0$ and $m = B$ distributions, but this time for a stronger field strength $B = 5$. The qualitative behaviour is the same, but the distributions have become more strongly localised. As in the planar and spherical monopole systems, this tendency of the distribution to be increasingly localised by stronger field strengths holds for all states, as illustrated clearly in Figure 5.5. The main result of our qualitative analysis, illustated again in Figure 5.4a, is that squashing the sphere has the effect of suppressing the probability of finding the particle near the poles, and increase the probability of finding the particle near the equator.

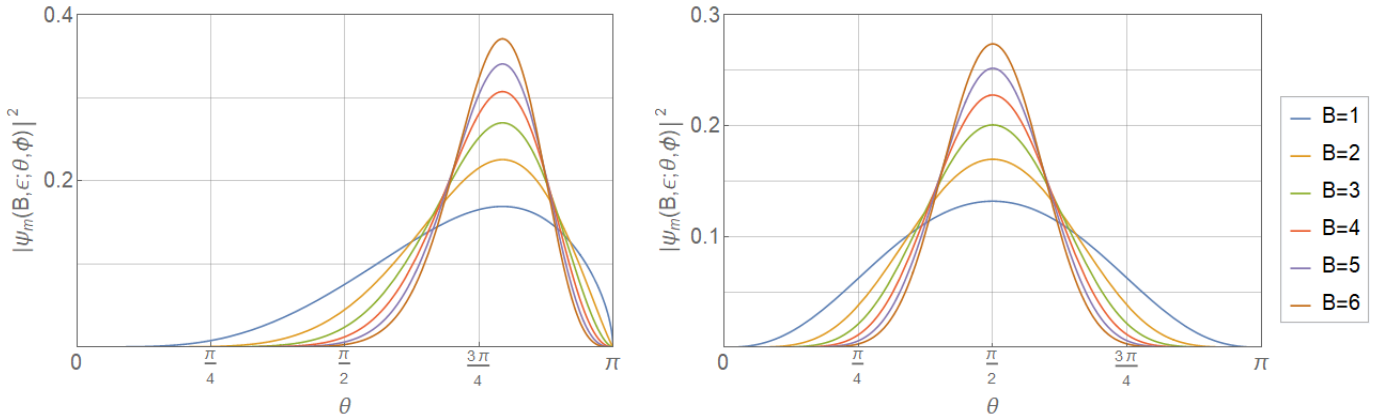

(a) $m = 0$ (b) $m = B$

Figure 5.5: $|\psi_m(B, \epsilon; r, \phi)|^2$ for $\epsilon = 0.2$ and various B.

Chapter 6

The Spherical Dipole System

In this chapter we will be considering a novel variant of the spherical monopole system in which the (physically unrealisable) monopole field is replaced by that of a dipole. We investigate the classical dynamics and then the quantum problem, finding the single particle state solutions and spectrum. We investigate these solutions in various limits, with special attention given to the strong-field limit. The work presented in this chapter is original and has been submitted for publication [40].

6.1 Classical Dynamics

To set up the system, we replace the magnetic monopole at the center of the Haldane sphere with two monopoles with charges $+b$ and $-b$, separated by a distance l and aligned along the z-direction. Taking the limit $l \to 0$ while holding bl fixed, the resulting magnetic field ,

$$\mathbf{B} = \frac{|\boldsymbol{\mu}|}{r^3}\left(2\cos\theta\,\widehat{\boldsymbol{r}} + \sin\theta\,\widehat{\boldsymbol{\theta}}\right), \tag{6.1}$$

is identical to that produced by a current loop enclosing a flat region with area A_{loop} in the xy-plane. In either case the magnetic moment is aligned in the positive z-direction with $|\boldsymbol{\mu}| = IA_{\text{loop}} = bl$. Associated to this dipole magnetic field is the vector potential

$$\begin{aligned}\boldsymbol{A} &= \frac{1}{r^2}\boldsymbol{\mu}\times\widehat{\boldsymbol{r}} \\ &= \frac{|\boldsymbol{\mu}|}{r^2}\sin\theta\,\widehat{\boldsymbol{\phi}}\,.\end{aligned} \tag{6.2}$$

The Lagrangian (in units of $c = 1$) for a particle of charge e and mass m, confined to move on a sphere of radius R concentric with the center of the dipole, is

$$L = \frac{1}{2}m\dot{\mathbf{x}}^2 + e\dot{\mathbf{x}}\cdot\mathbf{A}\,. \tag{6.3}$$

The resulting equations of motion

$$\begin{aligned}\ddot{\theta} &= \frac{1}{2}\sin 2\theta\left(\dot{\phi} + \frac{2e|\boldsymbol{\mu}|}{mR^3}\right)\dot{\phi}\,, \\ \ddot{\phi} &= -2\cot\theta\left(\dot{\phi} + \frac{e|\boldsymbol{\mu}|}{mR^3}\right)\dot{\theta}\,,\end{aligned} \tag{6.4}$$

can be numerically solved for a rich set of trajectories.

There is a unique set of initial conditions which yield a special set of trajectories. These are

$$\begin{aligned}\dot{\phi}(0) &= -\frac{2e|\boldsymbol{\mu}|}{mR^3}\,, \\ \dot{\theta}(0) &= 0\,.\end{aligned} \tag{6.5}$$

By inspection of (6.4), we see that this choice for $\dot{\theta}(0)$ ensures that $\dot{\phi}(t) = \dot{\phi}(0)$, which in turn ensures that $\dot{\theta}(t) = 0$ for all times. We thus recover closed circular orbits of constant latitude, and angular frequency $\omega = -2e|\boldsymbol{\mu}|/mR^3$. These orbits replicate those cyclotron orbits in the spherical monopole system which are confined to constant latitude. A representative example of such an orbit is plotted in Figure 6.1a, with the magnetic vector field illustrated in black.

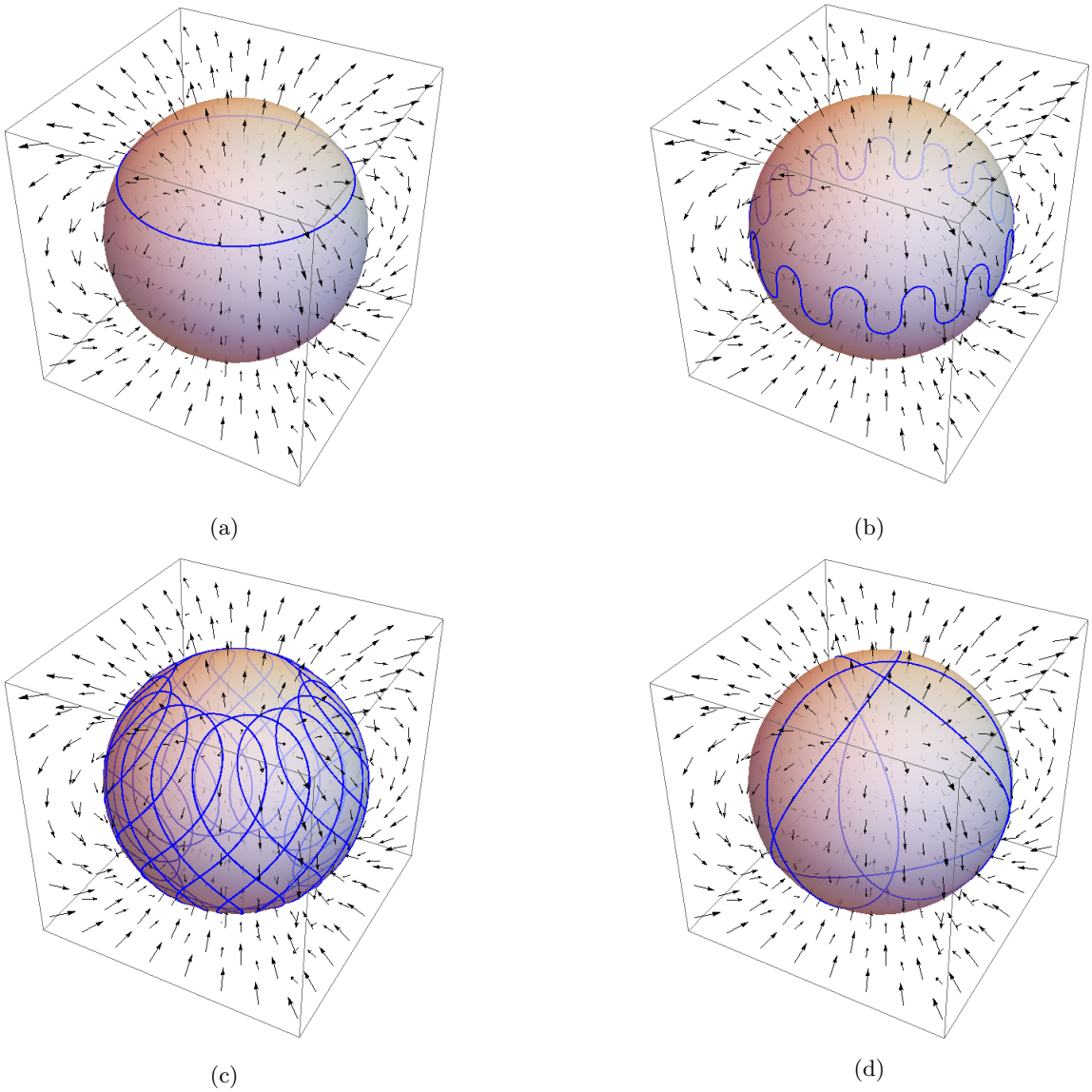

(a) (b) (c) (d)

Figure 6.1: Classical trajectories for various initial conditions.

Turning to more general initial conditions, Figure 6.1b illustrates a general characteristic of the classical trajectories, namely oscillation about the equator. Figure 6.1c shows the same behaviour but with the trajectory now highly delocalised, covering most of the sphere, and Figure 6.1d replicates this behaviour to a lesser extent. Note that all of the initial conditions for the trajectories plotted in Figure 6.1 have been fine tuned such that they yield periodic orbits which close after 'wrapping' around the sphere only once. More general initial conditions will lead to orbits which wrap around the sphere arbitrarily many times before returning to their starting point.

6.2 Quantum Mechanics

We now turn to the quantum formulation of the problem. As we have seen, the spherical monopole system shares many similarities with the planar system, and in the large R limit, the two problems converge. For the dipole system, this is no longer the case. Even if the particle is constrained by the initial conditions (6.5) to move on orbits of constant latitude, the magnetic field it experiences is no longer uniform. Intuitively, in the large radius limit when the sphere is nearly flat, we would expect that sufficiently close to the north pole the system reduces to the planar Landau problem but in an *inhomogeneous* magnetic field with azimuthal rotational symmetry. We begin our analysis hoping to make some of these notions more precise[1].

The Hamiltonian for the system is given (in units of $c = 1$) by

$$\begin{aligned} H &= \frac{1}{2m}(-i\hbar\nabla - eA)^2 \\ &= \frac{\hbar^2}{2mR^2}\left[-\frac{1}{\sin\theta}\frac{\partial}{\partial\theta}\sin\theta\frac{\partial}{\partial\theta} + \left(\frac{i}{\sin\theta}\frac{\partial}{\partial\phi} - Q\sin\theta\right)^2\right], \end{aligned} \tag{6.6}$$

where, to facilitate comparison with the spherical monopole system, we have defined

$$Q \equiv \frac{e|\boldsymbol{\mu}|}{\hbar R}\,. \tag{6.7}$$

Substituting into the Schrödinger equation and introducing a separable ansatz $\Psi(\theta,\phi) = e^{im\phi}\psi(\theta)$ yields the eigenvalue problem

$$\widetilde{E}\psi = -\frac{1}{\sin\theta}\frac{\partial}{\partial\theta}\left(\sin\theta\frac{\partial\psi}{\partial\theta}\right) + \frac{\left(m + Q\sin^2\theta\right)^2}{\sin^2\theta}\psi\,, \tag{6.8}$$

where, to avoid confusion between the mass of the particle and the quantum number labelling the eigenfunction, we define $\widetilde{E} \equiv 2mR^2E/\hbar^2$.

6.2.1 Mathieu Function Solutions

Implementing the change of variables $\varphi(\theta) = \sqrt{\sin\theta}\psi(\theta)$, (6.8) becomes

$$\frac{\partial^2\varphi}{\partial\theta^2} + \Big[\frac{1}{4}\Big(\frac{\cos^2\theta - 4m^2}{\sin^2\theta}\Big) + \frac{1}{2}(1 + 4mQ) - Q^2\sin^2\theta + \widetilde{E}\Big]\varphi = 0\,. \tag{6.9}$$

We now fix $m = \pm 1/2$, which reduces the first term in the square brackets to a constant. Using the identity $\sin^2\theta = (1 - \cos 2\theta)/2$, we then obtain

$$\frac{\partial^2\varphi}{\partial\theta^2} + \Big[\frac{1}{4} \pm Q - \frac{Q^2}{2} + \widetilde{E} + \frac{Q^2}{2}\cos 2x\Big]\varphi = 0\,. \tag{6.10}$$

We recognise this as a differential equation of the *Mathieu form*,

$$f''(x) + \big[a - 2q\cos 2\theta\big]f(x) = 0\,, \tag{6.11}$$

which has as solutions the linearly independent even and odd Mathieu functions $C(a,q;x)$ and $S(a,q;x)$ respectively.

Comparing coefficients in (6.10) and (6.11) and taking into account our change of variables, we obtain the general solution

$$\begin{aligned} \Psi_m(Q;\theta,\phi) &= \frac{AC\big(a,q;\theta\big) + BS\big(a,q;\theta\big)}{\sqrt{\sin\theta}}e^{im\phi}\,, \qquad m = -\frac{1}{2}\,,\frac{1}{2}\,, \\ a &= \frac{1}{4}(1 \pm 4Q - 2Q^2 + 4\widetilde{E})\,, \qquad q = -\frac{Q^2}{4}\,, \end{aligned} \tag{6.12}$$

[1]Note that the framework developed in Chapter 4 for finding LLL states in a non-homogenous magnetic field assumes small variations in magnetic flux density over a large constant background. It is thus not applicable to the spherical dipole system. In any case, we tackle the problem from first principles hoping to find the full single-particle Hilbert space, not just the LLL states.

where A and B are integration constants. By inspection we see that the denominator vanishes at $\theta = 0$ and $\theta = \pi$. The solution thus diverges unless the numerator also vanishes at these values. The even function $C(a, q; \theta)$ is in general non-zero at $\theta = 0$, so we set $A = 0$ to kill off this term. The odd Mathieu function $S(a, q; \theta)$ is always zero at $\theta = 0$, but is in general non-zero at $\theta = \pi$. For a given dipole field strength Q our solutions are therefore restricted to values of $\widetilde{E}$ for which $S(a, q; \pi) = 0$. This normalisability condition then quantises our energy spectrum via the relation in (6.12). The values of a for which this condition is satisfied are given by the *Mathieu characteristic values* $a_{r,q}$, which are functions of a positive integer r and the parameter q. We have thus found the single-particle eigenstates

$$\begin{aligned}
\Psi_{m,r}(Q;\theta,\phi) &= \mathcal{N}\frac{1}{\sqrt{\sin\theta}}S\big(a_{r,q},q;\theta\big)e^{im\phi} \\
&= \psi_{m,r}(Q;\theta)e^{im\phi}\,, \\
\widetilde{E}_{Q,m,r} &= a_{r,q} + \frac{Q^2}{2} - 2mQ - \frac{1}{4}\,, \qquad q = -\frac{Q^2}{4}\,, \\
m &= -\frac{1}{2}, \frac{1}{2}\,, \\
r &\in \mathbb{Z}\,,
\end{aligned} \tag{6.13}$$

where the normalisation constant $\mathcal{N}$ is given by

$$\mathcal{N}^{-2} = \int |\Psi_{m,r}(Q;\theta,\phi)|^2 dV\,. \tag{6.14}$$

In the following we will calculate $\mathcal{N}$ numerically on a case by case basis.

Wavefunctions

We will now plot a number of representative states to illustrate the general features of the Mathieu functions. In Figures 6.2a and 6.2b we plot $\psi_{m,r}(Q;\theta)$ against θ, ignoring the ϕ dependence which is not relevant to the probability distributions $|\Psi_{m,r}(\theta,\phi)|^2 = |\psi_{m,r}(\theta)|^2$ of the eigenstates.

We note a number of features. All states have zero amplitude at the poles. A state with quantum number r has $(r-1)$ nodes, and states of odd (even) r are symmmetric (antisymmetric) about $\theta = \pi/2$. Since the differential equation (6.10) is invariant under $m \to -m$, so too are the $\psi_{m,r}(Q;\theta)$. It is the full states $\Psi^m_n(Q;\theta,\phi)$ which carry the information about the sign of m in the phase factor $e^{im\phi}$.

The energy eigenvalues also know about the sign of m, as we can see from the expression for the spectrum in (6.13). Analytically we see that the $m = 1/2$ spectrum is simply the $m = -1/2$ spectrum shifted down by $2Q$, as pictured in Figures (6.2c) and (6.2d). Note that the spectrum is nonlinear in r. The eigenenergies increase with r, while the spacing between levels with adjacent r values also increases with r.

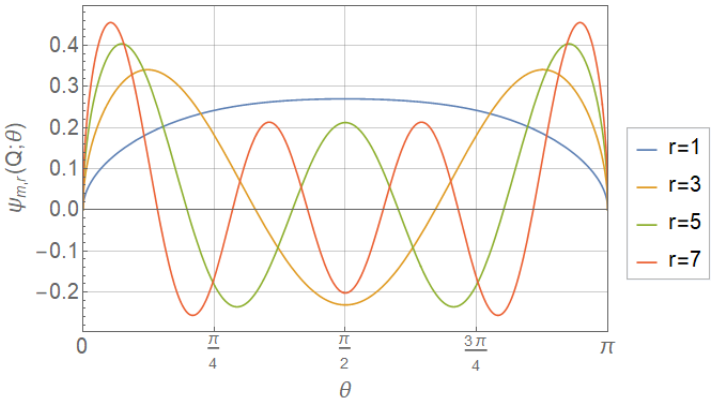

(a) Odd r states ($m = \pm 1/2$)

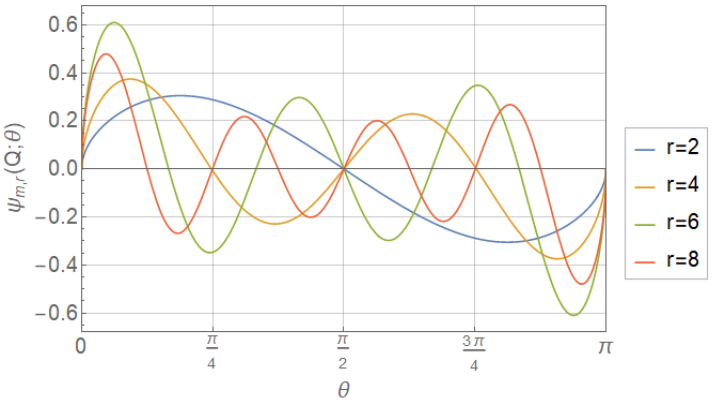

(b) Even r states ($m = \pm 1/2$)

(c) $m = -1/2$

(d) $m = 1/2$

Figure 6.2: Various states $\psi_{m,r}(Q;\theta)$ and their spectra $\widetilde{E}_{Q,m,r}$ for $Q = 1$.

A Note on the Mathieu Function Solutions

We do not perform a more detailed analysis of the Q dependence and the spectrum of the Mathieu function solutions for the following reason: the fact that we have chosen m to be non-integer means that our wave function is not single valued under $\phi \to \phi + 2\pi$.

We could consider rectifying this by implementing the gauge transformation

$$A_\phi^{\text{dip}} \to A_\phi^{\text{dip}} + \frac{n}{R\sin\theta}\,, \quad n \in \boldsymbol{C} \tag{6.15}$$

which leaves the magnetic field invariant, but changes the solutions as

$$\Psi(\theta,\phi) \to \Psi(\theta,\phi)e^{-ien\phi/\hbar}\,. \tag{6.16}$$

Making the choice $n = \pm\frac{\hbar}{2e}$ would then restore single-valuedness to the wavefunction. However, the gauge transformation (6.15) introduces a singularity at both poles into the otherwise everywhere regular gauge potential (6.2). We are forced to accept that to ensure both single-valuedness of our wavefunction and to preserve regularity of the vector potential, the quantum number m must be integer valued. We thus cannot regard the Mathieu function solutions outlined above as physical solutions to the spherical dipole system.

In the course of developing our full solutions to the spherical dipole system, it was the simplification of the eigenvalue problem (6.8) given by setting $m = \pm 1/2$, and the resulting Mathieu function solutions, which were noticed first and served as the entry point to obtaining the full solution outlined below. We have chosen here to present our results in the chronological order in which they were found, regardless of the fact that the Mathieu

solutions have been shown to be unphysical. We thus proceed now to present the general solution to the spherical dipole system.

6.2.2 Angular Oblate Spheroidal Solutions

We return to the Schrödinger equation (6.8). Changing variables to $z = \cos\theta$, we write the differential equation in the algebraic form

$$\frac{d}{dz}\left[\left(1-z^2\right)\frac{d}{dz}\right]\psi + \left[\lambda_l^m + Q^2 z^2 - \frac{m^2}{(1-z^2)}\right]\psi = 0, \tag{6.17}$$

where

$$\lambda_l^m \equiv \widetilde{E} - 2mQ - Q^2\,. \tag{6.18}$$

This is the *angular oblate spheroidal differential equation* [68]. Its solutions are the angular oblate spheroidal wavefunctions,

$$S_l^m(Q;z) = \sum_n d_n^{l,m}(Q) P_n^m(z)\,, \qquad l - |m| = 0, 1, 2, \ldots \tag{6.19}$$

where $P_n^m(z)$ are the associated Legendre functions, and the coefficient functions $d_n^{l,m}(Q)$ satisfy a three-term recursion relation [68]

$$\alpha_n d_{n+2} + (\beta_n - \lambda_l^m)\, d_n + \gamma_n d_{n-2} = 0\,, \tag{6.20}$$

where

$$\begin{aligned}
\alpha_n &= -\frac{(n+2m+1)(n+2m+2)}{(2n+2m+3)(2n+2m+5)}Q^2\,,\\
\beta_n &= (n+m)(n+m+1) - Q^2\frac{2(n+m)(n+m+1) - m^2 - 1}{(2n+2m+3)(2n+2m-1)}\,,\\
\gamma_n &= \frac{n(1-n)Q^2}{(2n+2m-1)(2n+2m-3)}\,.
\end{aligned} \tag{6.21}$$

The recursion relation may be solved by, for example, the method of continued fractions.

The angular spheroidal wave equation (6.17) has two regular singular points at $z = 1$ and $z = -1$, corresponding to the north and south poles of the sphere respectively. Using the fact that in the interval $z \in [-1, +1]$, the associated Legendre functions can be expressed as derivatives of Legendre polynomials of the first kind, $P_n^m(z) = (1-z^2)^{m/2} d^m P_n(z)/dz^m$, we rewrite the spheroidal wavefuctions (6.19) as

$$S_l^m(Q;z) = (1-z^2)^{m/2} \sum_n d_n^{l,m}(Q) \frac{d^m P_n(z)}{dz^m}\,, \tag{6.22}$$

In general, solutions that are finite at $z = \pm 1$ will diverge at $z = \mp 1$, but for a discrete set of values of the eigenvalues λ_l^m, the series will converge to solutions that are finite at both poles. These eigenvalues λ_l^m are fixed by the requirements that the wavefunction remain finite at $z = \pm 1$, and this normalisability condition quantises our energy spectrum via the relation in (6.18).

The spheroidal eigenvalues are real-valued and satisfy the conjugation relation $\lambda_l^m = \lambda_l^{-m}$ and the equality $\lambda_l^m < \lambda_{l+1}^m$. For a given value of m, the smallest value of the eigenvalue is that for which $l = |m|$. Also, for fixed m, the corresponding set of eigenfunctions with different l values are mutually orthogonal. Consequently, the full wavefunctions satisfy orthonormality with respect to both quantum numbers,

$$\left\langle \Psi_l^m \middle| \Psi_{l'}^{m'} \right\rangle = \delta_{l,l'}\delta_{m,m'}\,. \tag{6.23}$$

Contemplating these solutions in hindsight, the emergence of spheroidal symmetry should not be surprising since the presence of the dipole magnetic field breaks the rotational symmetry of the Haldane problem to that of the oblate spheroid.

Normalisation

There are a number of normalisation schemes for the angular oblate functions. In the Stratton-Morse scheme which will be most convenient for our purposes, S_l^m can be normalised by imposing that, near $z = 1$, it behaves like the associated Legendre functions P_l^m for all values of Q. This in turn requires that the expansion coefficients satisfy

$$\widetilde{\sum_n} \frac{(n+2m)!}{n!} d_n^{l,m}(Q) = \frac{(l+m)!}{(l-m)!} \,. \tag{6.24}$$

The tilde over the summation sign is an instruction to include only even values of n if $(l-m)$ is even and only odd values of n if $(l-m)$ is odd. With this, the normalisation constants are given by

$$\begin{aligned} \mathcal{N}^{-1} &= \int_{-1}^{1} \left(S_l^m(Q,z)\right)^2 \, dz \\ &= \widetilde{\sum_n} \left(d_n^{l,m}(Q)\right)^2 \left(\frac{2}{2n+2m+1}\right) \left(\frac{(n+2m)!}{n!}\right) . \end{aligned} \tag{6.25}$$

Wavefunctions

Drawing this all together, the normalised single-particle eigenstates are given by

$$\begin{aligned} \Psi_l^m(Q;\theta,\phi) &= \mathcal{N} e^{im\phi} (\sin\theta)^m \widetilde{\sum_n} d_n^{l,m}(Q) \frac{d^m P_n(\cos\theta)}{d\cos\theta^m} \\ &= \psi_l^m(Q;\theta) e^{im\phi} \,, \\ \widetilde{E}_{Q,l,m} &= \lambda_l^m + 2mQ + Q^2 \,, \\ m &\in \mathbb{Z} \,, \\ l &= |m|, |m|+1, ... \end{aligned} \tag{6.26}$$

Note that since the differential equation (6.17) is invariant under $m \to -m$, so too are the $\psi_l^m(Q;\theta)$. It is the full states $\Psi_l^m(Q;\theta,\phi)$ which carry the information about the sign of m in the phase factor $e^{im\phi}$, and differ in energy depending on this sign.

In Figure 6.3 we plot a number of states and their energies for $Q = 1$ to illustrate some general features of the angular oblate spheriodal wavefunctions. All $m = 0$ states take their maximum amplitude at the poles, illustrated in Figure 6.3a. All states with non-zero m have zero amplitude at the poles, illustrated for the $|m| = 1$ case in Figure 6.3b (note that there is no $l = 0$ state here). The number of nodes of the wavefunction is always equal to $l - |m|$. The eigenenergies increase with l, while the energy difference between adjacent states also increases with l. This yields the nonlinear spectrum pictured in Figures 6.3c and 6.3d.

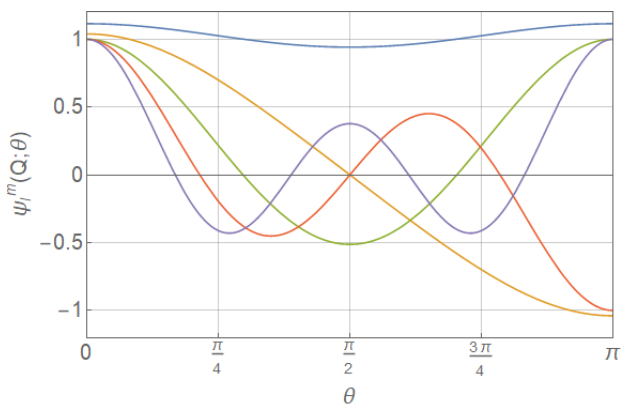

(a) $|m| = 0$ States

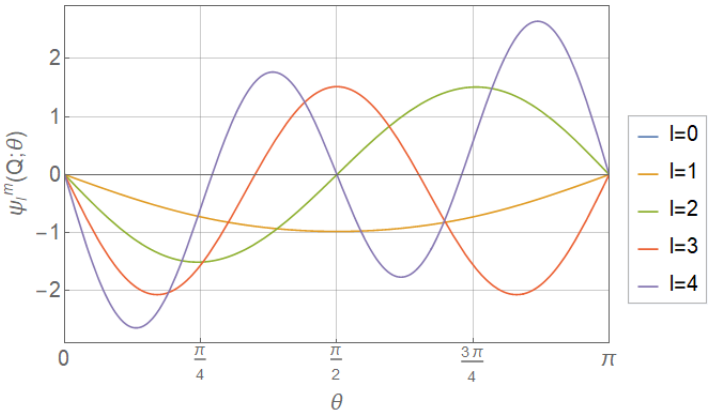

(b) $|m| = 1$ States

(c) $|m| = 0$ Spectrum

(d) $|m| = 1$ Spectrum

Figure 6.3: Various states $\psi_l^m(Q;\theta)$ and their spectrum $\widetilde{E}_{Q,l,m}$ for $Q = 1$.

6.2.3 Limiting Cases

We now attempt to develop some intuition for the physics of the system by studying the solutions (6.26) in some limiting cases: the weak-field limit, the free particle and near the north pole. We devote the next section entirely to the strong-field limit.

The Weak-Field Limit: $Q \ll 1$

From (6.7) we see that for fixed value of the magnetic dipole moment $\boldsymbol{\mu}$, the weak-field limit is obtained by taking the limit $R \to \infty$. Using the known power-series expansions for S_l^m and λ_l^m we can write down the corresponding expansions for the eigenstates and eigenenergies. We do this below to order Q^5.

$$
\begin{aligned}
\psi_l^m(Q;z) =& P_l^m(z) + \left[\frac{(l+m-1)(l+m)}{2(2l-1)^2(2l+1)}P_{l-2}^m(z) - \frac{(l-m+1)(l-m+2)}{2(2l+1)(2l+3)^2}P_{l+2}^m(z)\right]Q^2 \\
&- \left[\frac{(l+m-3)(l+m-2)(l+m-1)(l+m)}{8(2l-5)(2l-3)^2(2l-1)^2(2l+1)}P_{l-4}^m(z)\right. \\
&- \frac{1}{2(2l-1)}\left[\frac{(l+m-1)(l+m)((l-2)(l-1)+m^2-1)}{(2l-5)(2l-1)^3(2l+1)}\right. \\
&\left.- \frac{(l+m-1)(l+m)(l(1+l)+m^2-1)}{(2l-1)^3(2l+1)(2l+3))}\right]P_{l-2}^m(z) \\
&- \frac{1}{2}\left[\frac{(l-m-1)(l-m)(l+m-1)(l+m)}{4(2l-3)(2l-1)^4(2l+1)}\right. \\
&\left.+ \frac{(l-m+1)(l-m+2)(l+m+1)(l+m+2)}{4(2l+1)(2l+3)^4(2l+5)}\right]P_l^m(z) \\
&- \frac{1}{2(2l+3)}\left[\frac{(l-m+1)(l-m+2)(l(1+l)+m^2-1)}{(2l-1)(2l+1)(2l+1)^3}\right. \\
&\left.- \frac{(l-m+1)(l-m+2)((l+2)(l+3)+m^2-1)}{(1+2l)(2l+3)^3(2l+7)}\right]P_{l+2}^m(z) \\
&\left.+ \frac{(l-m+1)(l-m+2)(l-m+3)(l-m+4)}{8(2l+1)(2l+3)^2(2l+5)^2(2l+7)}P_{l+4}^m(z)\right]Q^4 + \mathcal{O}(Q^6)
\end{aligned}
\tag{6.27}
$$

$$
\begin{aligned}
E_{Q,l,m} =& \frac{\hbar^2}{2mR^2}\left[l(l+1) + \frac{2(l^2+l+m^2-1)}{(2l-1)(2l+3)}Q^2\right. \\
&- \left[\frac{(l-m-1)(l-m)(l+m-1)(l+m)}{2(2l-3)(2l-1)^3(2l+1)}\right. \\
&\left.\left.- \frac{(l-m+1)(l-m+2)(l+m+1)(l+m+2)}{2(2l+1)(2l+3)^3(2l+5)}\right]Q^4\right] + \mathcal{O}(Q^6)
\end{aligned}
\tag{6.28}
$$

Free Particle: $Q = 0$

From (6.27) and (6.28) it is clear that in the $Q \to 0$ limit we have

$$\psi_l^m(0;z) = P_l^m(z) \tag{6.29}$$

$$\widetilde{E}_{0,l,m} = l(l+1) \tag{6.30}$$

Thus our wavefunction reduces to the equation for a single spherical harmonic, as expected for a free particle confined to the surface of a sphere.

Near the North Pole: $\theta \to 0$

This limit corresponds to $z \to 1$. In the Stratton-Morse normalisation, the behaviour of S_l^m remains close to the associated Legendre function for all values of Q, and so, expanding in a power series in $(1-z^2)$, we recover

$$\Psi_l^m(Q;z) = \mathcal{N}\, e^{im\phi}(1-z^2)^{m/2}\sum_{k=0}^{\infty} c_{2k}^{l,m}(1-z^2)^k\,,$$

when $l-m$ is even, and where the coefficients $c_{2k}^{l,m}$ are expressed as a sum over the $d_{2k}^{l,m}$. A similar expression holds for $l-m$ odd.

6.2.4 The Strong-Field Limit: $Q \gg 1$

The most important limit we consider is the strong-field limit. The strong-field limit is relevant in the context of the surface physics of a neutron star where the magnetic dipole moment $|\boldsymbol{\mu}| \sim 10^{35}$ T m^{-3} and $R \sim 10^4$m. In this limit, $S_l^m(\theta, \phi)$ can be expanded in a series of Laguerre polynomials, giving a large-Q approximation to the single-particle eigenstate. We now plot a number of representative states for varying values of Q to observe the behaviour of the system as it approaches the strong-field limit. In Figure 6.4 we plot states with $0 \leq l + m \leq 4$, while in Figure 6.5 we plot states with $4 \leq l + m \leq 6$. The relevance of this distinction with respect to the quantity $l + m$ will become apparent shortly.

In both Figures 6.4 and 6.5 we see that for $Q = 1$ the particles are relatively delocalised over the entire sphere. As we increase the field strength to $Q = 10$, the amplitude around the equator becomes suppressed. Further increasing the field strength to $Q = 20$, and then $Q = 50$, the states become progressively more localised around the poles with negligible amplitude in an expanding region surrounding the equator. Note that comparing Figures 6.4 and 6.5, we see that for a given $Q > 1$, states with smaller $l - |m|$ values are more strongly localised around the poles than states with greater $l - |m|$.

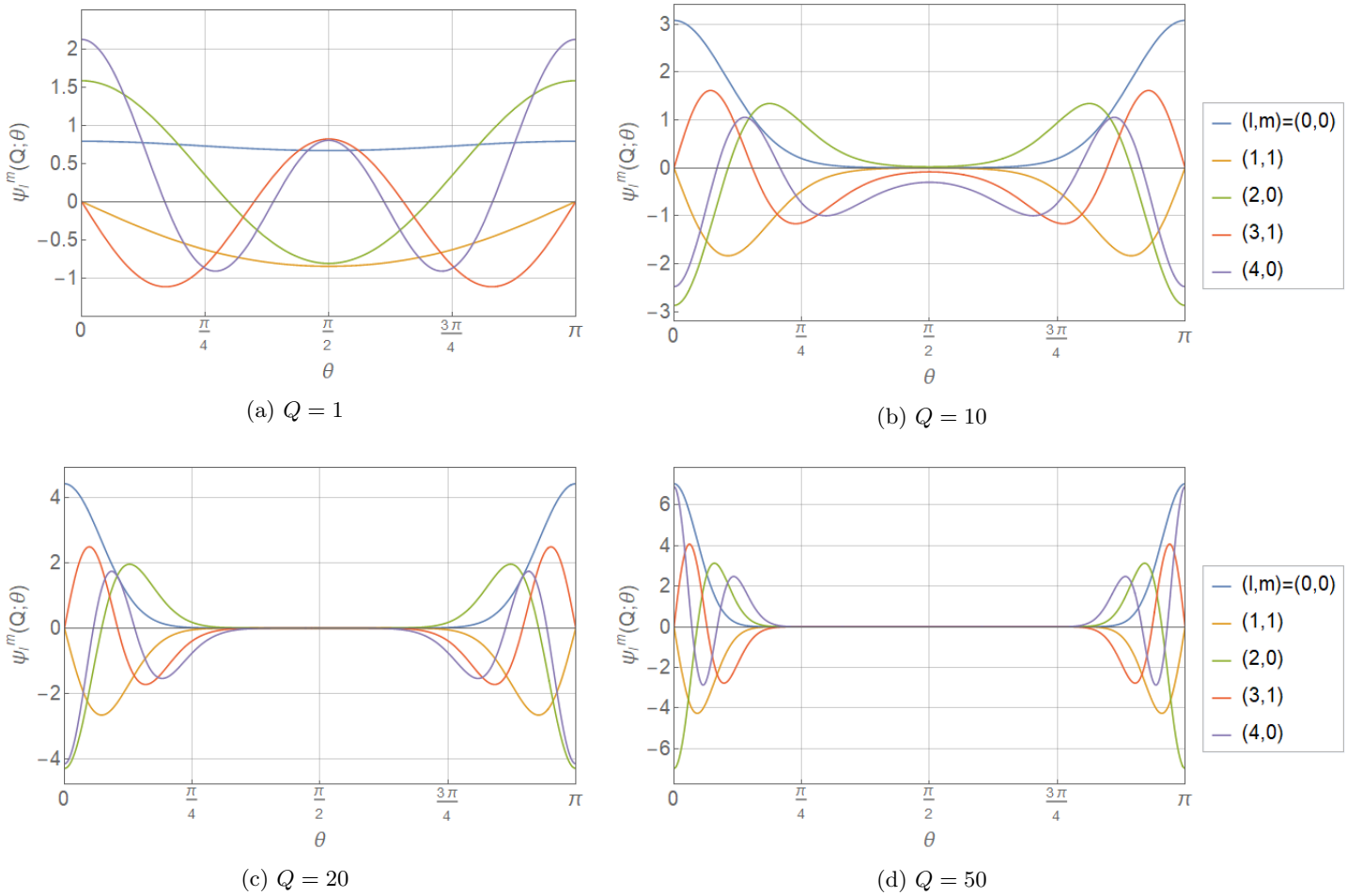

(a) $Q = 1$

(b) $Q = 10$

(c) $Q = 20$

(d) $Q = 50$

Figure 6.4: $\psi_l^m(Q;\theta)$ for various l, m and Q.

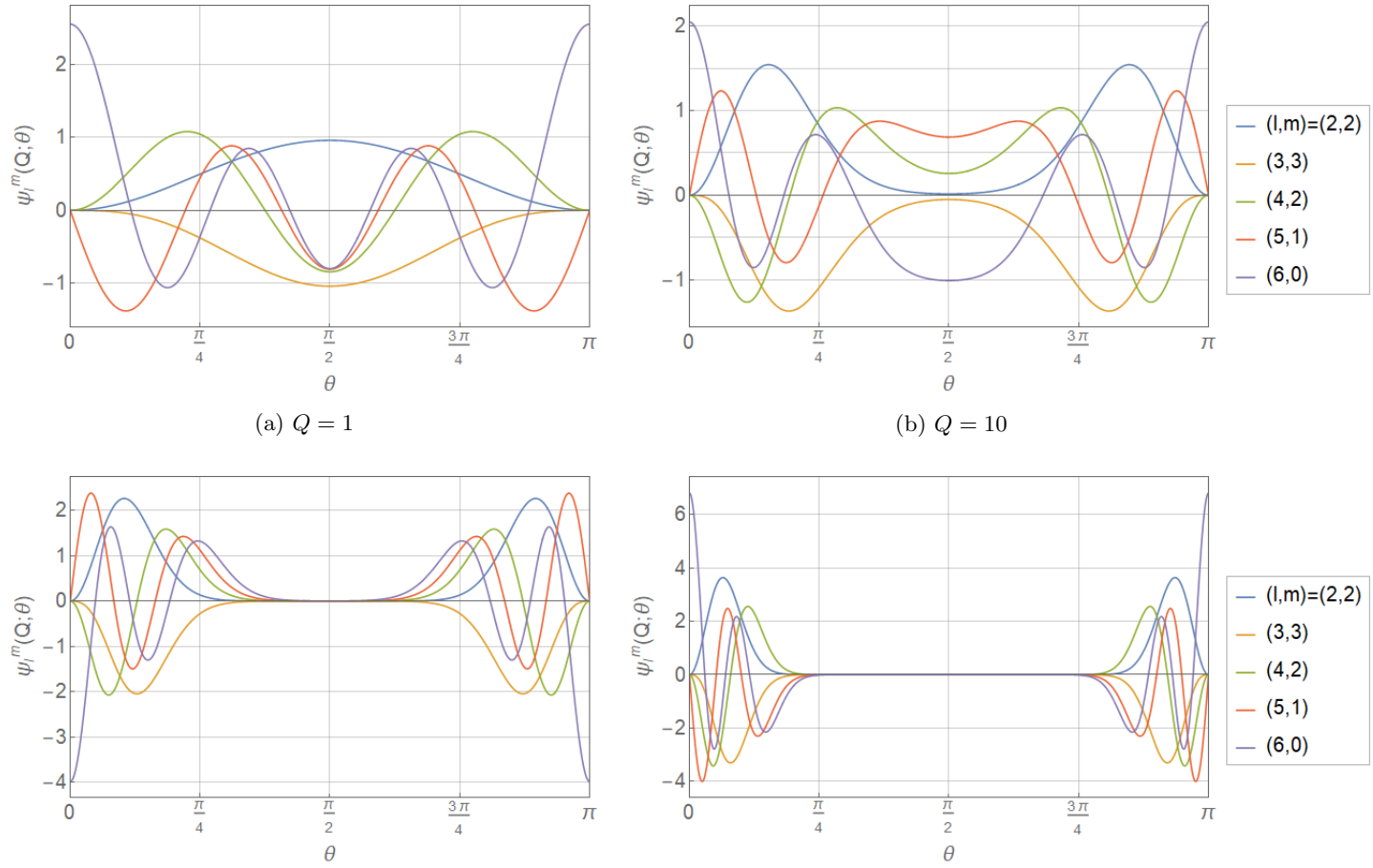

(a) $Q = 1$

(b) $Q = 10$

(c) $Q = 20$

(d) $Q = 50$

Figure 6.5: $\psi_l^m(Q;\theta)$ for various l, m and Q.

We have found that in the strong-field limit, our states become highly localised in the region surrounding the poles. This localisation effect appears to be stronger for states with lower values of the combination of quantum numbers $l - m$. In the dipole magnetic field configuration, the regions surrounding the poles are the regions on the sphere where the field configuration most closely approximates a field that is constant and perpendicular to the surface of the sphere. Given then that in the strong-field limit our states become confined to a region of approximately uniform magnetic field, we expect the energy spectrum to exhibit an approximate Landau level structure. We now proceed to make this intuition precise.

In the limit $Q^2 \gg m^2$ [69, 70], the spheroidal eigenvalues become

$$\lambda_l^m = 2\big[l + 1 - \mathrm{mod}(l - m, 2)\big]Q + \mathcal{O}(1)\,. \tag{6.31}$$

If m is integer valued, it follows that $\mathrm{mod}(l - m, 2) = \mathrm{mod}(l + m, 2)$. Using this and substituting into our expression for the energy spectrum (6.18), yields the following expression for the spectrum in the strong-field limit

$$\widetilde{E}_{Q,l,m} = Q^2 + 2\big[l + m + 1 - \mathrm{mod}(l + m, 2)\big]Q + \mathcal{O}(1)\,. \tag{6.32}$$

This result exhibits a number of noteworthy features:

1. With regard to quantum numbers, the spectrum depends only on the combination $l + m$. The strong-field limit spectrum therefore exhibits an (approximate) Landau level structure, where all states of the same $l + m$ are (approximately) degenerate.

2. The (approximate) Landau levels are evenly spaced, with spacing $2Q$.

3. Since m can take negative values, the (approximate) degeneracy per Landau level is *infinite*.

4. Due to the modulo term, the energies of states with pairwise adjacent $l+m$ values converge in the strong-field limit.

5. The lowest Landau level is comprised of all states for which $m \leq 0$ and $l = m$ or $l = m+1$.

6. Since the expression is valid in the limit $Q^2 \gg m^2$, in the strong-field limit we expect this Landau level structure to break down for states with very large m.

We illustrate these features by plotting the energy spectrum for a selection of states in Figure 6.6 ($m \geq 0$) and Figure 6.7 ($m \leq 0$) for various values of Q. The spectrum is calculated numerically for states of various l and m using the general expression (6.18), and is plotted against the strictly non-negative combination of quantum numbers $l - |m|$. The analytic results for the spectrum in the strong-field limit (6.32), neglecting the $\mathcal{O}(1)$ term, are then plotted for comparison as gray dashed lines. Note that in Figures 6.6g and 6.6h we have zoomed in on the lower half of the spectrum plotted in Figures 6.6e and 6.6f.

Observe how as Q increases the spectrum converges to the Landau level structure given by the strong-field analytic result (6.32). Figure 6.6 (6.6d in particular) illustrates that the pairwise convergence due to the modulo term taking place faster in Q for states with lower l and m values. Figure 6.7 illustrates that each Landau level will have infinite degeneracy as a result of the negative m states, since all states with the same $l - |m|$ values become degenerate in the large-Q limit.

Recall that for a given $Q > 1$, states with smaller $l - |m|$ are more strongly localised around the poles than states with greater $l - |m|$. Intuitively, larger $l - |m|$ states thus experience a more varied magnetic field. We expect this field inhomogeneity to perturb their energies, breaking the Landau level degeneracy. This is observed in Figures 6.6e, 6.6f and 6.7e, 6.7f where we see the Landau level degeneracy breaking as $l - |m|$ increases, as the energy eigenvalues gradually drift away from the gray dashed lines of the Landau levels. Increasing Q (thereby further localising the states at the poles) suppresses this degeneracy breaking effect, as can be seen by comparing for instance Figures 6.6g and 6.6h (or Figures 6.7e and 6.7f).

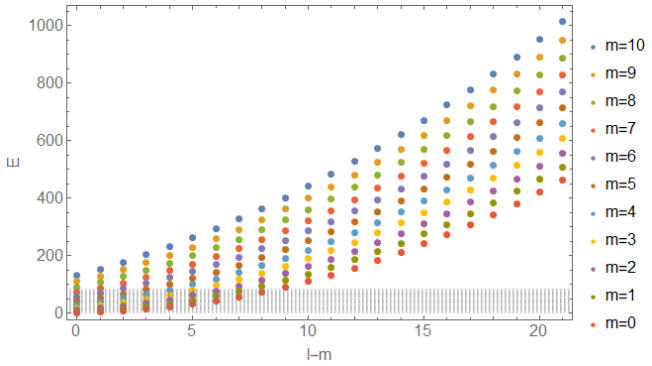

(a) $Q = 1$

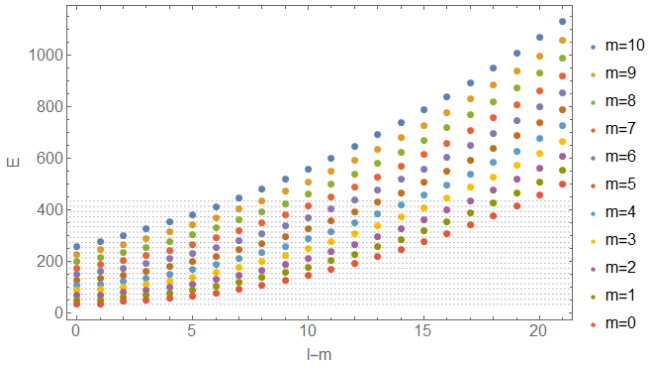

(b) $Q = 5$

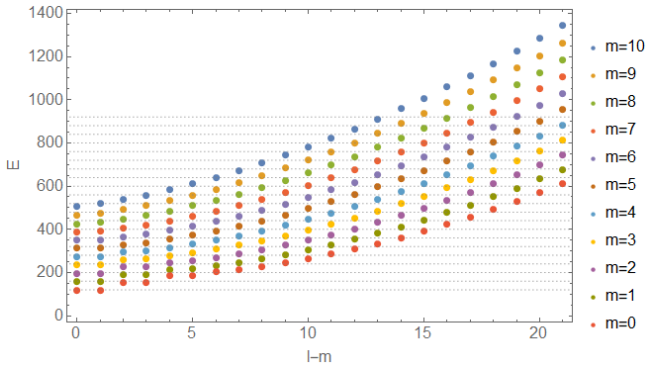

(c) $Q = 10$

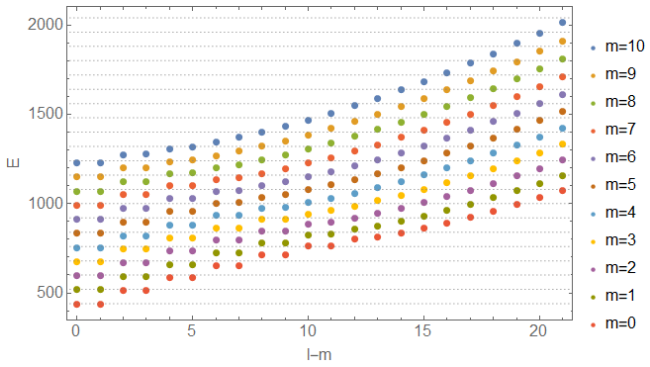

(d) $Q = 20$

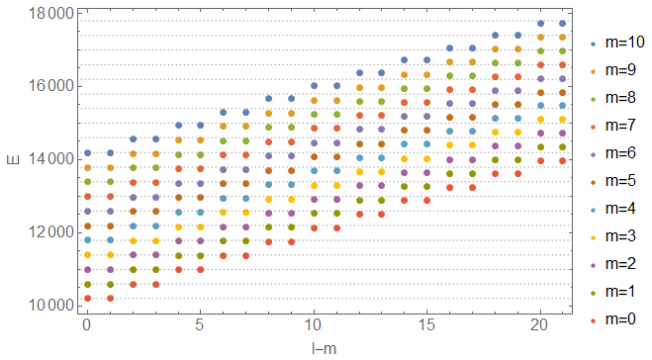

(e) $Q = 100$

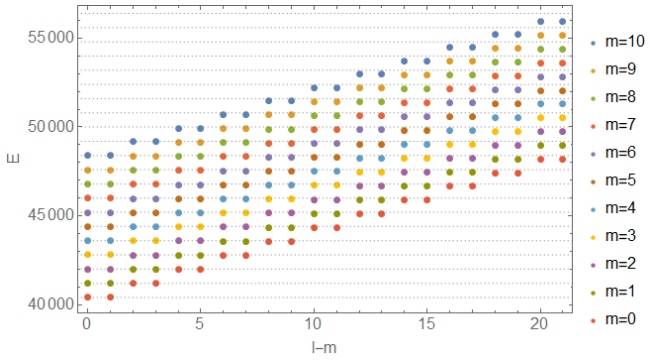

(f) $Q = 200$

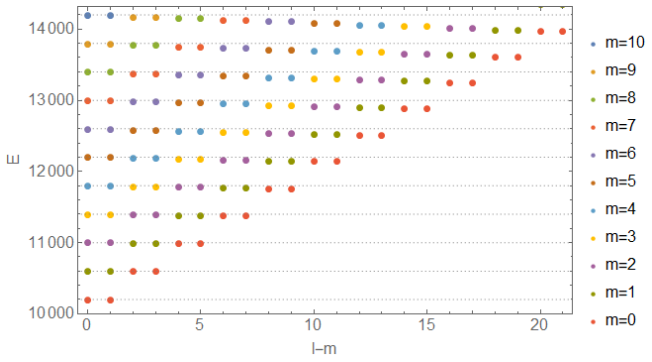

(g) $Q = 100$ (Partial Spectrum)

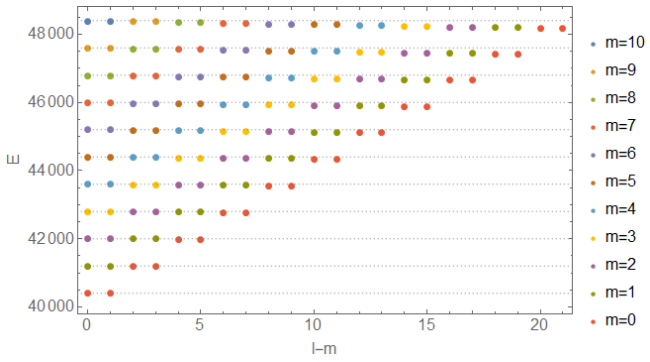

(h) $Q = 200$ (Partial Spectrum)

Figure 6.6: Energy spectra for $m \geq 0$ states.

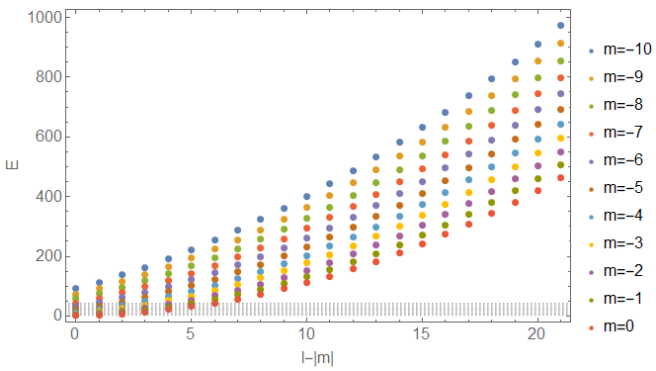

(a) $Q = 1$

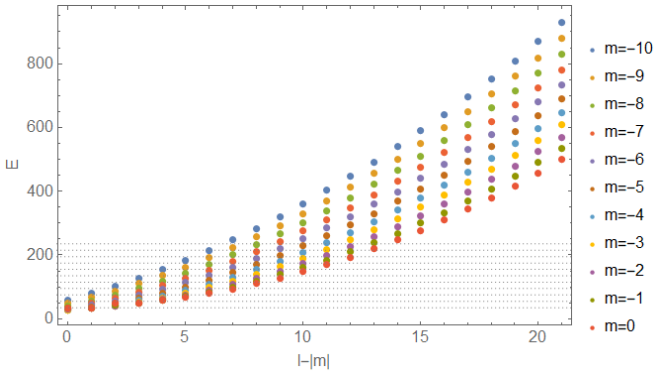

(b) $Q = 5$

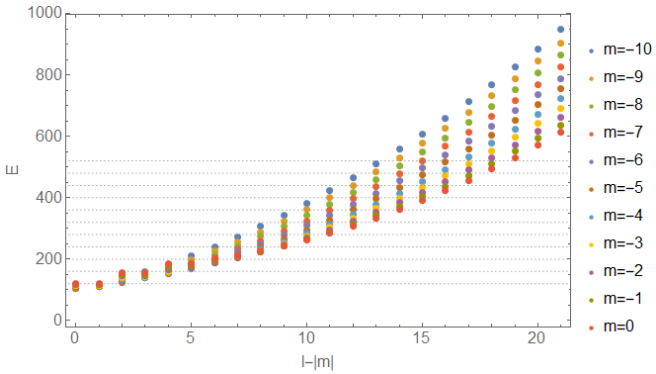

(c) $Q = 10$

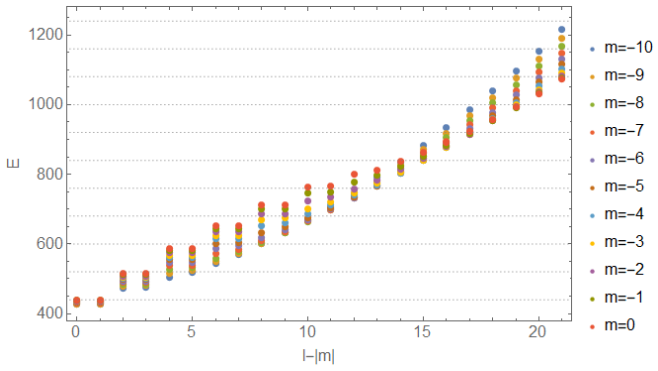

(d) $Q = 20$

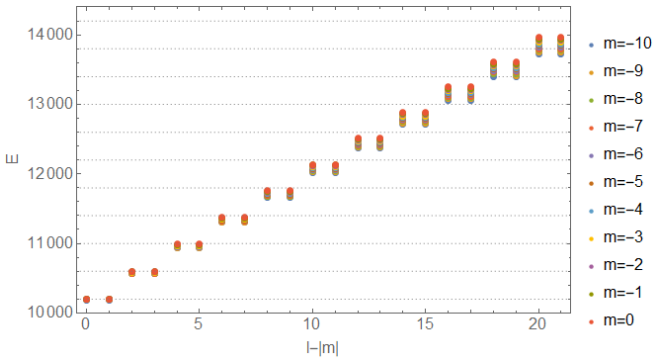

(e) $Q = 100$

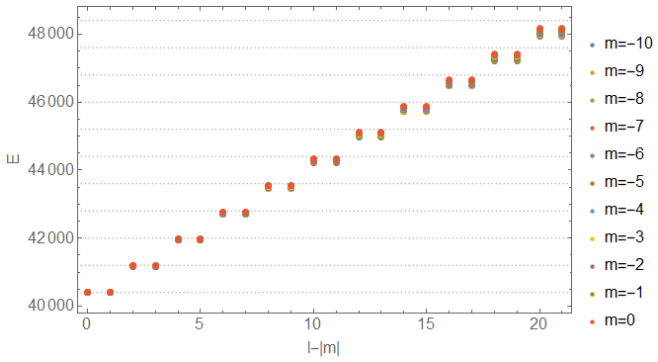

(f) $Q = 200$

Figure 6.7: Energy spectra for $m \leq 0$ states.

Chapter 7

Conclusion

7.1 Thesis Summary

We began this thesis by studying the two well-understood problems of charged particles confined to the plane in a constant magnetic field, and to the surface of a sphere in a monopole magnetic field, in Chapters 2 and 3 respectively. The entire single-particle Hilbert space and energy spectrum was found, and all features of the planar system were shown to emerge in the infinite radius limit of the spherical system. These results were then synthesized in Chapter 4 into a general framework for treating charged particles on the surface of a two-dimensional Kähler manifold, for the cases of both constant and non-constant magnetic flux densities.

In Chapter 5, we applied the framework developed in Chapter 4 to find perturbative results for the single-particle lowest Landau level states on the 'squashed sphere' (parameterised by a squashing parameter ϵ, with $\epsilon = 0$ corresponding to the unit sphere and $\epsilon > 0$ corresponding to the spheroid with unit polar radius and equatorial radius $1 + \epsilon$). We did this for both the constant and non-constant flux cases using monopole-like background magnetic fields. While 'unphysical', the monopole-like fields considered were best suited to our aim of applying the framework developed in Chapter 4 to investigate the effect of perturbing the geometry on the LLL states in both the uniform and non-uniform flux cases. The constant flux solutions were shown to be redundant, in the sense that they are only reliable for values of the squashing parameter in the regime $0 \leq \epsilon \leq 0.3$, and in this regime they are indistinguishable from the non-constant flux states. The non-constant flux states, on the other hand, are reliable for squashing parameter values in the regime $0 \leq \epsilon \leq 1$.

The tendency of states to be increasingly localised in stronger magnetic fields, which we observed in the spherical monopole and planar systems, was found to remain true in the squashed sphere system. The primary new effect we observed was the following: squashing the sphere was found to suppress the probability of finding the particle near the poles, and increase the probability of finding the particle near the equator. The particles effectively become localised in a band centred at the equator as the sphere is squashed.

In Chapter 6 we found the entire single-particle Hilbert space of the spherical dipole system. The wavefunctions are given, up to normalisation and complex phase, by the angular oblate spheroidal wavefunctions $S_l^m(Q;\theta)$. Unlike the monopole case, the net magnetic flux through the sphere vanishes for the dipole, making the problem globally topologically trivial. Nevertheless, it exhibits a remarkably rich structure. For a given field strength Q, the $l = m = 0$ state is the lowest energy state, and is only slightly localised around the poles, while states of higher energy are in general delocalised over the entire sphere. The energy spectrum is non-linear in the quantum numbers.

However, as the magnetic field becomes stronger, all states become increasingly localised around the poles, and are thus confined to a region of approximately constant magnetic flux density. This localisation effect is stronger for states of lower $l - |m|$. In the strong-field $Q \gg 1$ limit, the energy levels exhibit an approximate Landau level structure: the energies of states have only a linear dependence on the combination of quantum numbers $l + m$, with constant spacing between levels proportionate to Q. Unlike in the spherical monopole system, each level is infinitely degenerate, due to the negative m states. The LLL is comprised of states with $m \leq 0$ and $l = m$ or $l = m + 1$. The

degeneracy increasingly breaks down in the higher Landau levels as states with large $l - |m|$ are less localised around the poles and therefore experience more degeneracy-breaking magnetic field inhomogeneity. For sufficiently high Landau levels we therefore expect level crossing to cause the Landau level structure to disappear completely. The lower Landau levels however, in particular the LLL, remain approximately degenerate and maintain a clear Landau level structure.

7.2 Outlook

The most significant results presented in this paper, with the most prospects for further research, have concerned the spherical dipole system. I will here suggest a few directions in which these results can be expanded, which although outside of the scope of this thesis, will hopefully form the basis for future research.

In solving the spherical dipole system, we considered spinless charged particles. The first step would be to extend these results to the non-zero spin case, in particular to electrons with spin 1/2. This would entail solving the Schrödinger equation for the Pauli Hamiltonian which encodes spin. Another extension of the present work would be to consider the spherical dipole system in the presence of an applied electric field, to see which of the phenomena associated to the QHE are observed (in particular in the strong-field limit where we expect a Landau level structure to emerge).

With regards to possible experimental prospects for this research, we earlier noted that the dipole field we have considered is physically realisable, unlike the monopole field originally considered by Haldane. As experimental capabilities increase and the possibility of producing two-dimensional graphene spheres becomes more likely, the spherical dipole system could indeed be physically realisable in the future. It may present an opportunity to empirically test some of the theoretical predictions for quantum Hall states on compact geometries. This would however require the extension of our results to the relativistic case relevant for graphene, which would entail solving the Dirac equation instead of the Schrödiger equation.

Our consideration of the surface physics of neutron stars and astrophysical quantum matter (mentioned in the Introduction) served much more as the initial spark which lead us to consider the unsolved spherical dipole system, than as the focus of this thesis. Indeed any detailed assessment of the applicability of our model to neutron star physics was by no means within the scope or intention of this work. It is at this stage however worth briefly returning to the topic. We have only scratched the surface of the class of problems we have considered and are left with many more questions than answers. Quantum Hall systems and their variants are at this stage a staple of contemporary condensed matter physics. However, with the possible exception of high energy theory, they remain largely unknown (at least in their details) outside the community. On the other hand, strongly magnetic, compact astrophysical objects like neutron stars are one of the exciting new frontiers of contemporary physics. Rapidly increasing sensitivities in astrophysical observations and forthcoming experiments focused on pulsars [71] promise an unprecedented opportunity to study quantum matter under these extreme conditions [40]. While much effort has been devoted to understanding the processes in the interior of such objects, comparatively little study has gone into examining surface phenomena, at least from the perspective of quantum matter. Given the difficulty of probing neutron stars, the question of how to extract the condensed matter physics from neutron star observations remains pertinent [40]. Our intent in Chapter 6 of this thesis, a version of which has been submitted for publication [40], was as much to study the novel physics of particles in dipolar fields, as it was to bring to the attention of both the condensed matter and astrophysics communities a potentially new and remarkable class of problem. We hope that, if nothing else, it will stimulate further ideas in this direction.

Appendix A

Laguerre and Jacobi Polynomial Relations

The Laguerre polynomials $L_n^\alpha(x)$ satisfy the differential-difference equation

$$x\frac{d}{dx}L_n^\alpha(x) = nL_n^\alpha(x) - (n+\alpha)L_{n-1}^\alpha(x)\,, \tag{A.1}$$

and the difference relations

$$L_n^{\alpha-1}(x) = L_n^\alpha(x) - L_{n-1}^\alpha(x)\,, \tag{A.2}$$

$$xL_n^{\alpha+1}(x) = (x-n)L_n^\alpha(x) + (\alpha+n)L_{n-1}^\alpha(x)\,. \tag{A.3}$$

The Jacobi polynomials $P_n^{(\alpha,\beta)}(x)$ satisfy the differential-difference equation

$$(2n+\alpha+\beta)(1-x^2)\frac{d}{dx}P_n^{(\alpha,\beta)}(x) = n[\alpha-\beta-(2n+\alpha+\beta)x]P_n^{(\alpha,\beta)}(x) + 2(n+\alpha)(n+\beta)P_{n-1}^{(\alpha,\beta)}(x)\,, \tag{A.4}$$

and the difference relations

$$P_n^{(\alpha,\beta-1)}(x) - P_n^{(\alpha-1,\beta)}(x) = P_{n-1}^{(\alpha,\beta)}(x)\,, \tag{A.5}$$

$$(1-x)P_n^{(\alpha+1,\beta)}(x) + (1+x)P_n^{(\alpha,\beta+1)}(x) = 2P_n^{(\alpha,\beta)}(x)\,, \tag{A.6}$$

$$(2n+\alpha+\beta)P_n^{(\alpha-1,\beta)}(x) = (n+\alpha+\beta)P_n^{(\alpha,\beta)}(x) - (n+\beta)P_{n-1}^{(\alpha,\beta)}(x)\,, \tag{A.7}$$

$$(2n+\alpha+\beta)P_n^{(\alpha,\beta-1)}(x) = (n+\alpha+\beta)P_n^{(\alpha,\beta)}(x) - (n+\alpha)P_{n-1}^{(\alpha,\beta)}(x)\,. \tag{A.8}$$

Appendix B

Conformal Map from the Spheroid to the Plane

For a surface with orthogonal coordinates (θ, ϕ) and line element

$$ds^2 = E(\theta,\phi)d\theta^2 + G(\theta,\phi)d\phi^2\,, \tag{B.1}$$

E and G are known as the Gaussian fundamental quantities.

The sphere of radius R with line element

$$ds^2 = R^2 d\theta_s^2 + R^2\sin^2\theta d\phi_s^2\,, \tag{B.2}$$

where $0 < \theta_s < \pi$ and $0 \le \phi_s < 2\pi$, has Gaussian fundamental quantities

$$e = R^2\,, \quad g = R^2\sin^2\theta\,. \tag{B.3}$$

The spheroid, with equatorial and polar radii a and b respectively, has line element

$$ds'^2 = (a^2\cos^2\theta + b^2\sin^2\theta)d\theta^2 + a^2\sin^2\theta d\phi^2\,, \tag{B.4}$$

where $0 < \theta < \pi$, $0 \le \phi < 2\pi$, and Gaussian fundamental quantities

$$E = (a^2\cos^2\theta + b^2\sin^2\theta)\,, \quad G = a^2\sin^2\theta\,. \tag{B.5}$$

We would like to construct a conformal map

$$\theta = \theta(\theta_s)\,, \quad \phi = \phi(\phi_s)\,, \tag{B.6}$$

between these two surfaces. The following expression, relating the Gaussian fundamental quantities of the two metrics, then expresses the condition that this map be conformal [38]

$$\Big(\frac{\partial\theta_s}{\partial\theta}\Big)^2\frac{E}{e} = \Big(\frac{\partial\phi_s}{\partial\phi}\Big)^2\frac{G}{g} \tag{B.7}$$

We first fix $\phi_s = \phi$. Substitution then yields

$$\Big(\frac{\partial\theta_s}{\partial\theta}\Big)^2\frac{R^2}{a^2\cos^2\theta + b^2\sin^2\theta} = \frac{R^2\sin^2\theta_s}{a^2\sin^2\theta} \tag{B.8}$$

$$\Rightarrow \frac{d\theta_s}{\sin\theta_s} = \frac{\sqrt{a^2\cos^2\theta + b^2\sin^2\theta}}{a\sin\theta}d\theta\,. \tag{B.9}$$

Integrating this expression yields

$$\log\left(\tan\left(\frac{\theta_s}{2}\right)\right) - C = \int \sqrt{(b/a)^2 + \cot^2\theta}\, d\theta\,, \tag{B.10}$$

where C is an integration constant. We rewrite the right hand side as follows

$$\int \sqrt{(b/a)^2 + \cot^2\theta}\, d\theta = \int_{\pi/2}^{\theta} \sqrt{(b/a)^2 + \cot^2 v}\, dv + \log(a/b)\,, \tag{B.11}$$

where the constant term is obtained by evaluating the anti-derivative of the integrand at $\theta = \pi/2$. Substituting back into (B.10) yields

$$\log\left(\tan\left(\frac{\theta_s}{2}\right)\right) = \int_{\pi/2}^{\theta} \sqrt{\left(\frac{b}{a}\right)^2 + \cot^2 v}\, dv + \log(a/b) + C\,. \tag{B.12}$$

Exponentiating and then inverting both sides, we obtain

$$\cot\left(\frac{\theta_s}{2}\right) = A\frac{b}{a}e^{-h(\theta)}\,, \tag{B.13}$$

where $A \equiv e^{-C}$, and we have defined

$$h(\theta) \equiv \int_{\pi/2}^{\theta} \sqrt{\left(\frac{b}{a}\right)^2 + \cot^2 v}\, dv\,. \tag{B.14}$$

Imposing the initial condition $\theta_s(\pi/2) = \pi/2$ fixes $A = a/b$. Thus our conformal map from the sphere with coordinates (θ_s, ϕ_s) to the spheroid with coordinates (θ, ϕ) is given by

$$\cot\left(\frac{\theta_s}{2}\right) = e^{-h(\theta)}, \qquad \phi_s = \phi\,. \tag{B.15}$$

Finding the conformal map from the spheroid to the plane is now straightforward. The standard stereographic projection conformally maps the sphere of radius R to the plane with standard polar coordinates (r, ϕ_p). This map is given by

$$r = 2R\cot\left(\frac{\theta_s}{2}\right), \qquad \phi_p = \phi\,. \tag{B.16}$$

To obtain a conformal mapping from the spheroid to the plane, we simply pull the stereographic projection back to the spheroid. The resulting conformal map is given by

$$r = 2Re^{-h(\theta)}\,, \quad \phi_p = \phi\,, \tag{B.17}$$

where

$$h(\theta) = \int_{\pi/2}^{\theta} \sqrt{\left(\frac{b}{a}\right)^2 + \cot^2 v}\, dv\,. \tag{B.18}$$

Bibliography

[1] S.M. Girvin, *The Quantum Hall Effect: Novel Excitations and Broken Symmetries* (1999) arXiv:cond-mat/9907002

[2] K. v Klitzing, G. Dorda and M. Pepper, *New Method for High-Accuracy Determination of the Fine-Structure Constant Based on Quantized Hall Resistance* (1980) Phys. Rev. Lett. 45 494.

[3] D.C. Tsui, H.L. Stormer and A.C. Gossard, *Two-Dimensional Magnetotransport in the Extreme Quantum Limit* (1982) Phys. Rev. Lett. 48 1559.

[4] T. Can, M. Laskin and P.B. Wiegmann, *Geometry of Quantum Hall States: Gravitational Anomaly and Transport Coefficients.* (2015) arXiv:1411.3105v3

[5] M. Bander, *Fractional quantum hall effect in nonuniform magnetic fields* (1990) Phys. Rev. B41 9028

[6] R.B. Laughlin, *The Anomalous Quantum Hall Efect: An Incompressible Quantum Fluid with Fractionally Charged Excitations* (1983) Phys. Rev. Lett. 50, 1395

[7] R. B. Laughlin, *Quantized Hall Conductivity in Two Dimensions* (1981) Phys. Rev, B23 5632

[8] H. Grosse, A. Martin and J. Stubbe, *Splitting of Landau levels in nonconstant magnetic fields* (1993) Phys. Lett. A **181**, 7. doi:10.1016/0375-9601(93)91115-L

[9] R. Iengo and D. Li, *Quantum mechanics and quantum Hall effect on Riemann surfaces.* (1993) arXiv:hep-th/9307011v1

[10] Y. Deng and H.W.J Blote, *Conformal invariance and the Ising model on a spheroid.* (2003) Phys. Rev. E 67, 036107

[11] F.D.M. Haldane, *Fractional Quantization of the Hall Effect: A Hierarchy of Incompressible Quantum Fluid States.* (1983) Phys. Rev. Lett. 51, 605–608.

[12] C. Nayak, S.H. Simon, A. Stern, M. Freedman, and S.D. Sarma, *Non-Abelian Anyons and Topological Quantum Computation* (2008) Rev. of Mod. Phys., 80(3):1083

[13] F. Wilczek, *Fractional Statistics and Anyon Superconductivity* (1990) World Scientifi
c.

[14] X.-G. Wen, *Vacuum Degeneracy of Chiral Spin State in Compactified Spaces* Phys. Rev. B, 40, 7387 (1989)

[15] X.-G. Wen, *Topological Orders in Rigid States* (1990) Int. J. Mod. Phys. B. 4: 239.

[16] A. Kitaev and J. Preskill, *Topological Entanglement Entropy* (2006) Phys. Rev. Lett. 96, 110404

[17] G.V. Dunne, *Hilbert Space for Charged Particles in Perpendicular Magnetic Fields.* (1991) Annals of Physics 215,233-263

[18] M. Abramowitz and I. Stegun, *Handbook of Mathematical Functions.* (1984) Verlag Harri Deutsh, Thun, Switzerland

[19] G. Szegö, *Orthogonal Polynomials.* (1967) Amer. Math. Soc., Providence, RI

[20] P. Dirac, (1931) Proc. R. Soc. London A 133, 60

[21] I. Tamm, (1931) Z. Phys. 71, 141

[22] L. Landau and E. Lifschitz, *Quantum Mechanics: Non-Relativistic Theory.* (1977) 3rd ed., Pergamon, Oxford, page 136

[23] D. Tong, *The Quantum Hall Effect: TIFR Infosys Lectures.* (2016) http://www.damtp.cam.ac.uk/user/tong/qhe.html.

[24] S. Klevtsov, *Random normal matrices, Bergman Kernel and projective embeddings.* (2014) JHEP 1-19

[25] R. Alicki, J.R. Klauder and J. Lewandowski, *Landau Level Ground-State Degeneracy, and Its Relevance for a General Quantization Procedure.* (1993) arXiv:gr-qc/9312006v1

[26] Y. Aharonov and A. Casher, *Ground state of a spin-1/2 particle in a two-dimensional magnetic field.* (1979) Phys. Rev. A 19 2461–2462

[27] P. Maraner, *Landau ground state on Riemann surfaces.* Modern Physical Letters A 07 (1992) 2555.

[28] L. Landau, Z. Phys. 64, 629 (1930).

[29] A. H. MacDonald, Phys. Rev. B 30, 3550 (1984).

[30] S. M. Girvin and T. Jach, Phys. Rev. B 28, 4506 (1983).

[31] D. P. Arovas, Ph.D. thesis, University of California, Santa Barbara (1986).

[32] M. Greiter, *Landau Level Quantization on the Sphere.* (2011) arXiv:1101.3943v4

[33] R. Gilmore, *Lie Groups, Lie Algebras and Some of Their Applications* (1974) Wiley, New York

[34] T.T. Wu and C.N. Yang, *Dirac Monopole Without Strings: Monopole Harmonics* (1976) Nucl. Phys. B, 365

[35] S.M. Girvin and T. Jach, *Formalism for the quantum Hall effect: Hilbert space of analytic functions* (1984) Phys. Rev. B, 29 5617

[36] V. Bargman, (1962) Rev. Mod. Phys. 34, 829

[37] P. Maraner, *Landau Ground State on Riemann Surfaces* (1992) Modern Physics Letters A, Vol. 7, No. 27, 2555-2558

[38] D.B. Thompson, M.P. Mepham and R.R. Steeves, *The Stereographic Double Projection* (1977) Department of Geodesy and Geomatics Engineering, University of new Brunswick

[39] P. Richardus and R.K. Adler, *Map Projections* (1972) Amsterdam, Oxford (North-Holland Publishing Company)

[40] J. Murugan, J. P. Shock and R. P. Slayen, *Astrophysical Quantum Matter: Spinless charged particles on a magnetic dipole sphere* (2018) arXiv:1811.03109 [hep-th]

[41] P.A.M. Dirac, *Quantised Singularities in the Electromagnetic Field* (1931) Proc. Roy. Soc. London. Ser. A 133, 60

[42] M. V. Berry, *Quantal phase factors accompanying adiabatic changes*, Proc. R. Soc. A 392, 45 (1984).

[43] B. I. Halperin, *Quantized Hall conductance, current-carrying edge states, and the existence of extended states in a two-dimensional disordered potential*, Phys. Rev. B 25, 2185 (1982).

[44] B.I. Halperin, *Statistics of Quasiparticles and the Hierarchy of Fractional Quantized Hall States.* Phys. Rev. Lett., 52(18):1583, 1984.

[45] J. Jain, *Composite Fermions* Cambridge University Press. doi:10.1017/CBO9780511607561

[46] D. Thouless, M. Kohmoto, M. Nightingale and M. den Nijs, *Quantized Hall Conductance in a Two-Dimensional Periodic Potential* Phys. Rev. Lett. 49, 405 (1982).

[47] G. Moore and N. Read, *NonAbelions in the Fractional Quantum Hall Effect*, Nucl. Phys B360 362 (1991)

[48] N. Read and E. Rezayi, *Beyond paired quantum Hall states: parafermions and incompressible states in the first excited Landau level* cond-mat/9809384

[49] T. Senthil, N. Seiberg, E. Witten and C. Wang, *A Duality Web in 2+1 Dimensions and Condensed Matter Physics* (2016) ArXiv:1606.01989.

[50] A. Zee, *Quantum Hall Fluids* (1995) arXiv:cond-mat/9501022

[51] S. C. Zhang, T. Hansson and S. Kivelson, *Effective-Field-Theory Model for the Fractional Quantum Hall Effect* Phys. Rev. Lett. 62, 82 (1989)

[52] S.C. Zhang, *The Chern-Simons-Landau-Ginzburg Theory of the Fractional Quantum Hall Effect*, Int. Jour. Mod. Phys. B6 (1992).

[53] R. Shankar, *Topological Insulators - A review* (2018) arXiv:1804.06471

[54] M. Sato and Y. Ando, *Topological superconductors: a review* (2016) arXiv:1608.03395

[55] F. Haldane and E. Rezayi, *Periodic Laughlin-Jastrow wave functions for the fractional quantized Hall effect* Phys. Rev. B **31**, no. 4, 2529 (1985). doi:10.1103/PhysRevB.31.2529

[56] S. Klevtsov, *Random normal matrices, Bergman kernel and projective embeddings*, JHEP 2014 (1) (2014) 1–19.

[57] J. E. Avron, R. Seiler and P. G. Zograf, *Viscosity of quantum Hall fluids*, Phys. Rev. Lett. 75 (1995) 697–700.

[58] P. Levay, *Berry phases for Landau Hamiltonians on deformed tori*, J. Math. Phys. 36 (6) (1995) 2792–2802.

[59] P. Levay, *Berry's phase, chaos, and the deformations of Riemann surfaces*, Phys. Rev. E 56 (1997) 6173–6176.

[60] E. Witten, *Topological quantum field theory* Volume 117, Number 3 (1988), 353-386.

[61] X. G. Wen and Q. Niu, *Ground-state degeneracy of the fractional quantum Hall states in the presence of a random potential and on high-genus Riemann surfaces* (1990) Phys. Rev. B **41**, 9377. doi:10.1103/PhysRevB.41.9377

[62] https : //tinyurl.com/y78w9xw3

[63] S. Bellucci and P. Onorato, Phys. Rev. B **82**, 205305 (2010). doi :10.1103/PhysRevB.82.205305

[64] J. Heyl and I. Caiazzo, *Strongly Magnetized Sources: QED and X-ray Polarization* Galaxies **6**, no. 3, 76 (2018) doi:10.3390/galaxies6030076 [arXiv:1802.00358 [astro-ph.HE]].

[65] C. Störmer, Arch. Sci. Phys. Nat, **24** (1907)

[66] A.J. Dragt, *Trapped Orbits in a Magnetic Dipole Field* Reviews of Geophysics **3**, 2 (1965) doi:10.1029/RG003i002p00255

[67] G. Fano, F. Ortolani and E. Colombo, *Configuration-interaction calculations on the fractional quantum Hall effect* Phys. Rev. B **34**, 2670 (1986). doi:10.1103/PhysRevB.34.2670

[68] P.M. Morse and H. Feshbach, McGraw-Hill Book Co. Inc., New york NY (1953)

[69] E. Berti, V. Cardoso and M. Casals, *Eigenvalues and eigenfunctions of spin-weighted spheroidal harmonics in four and higher dimensions* Phys. Rev. D **73**, 024013 (2006) Erratum: [Phys. Rev. D **73**, 109902 (2006)] doi:10.1103/PhysRevD.73.109902, 10.1103/PhysRevD.73.024013 [gr-qc/0511111].

[70] S. Hod, *Eigenvalue spectrum of the spheroidal harmonics: A uniform asymptotic analysis* Phys. Lett. B **746**, 365 (2015) doi:10.1016/j.physletb.2015.05.036 [arXiv:1506.04148 [gr-qc]].

[71] M. Kramer and B. Strappers, [arXiv:1507.04423 [astro-ph.IM]].